The Synthesis and Characterization of A New Kind of Tagged Ru-Pt Bimetallic DNA Binding Agent

Zhenglai Fang

Thesis submitted to the Faculty of the
Virginia Polytechnic Institute and State University
in partial fulfillment of the requirements for the degree of

Master of Science
in
Chemistry

Prof. Karen J. Brewer, Chair
Prof. Brenda S.J. Winkel, Co-Chair
Prof. David G.I. Kingston
Prof. Brian E. Hanson

October 23, 2000
Blacksburg, VA

Keywords: ruthenium, platinum, DNA, binding, cisplatin, supramolecular

The Synthesis and Characterization of A New Kind of Tagged Ru-Pt Bimetallic DNA Binding Agent

Zhenglai Fang

(Abstract)

The goal of this project was to design a new kind of tagged supramolecular structural motif. These systems are modular in design and able to bind to DNA. The motif can be represented as TAG-LA-BL-BAS (TAG = NMR active phosphine ligand, LA = light absorber, BL = bridging ligand and BAS = bioactive site). The TAG provides a NMR probe for the characterization of supramolecular complexes as well as for the future investigation of the metal complex–DNA interaction process. In this project the phosphorous ligand PEt_2Ph was selected as the TAG due its ability to provide an easy ^{31}P NMR probe in the research. The LA represents the light absorber which could be photoexcited by photons of proper energy, here a $Ru^{II}(tpy)(PEt_2Ph)(BL)$ chromophore is used. The bridging ligands are those bidentate polyazine ligands that can connect two metal center together in a polymetallic system and have a low energy π^* orbital. The BAS represents the bioactive sites for binding to DNA, in this case the cis-$Pt^{II}Cl_2$ moiety based on previous studies with cisplatin.

The Ru-Pt bimetallic complexes $[(tpy)Ru(PEt_2Ph)(BL)PtCl_2](PF_6)_2$ (BL = bpm or dpp) and their precursors were designed, successfully synthesized and characterized. The synthesis followed a building block approach, allowing variation of the supramolecular system. The final bimetallic complexes were made without need for Al_2O_3 column chromatograph, important due to the presence of the labile $Pt^{II}Cl_2$ center.

The bimetallic complexes and all of their monometallic precursors were fully characterized by FAB MS, electrochemistry, electronic absorption and ^{31}P NMR spectroscopy. The Ru-Pt bimetallic complex containing the bpm bridging ligand and its precursors were also characterized by ^{1}H NMR. The FAB MS spectra of the complexes is characterized by the appearance of the parent ion peaks $[M\text{-}PF_6]^+$ and $[M\text{-}2PF_6]^+$. The cyclic voltammogram of all complexes show metal based oxidation(s) and ligand based reductions. The electronic absorption spectra of the complexes are characteristic of the lowest lying Ru→BL MLCT (metal to ligand charge transfer) transition with higher energy bridging and terminal ligand based π→π* transitions. The electronic absorption data are consistent with the electrochemical data. The ^{31}P NMR technique provides an efficient and easy characterization method for the complexes, showing the utility of this structural moiety.

The DNA binding activity of the bimetallic complexes were studied by non-denaturing agarose gel electrophoresis and the results show that these tagged bimetallic complexes can bind to DNA through the cis-$Pt^{II}Cl_2$ moiety. This binding has a more pronounced retardation effect on DNA migration than cis-$[Pt(NH_3)_2Cl_2]$ (cisplatin), but less than $[Ru(bpy)_2(dpq)PtCl_2](CF_3SO_3)_2$. The DNA binding study establishes these bimetallic complexes with a NMR tag ligand, PEt_2Ph, as a new kind of DNA binding agent.

Table of Contents

List of Figures

List of Tables

Abbreviations

BAS	bioactive site
bpm	2,2’-bipyrimidine
bpy	2,2’-bipyridine
CT	charge transfer
dpb	2,3-bis(2-pyridyl)benzoquinoxaline
dpq	2,3-bis(2-pyridyl)quinoaline
HOMO	highest occupied molecular orbital
LA	light absorber
LF	ligand field
LUMO	lowest unoccupied molecular orbital
MLCT	metal to ligand charge transfer
tpy	2,2’:6’,6’’-terpyridine

Acknowledgements

I should thank my grand mother, my parents and my brother for my upbringing and for the support of my receiving high education. I believe the value they helped me to develop is ever the best gift for me along my way of life.

I should also thank Professor Karen J. Brewer for her mentoring during my graduate career at Virginia Tech and even right now at Columbia. Her guidance and encouragement were indispensable in my success at Virginia Tech and will be, I believe, in my future professional life. I should also thank Dr. Winkel for her sincere help with the DNA binding study and Dr. Hanson for the interpretation of the ^{31}P NMR. Help from other Brewer's group members is also appreciated.

NSF (National Science Foundation), OSER/Carilion Biomedical and Virginia Tech provided much appreciated financial support throughout this work.

Chapter 1: Introduction

Light absorption and electronic absorption spectroscopy

LA is a light absorber molecule. When it absorbs a photon of light, it goes into an electronically excited state. Eq (1).

Absorption of Light

$$LA + h\nu \rightarrow LA^* \qquad (1)$$

A simplified two orbital picture of a light absorber (LA) would consist of a filled orbital and a higher energy empty orbital. Absorption of a photon of light of the proper energy would promote an electron from the lower energy orbital to the higher energy orbital, generating an excited state of the light absorber (Figure 1.1). The excited state of the light absorber possesses a number of unique chemical properties and thus gives rise to

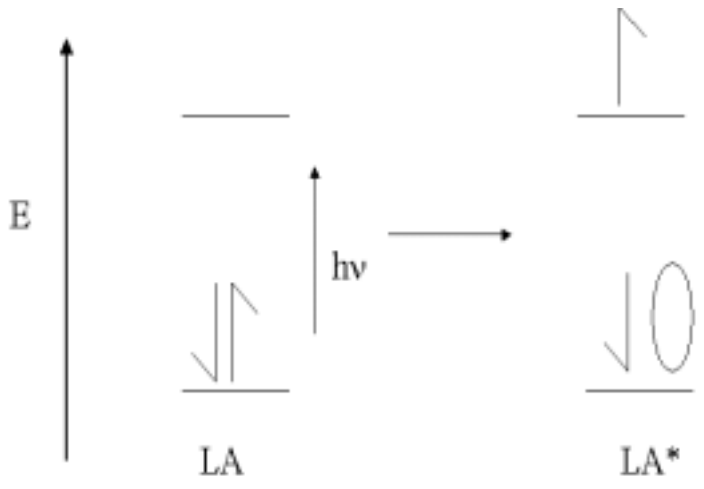

Figure 1.1 Light absorption process by a light absorber

some unique reactivity. An obvious example is that the excited state of a light absorber is both a better oxidizing agent and reducing agent than the ground state of a light absorber. This is pretty straightforward: it is comparatively easy to remove the promoted electron from the higher energy orbital making oxidation easier. At the same time it is also relative easy to put an electron into the hole generated by the electron promotion, making reduction easier.

The octahedral d^6 transitional metal ruthenium complexes with polypyridyl ligands are widely used as light absorbers. This is because these complexes are generally photostable and under many circumstances are able to undergo excited electron transfer.[1-3] One well-studied example would be $[Ru(bpy)_3]^{2+}$, where bpy = 2,2'-bipyridine.

Figure 1.2 shows the molecular orbitals of the ruthenium metal center using the linear combination of atomic orbitals (LACO) description. The boxes in the diagram represent sets of orbitasl of slightly varied energy. In these complexes, the highest occupied molecular orbital (HOMO) is located on the ruthenium based $d\pi$ orbital and the lowest unoccupied molecular orbital (LUMO) is located on the ligands baesd π^* orbital.

When a light-absorbing molecule absorbs a photon of light, an electron could be promoted from any occupied orbital to any unfilled orbital. Symmetry considerations and the amount of overlap between the two orbitals determine the strength of a particular transition. The major electronic transitions that occur in ruthenium pseudo octahedral d^6 complexes of the polyazine ligands are ligand based $\pi \rightarrow \pi^*$, metal-to-ligand charge transfer (MLCT), and the ligand field transitions. The intensity of a transition is determined by selection rules. In order for a transition to be fully allowed, the transition must be both Laporte and spin allowed, conditions typically met for MLCT and $\pi \rightarrow \pi^*$ transitions.

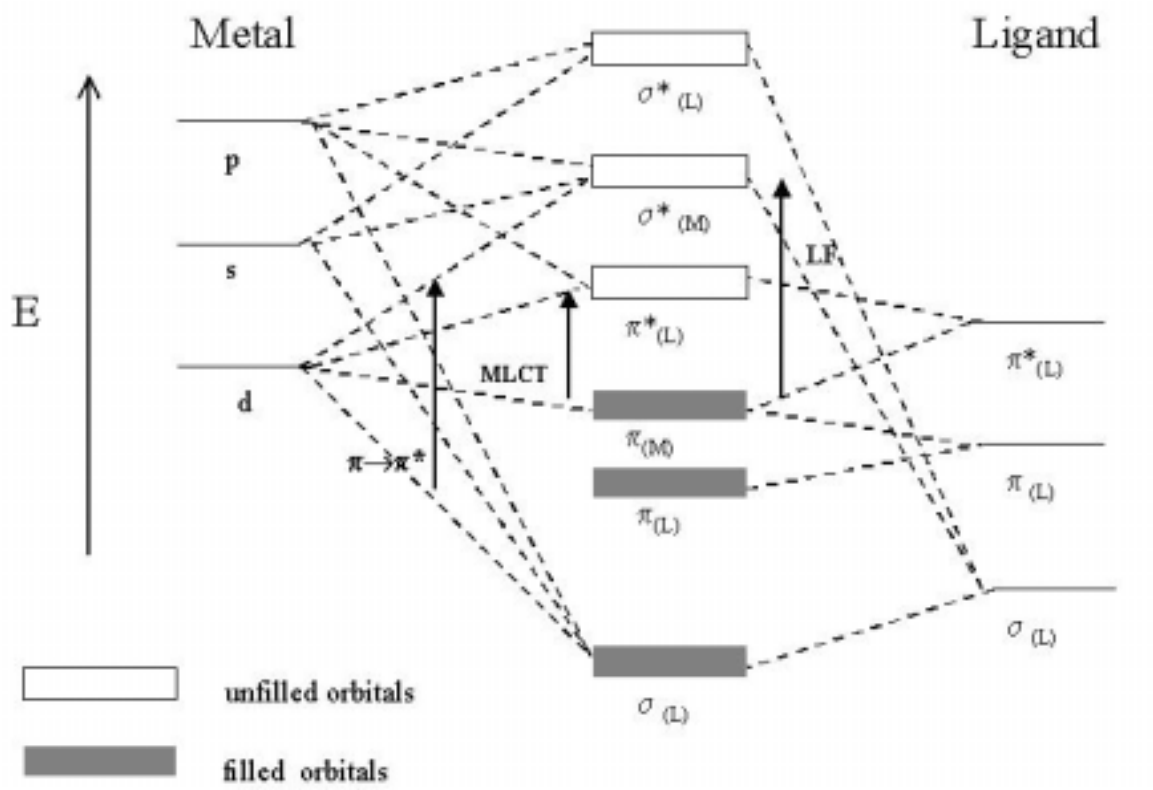

Figure 1.2 Block diagram of molecular orbital of a d^6 octahedral complex and some of its possible electronic transitions

Cyclic voltammetry

Cyclic voltammetry measures the potential at which a molecule is either oxidized or reduced.[4] Here a simplified 2-orbital model is used in the explanation of the electrochemical reduction and oxidation of a compound. In the 2-orbital model, a molecule has one filled lower-energy orbital and one unfilled higher-energy orbital. The electrochemical oxidation process is the transfer of an electron from the filled orbital of the compound in the solution to the electrode. The electrochemical reduction process is the transfer of an electron from the electrode to the empty higher energy orbital of the compound in the solution. As the external voltage is scanned, a point is reached where the electrons at the electrode surface have higher energy than the energy of the empty

orbital in the compound and these electrons are then transferred to that compound. This is how the reduction of a compound occurs (Figure 1.3). In contrast, when the electrons in the filled orbital of the compound have higher energy than those electrons on the electrode with some potential, the electrons are transferred to the electrode from the filled orbital in the compound. This is how the oxidation process occurs (Figure 1.3).

The energy of the orbitals of a compound can be determined by measuring the potential of the electrons in the electrode as the oxidation and reduction processes occur. The energy of the electrons are related to the potential of electrons in the electrode by the equation $\Delta G = - nFE$, where ΔG is the Gibbs free energy, n is the number of the electrons transferred, F is the Faraday's constant, and E is the potential.

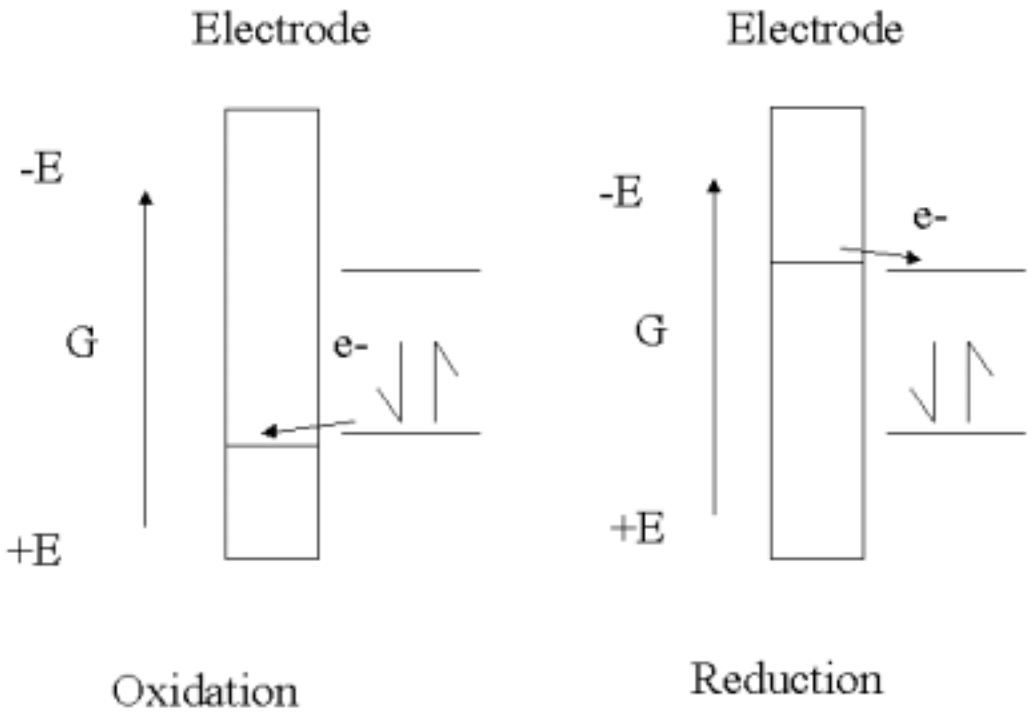

Figure 1.3 The electrochemical oxidation and reduction of a compound

In cyclic voltammetry, the potential of the electrode is cycled through the region where oxidations and reductions of the compound in solution occur and the current is measured as electrons flow to or from the electrode. A sample cyclic voltammogram of ferrocene ($FeCp_2$) in CH_3CN is shown in Figure 1.4. As the potential is scanned from zero/positive, ferrocene is oxidized. As ferrocene at the surface of the electrode is oxidized, the current eventually reaches a maximum. This is called the anodic peak current, $\boldsymbol{i}_p^a$, and occurs at the anodic peak potential, E_p^a. After the majority of the sample at the electrode surface is oxidized, the current is determined by the mass transport of the unoxidized sample from the bulk solution to the electrode surface and the current drops. As the potential is cycled back in the negative direction toward 0, the current reaches a maximum as $FeCp_2^+$ is reduced back to $FeCp_2$. This maximum current is called the cathodic peak current, $\boldsymbol{i}_p^c$, and occurs at the cathodic peak potential, E_p^c. A reversible redox reaction is one in which there are no chemical steps after the oxidation or reduction and occurs with fast electron transfer rate. The theoretical peak separation for a reversible reaction, $\Delta E_p = E_p^a - E_p^c$, is 59 mV/n where n is the number of the electrons in the redox process and $\boldsymbol{i}_p^c/\boldsymbol{i}_p^a = 1$.The half potential, $E_{1/2}$, is defined as $(E_p^a + E_p^c)/2$.

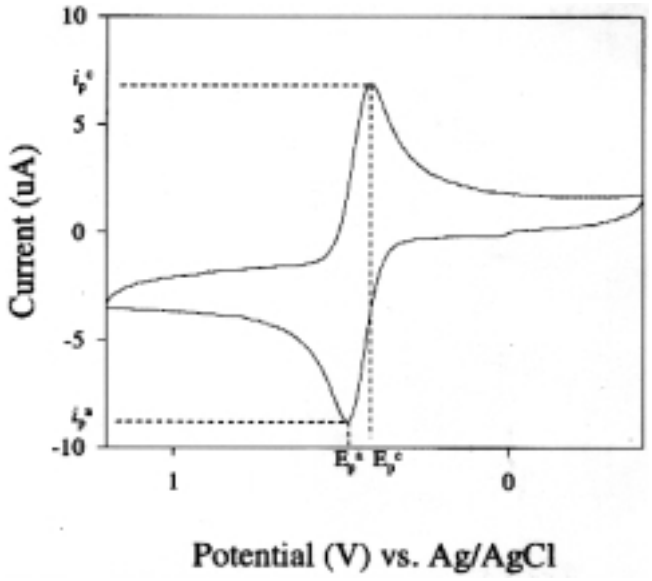

Figure 1.4 Cyclic voltammogram of ferrocene, $Fe(C_5H_5)_2$

Ruthenium chromophores, tridentate terpyridine ligand and polyazine bridging ligand

Since the discovery of the photophysical properties of $[Ru(bpy)_3]^{2+}$ much work has been done on the properties of related ruthenium(II) polypyridyl complexes and their applications in solar energy conversion, electron transfer and the construction of luminescent supramolecular polymetallic complexes.[1-3,5-7] The properties of ruthenium(II) complexes can be tuned through the variation of the ligands attached. Recently ruthenium(II) complexes with polypyridyl ligands have been widely used as building blocks for the luminescent supramolecular metal complexes.[8] In these polymetallic supramolecular systems, bridging ligands are commonly used to hold the metal centers together. These complexes could possibly be used as molecular devices for various photoinitiated processes including energy and electron transfer. In those systems specially designed for photoinitiated charge separations, a chromophore absorbs a photons of light and intramolecular electron transfer occurs involving a suitable oxidative or reductive quencher to produce a separation of charge. This charge-separated state of the supramolecular system could be utilized to perform many useful complex functions.

The tridentate ligand tpy (tpy = 2,2':6',2''-terpyridine, Figure 1.5) is seldom used in the construction of supramolecular systems. This is largely due to the nonemissive nature as well as the short excited life time of those tpy-containing complexes such as $[Ru(tpy)_2]^{2+}$. It has been shown that the short excited lifetime of the MLCT state of the complex $[Ru(tpy)_2]^{2+}$ is due to a ligand field (LF) state that is thermally accessible at RT.[9-11] The thermal accessibility of this LF state is attributed to the non-ideal bite angle (158^0 instead of 180^0) of the tpy ligand.[12,13] Despite the limited lifetime of the excited state of $[Ru(tpy)_2]^{2+}$, systems with observable emission still could be formed with the tridentate ligands when the energy difference between the lowest ^{3}MLCT and the low-lying ligand field states are greater than in $[Ru(tpy)_2]^{2+}$.[9] Tridentate ligands eliminate the possibility of geometric isomers which could bring about two obvious advantages: the elimination of

the problem of separating or studying a mixture of isomers and the ability to design complexes in which the distance of the electron or energy transfer could be controlled. Because of these advantages, the tridentate ligand tpy was used to construct our supramolecular system in this project.

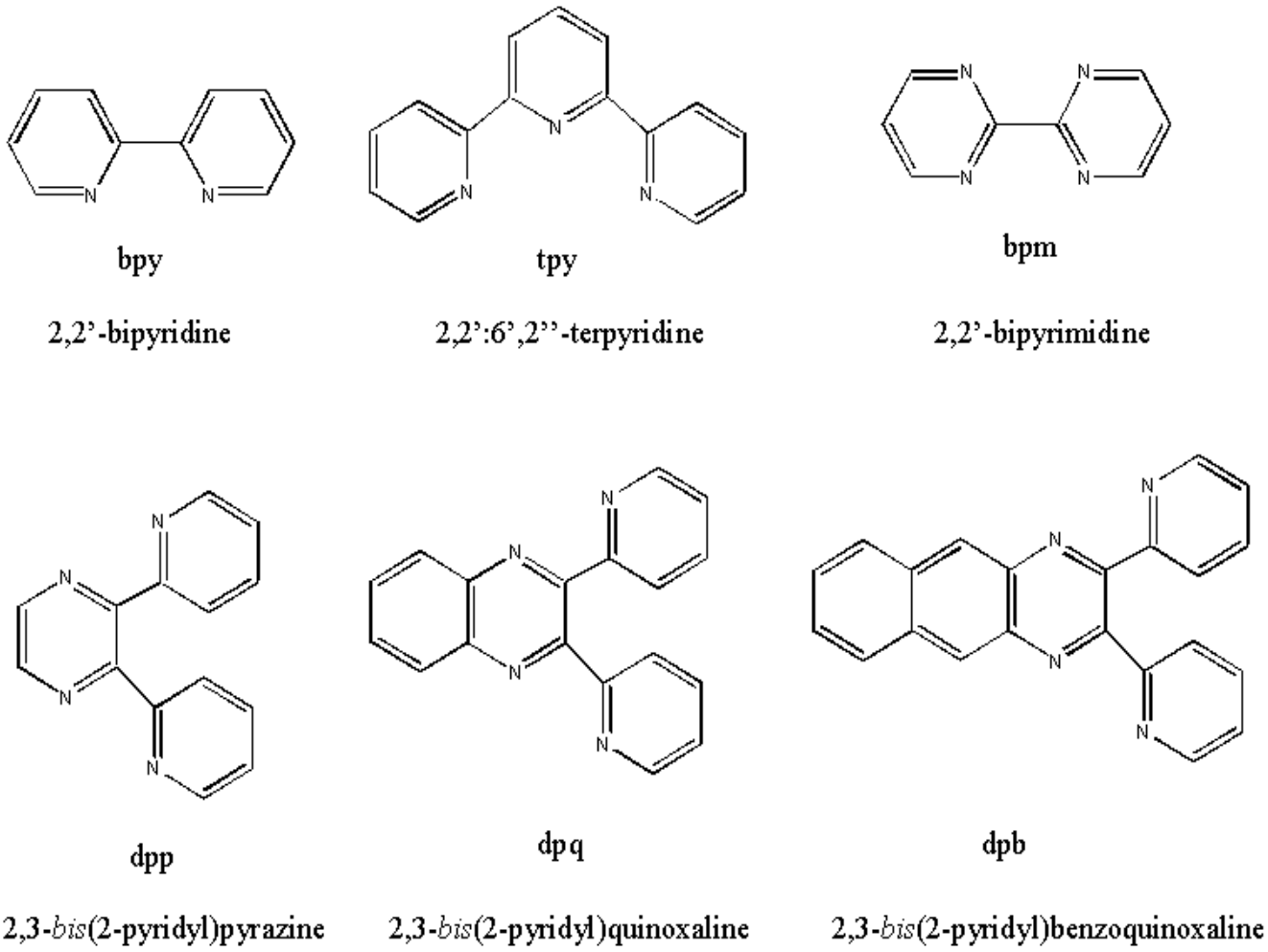

Figure 1.5 Terminal ligands bpy, tpy and bridging ligands bpm, dpp, dpq and dpb.

In the construction of a polymetallic supramolecular species, bridging ligands covalently connect the different metal centers but also determine many characteristics of the complex. Bidentate polyazine bridging ligands have been widely used in the construction of polymetallic complexes. Generally these bridging ligands can be grouped into the asymmetrical A-B type ligands and the symmetrical A-A type ligands. In the asymmetrical A-B type polyazine bridging ligands, the two nitrogen donors to one metal center are nonequivalent. In contrast, the nitrogen donors from the A-A type polyazine bridging ligands to a metal center are equivalent.

Some of the most widely used A-B type polyazine bridging ligands include dpp (2,3-bis(2-pyridyl)pyrazine), dpq (2,3-bis(2-pyridyl)quinoxaline and dpb (2,3-bis(2-pyridyl)benzoquinoxaline) (Figure 1.5).[14-17] The use of these bridging ligands is a disadvantage in terms of controlling the stereochemistry of the resulting polymetallic complexes.

One of the most heavily used A-A type polyazine bridging ligands is bpm (2,2'-bipyrimidine) (Figure 1.5). It has been used in building a series of polymetallic systems.[18-21] The supramolecular systems incorporating this symmetrical ligand have well-define stereochemistry. The bpm ligand does bring some disadvantages in the construction of polymetallic complexes. First, the small size of this ligand holds the bridged metals very close and this sometimes could prevent the synthesis of the polymetallic complexes. Secondly, it would be quite difficult to add any electron withdrawing or donating groups to the bpm ligand and the modified bpm ligand would probably interfere sterically with the synthesis of the polymetallic complexes. So it is difficult to tune the electronic properties of the polymetallic complexes with a bpm type bridging ligand.

Ru-Pt mixed mixed-metal complexes and their application as anticancer agents

The luminescent ruthenium(II)/platinum(II) binuclear complexes have recently been studied by Rillema[22] and Yam[23], most notably $[(bpy)_2Ru(dpp)PtCl_2](PF_6)_2$. The electrochemical behavior and the electronic absorption properties of these complexes have been studied. The electrochemical study shows that the bridging ligand in the dpp based bimetallic complexes have a characteristically more positive first reduction potential ($E_{1/2}$ = -0.54 V) relative to the monometallic system ($E_{1/2}$ = -1.06 V), which is attributed to the attachment of the electron-deficient $Pt^{II}Cl_2$ moiety.[23] This attachment leads to a stabilization of the dpp based π^* acceptor orbital. The ruthenium(II) based oxidation was observed to shift to a more positive potential ($E_{1/2}$ = +1.57 V for the bimetallic complex and $E_{1/2}$ = +1.31 V for the monometallic complex); $[(bpy)_2Ru(dpp)PtCl_2](PF_6)_2$ shows an irreversible oxidation in the cyclic voltammogram observed by Yam and later assigned by Brewer et al as platinum(II) in nature.[24a] The electronic absorption study shows that the metal-to-ligand charge transfer transitions (MLCT) between the ruthenium(II) metal center and the bridging ligand red shifts in the bimetallic complex relative to the corresponding ruthenium(II) monometallic complexes (505 vs 464 nm respectively). [23] This red shift of the MLCT transitions is consistent with the coordination of the electron-deficient platinum metal center as suggested by the more positive first reduction of the bridged bridging ligand.

Previously in the Brewer group, Milkevitch synthesized and characterized the supramolecular systems $[(bpy)_2Ru(BL)PtCl_2](PF_6)_2$ (BL = 2,3-bis(2-pyridyl)quinoxaline and 2,3-bis(2-pyridyl)benzoquinoxaline) as a new kind of DNA-binding agents.[24] In these bimetallic systems the ruthenium(II) metal center and platinum(II) metal center are covalently coupled by two different bridging ligands, allowing possible intramolecular energy and electron transfer. Brewer postulated and later showed that incorporation of the $Pt^{II}Cl_2$ moiety into the system allows the potential binding to DNA through the platinum site.[25-27]

McMillin and coworkers have shown that $[Pt(tpy)X]^+$ (X = Cl, OH and CH_3CN) complexes can bind to DNA intercalatively through the terminal ligand tpy[28] as well as covalently through the platinum(II) site. But intercalation of tpy to DNA is only observed in square planar complexes but not in octahedral complexes.

The Ru-Pt bimetallic complexes were made by a building-block approach allowing easy modification of the electronic properties of the complexes. The electronic absorption spectroscopic and electrochemical characterization of these complexes show that the substitution of dpq and dpb for dpp gives rise to a series of complexes with easily tunable spectroscopic and redox properites. The DNA-binding activities of these complexes were well studied by agarose gel electrophoresis. The results established these complexes as a new kind of DNA-binding agent.

Cisplatin and analog research

Cisplatin is one of the most potent and widely-used anticancer drugs known. Its formal name is cis-diamminedichloroplatinum(II), abbreviated to cis-DDP. It was discovered to possess the antitumor activity in 1969 by Rosenberg.[25, 29] Cisplatin enters human cells by diffusion, where it is converted to its active form[30] shown in Eq. (2):

$$Pt(NH_3)_2Cl_2 + 2H_2O \Leftrightarrow [Pt(NH_3)_2(H_2O)_2]^{2+} + 2Cl^- \qquad (2)$$

This ligand substitution equilibrium shifts to the right side due to the lower intracellular chloride concentration. The active aquated species $[Pt(NH_3)_2(H_2O)_2]^{2+}$ is a bifunctional electrophilic agent[31] and previous studies show that it binds to DNA forming about 90% 1,2-intrastrand crosslink, preferentially to two N^7-guanine (Figure 1.6) sites.[32,33] This

adjacent crosslink causes severe distortion to the DNA double helix by introducing significant disruptions in the DNA base stacking to accommodate the coordination requirements of the square planar platinum(II) atom. This distortion causes a degree of unwinding and significant bending from the site of attachment[32-34] and is believed to be responsible for the prevention of DNA transcription. Although cisplatin has also been found to be able to form interstrand crosslinks in the DNA duplex, its cytotoxicity[34] has been widely accepted to result primarily from its formation of intrastrand crosslinks in DNA.

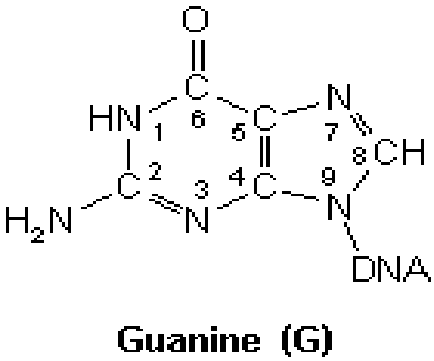

Guanine (G)

Figure 1.6 DNA nucleic acid residue — Guanine

Although cisplatin is a very effective drug for cancer chemotherapy, there are restrictions in cisplatin's clinical use due to cumulative drug resistance and toxic effects. Due to these limitations, an active new area of cisplatin analog[35-41] research has developed. Today, cisplatin analogs containing DACH[39,40] (diaminocyclohexane) and the CBDCA[41,42] (cyclobutanecarboxylato) ligand have been developed. Some platinum^{IV} complexes have been designed and show potential for oral adminstration.[35,43]

Recent work has shown that many mono- and bimetallic complexes of the platinum group metals incorporating planar aromatic ligands with extended π-systems can interact with DNA.[28a, 44-52] Studies on several polypyridyl compounds of the ruthenium, osmium,

cobalt, nickel, rhodium and platinum indicate that these complexes bind to DNA, often in an intercalative fashion. Barton et al have demonstrated that $[Ru((bpy)_2(dppz)]^{2+}$, $[Ru(phen)_2(dppz)]^{2+}$, and $[Os(phen)_2(dppz)]^{2+}$ show enhanced photoluminescence in the presence of DNA (phen =1,10-phenathroline; dppz = dipyrido[3,2-a:2',3'-c]phenazine).[44] They attribute this to the intercalation of the dppz ligand into the DNA double helix. Murphy and co-workers have demonstrated that bimetallic complexes of ruthenium can interact with DNA. Studies on the ruthenium bimetallic complex $\{[(NH_3)_4Ru]_2(dpb)\}^{4+}$ indicate that the planar dpb bridging ligand intercalates into DNA.[51]

Agarose gel electrophoresis experiment for DNA binding study

The DNA binding study of Ru-Pt bimetallic complexes is performed by non-denaturing agarose gel electrophoresis. Gel electrophoresis[53] is an important molecular biology tool. It could be used along with other methods to study DNA, the site of an insertion or deletion, or the presence of a point mutation, and to assess the quality and quantity of DNA present in a sample etc.

Gel electrophoresis is a method for separating chemical compounds based on their size and charge. Gel electrophoresis of DNA can be carried out in agarose, polyacrylamide, or agarose-acrylamide composite gels. The most common method allows the separation of the duplex DNA fragments at neutral pH values, which is called the non-denaturing gel electrophoresis. Denaturing agarose gels are used for the analysis of single-stranded DNA fragments. Since in this project only nondenaturing gel electrophoresis is used, only non-denaturing gel agarose system is discussed here.

In the electrophoresis experiments, the DNA duplex fragments are placed in wells in solidified agarose gel and subjected to an electrical field. Under these conditions the DNA is negatively charged so fragments that are loaded into a sample well at the cathode

(-) end of a gel move through the gel toward the anode (+). The electrophoretic mobility of DNA fragments is dependent on its size, shape and the overall charge. Longer or larger molecules have difficulty traveling through the gel; they become entangled in the gel matrix. Shorter or smaller molecules migrate through the agarose matrix faster and thus travel farther in a given time period. Similar sized fragments travel at relatively the same speed and form a tight "band" when stained. More negatively charged DNA fragments move faster through the gel than the less negatively charged fragments.

The DNA gels used in these experiments are made of agarose, a highly purified agar, which is heated and dissolved in a buffer solution. The agarose molecules form a matrix with pores. The more concentrated the agarose, the smaller the pores. Agarose gels can be used to analyze double-stranded DNA fragments from 70-base-pairs(bp) (3% agarose gel, w/v) to 800,000 bp (0.1% agarose gel).[54] In this project 0.8% agarose gel is used because our cut plasmid DNA is approximately 3000 in length.
DNA is colorless in the visible region and must be stained for visualization. It can be stained with either fluorescent or chemical dyes.[53] In this research ethidium bromide, an ultraviolet (UV) fluorescent stain, is used because it shows very small amounts of DNA and is fast to use. Its fluorescence is much higher when intercalated into the DNA double helix. The disadvantage of it is that it is a carcinogen. One alternative to the ethidium bromide is methylene blue, a chemical dye, which binds to DNA.

Goal of this project

Based on the previous DNA-binding study in the Brewer group, the goal of this project is to design a new kind of supramolecular structural motif using a tpy ligand and adding a phosphine ligand to the remote metal center. These systems will be modular in design and able to bind to DNA. The motif of these complexes can be represented as TAG-LA-BL-BAS (TAG = NMR active phosphine ligand, LA = light absorber, BL = bridging

ligand and BAS = bioactive sites). The TAG will provide a NMR probe for the characterization of supramolecular complexes as well as for the future investigation of the metal complex–DNA interaction process. In this project the phosphine ligand PEt_2Ph was selected as the TAG due its ability to provide an easy ^{31}P NMR probe. The LA represents the light absorber which could be photoexcited by photons of proper energy; here we use a $Ru^{II}(tpy)(PEt_2Ph)(BL)$ chromophore. The bridging ligands used here are bidentate polyazine ligands that can connect two metal centers together in a polymetallic system and have a low energy π^* orbital. The BAS represents the bioactive site for binding to DNA and the cis-$Pt^{II}Cl_2$ moiety is chosen as the BAS based on the previous studies of cisplatin.

Chapter 2: Experimental

Material

All chemicals were obtained from Aldrich Chemical Co. and used as received unless otherwise noted. HPLC grade acetonitrile was obtained from Baxter Scientific. The supporting electrolyte for the electrochemistry was tetrabutalammonium hexafluorophosphate, prepared by the metathesis of tetrabutalammonium bromide with potassium hexafluorophosphate, recrystallized twice from ethanol, dried under vacuum, and stored in a vacuum desiccator. Adsorption alumina (80-200 mesh) was obtained from Fisher Scientific. $TlPF_6$ was obtained from Strem Chemicals. PEt_2Ph and cis-$[Pt(NH_3)_2Cl_2]$ (cisplatin) were obtained from Aldrich Chemical Co. Bacteriophage lambda DNA was obtained from Pharmacia. The plasmid, pBluescript KS+, was obtained from Stratagene, and all materials used in amplification and purification of plasmid DNA were purchased from Fisher. Electrophoresis-grade low EEO agarose, tris(hydroxymethyl)-aminomethane(Tris), boric acid and ethidium bromide were also obtained from Fisher. *EcoRI* and *HindIII* restriction endonucleases were purchased from Promega. $[Ru(tpy)Cl_3]$[55] (tpy = 2,2':6',6''-terpyridine), $[Ru(tpy)(Cl)(dpp)](PF_6)$[56], and $Pt(dmso)_2Cl_2$[19b,22a,57] were prepared as previously reported.

Synthesis

Column Chromatography

Purification of the ruthenium precursor complexes was achieved by chromatography on Fisher adsorption alumina, Al_2O_3. Other forms of alumina may be too active and not release the desired products. Typically a 8 ~ 10 cm column (3.2 cm in diameter) was

prepared by filling the glass column with the 3:2 (V/V) toluene/acetonitrile eluent and adding solid Al_2O_3 with the eluent flowing. This ensures tight packing of the solid phase. The crude product was then dissolved in a minimal amount (ca. 20 mL) of the same eluent and filtered to remove insoluble materials. The product solution was carefully added onto the solid Al_2O_3 support and eluted with the same 3:2 toluene/acetonitrile mixture. The products are colored, thus visual inspection of each column dictates product band collection.

Synthesis of [(tpy)RuCl(bpm)](PF$_6$)

Ru(tpy)Cl_3 (0.43 g, 1.0 mmol), 2,2'-bipyrimidine (0.24 g, 1.5 mmol) and triethylamine (4.0 mL, 29 mmol) were heated at reflux in 40 mL 2:1 (V/V) ethanol/water for 5 hours. The reaction mixture was added into 10 mL of saturated KPF_6 aqueous solution to induce the precipitation of the crude dark product. The solvent was removed by vacuum filtration. Purification was achieved using alumina chromatography with 3:2 toluene/acetonitrile as eluting solvent. The first, red product band was collected and the solvent was removed by rotary evaporation. The product was then dissolved in ca. 20 mL acetonitrile and flash-precipitated in ca. 200 mL diethyl ether. The product was collected by vacuum filtration and dried under vacuum. Yield: 0.45 g, 0.67 mmol, 67%. ^{1}H NMR: 10.04(dd), 9.29(dd), 8.72(dd), 8.50(d), 8.38(d), 8.14(t), 8.05(dd), 7.92(m), 7.75(d), 7.68(dd), 7.29(m) and 7.06(dd). ^{31}P NMR: -143.26(m). $E_{1/2}$ (V vs. Ag/AgCl): +1.01, -1.15, -1.56. λ_{max}^{abs} = 516 nm. The FAB MS data are summarized in Table 2.1.

Table 2.1 FAB Mass spectral data for $[(tpy)RuCl(bpm)](PF_6)$[a,b]

m/z	rel. abund	assignment
528	100	$[(tpy)Ru(Cl)(bpm)]^+$
492	14	$[(tpy)Ru(bpm)]^+$
460	24	$[(tpy)Ru(CH_3CN)_3]^+$
370	19	$[(tpy)Ru(Cl)]^+$
334	31	$[Ru(tpy)]^+$

[a] tpy = 2,2':6',6''-terpyridine and bpm = 2,2'-bipyrimidine.

[b] See Appendix 1 (Page 95) for the spectrum.

Synthesis of $[(tpy)Ru(CH_3CN)(bpm)](PF_6)_2$

$[Ru(tpy)Cl(bpm)](PF_6)$ (0.67 g, 1.0 mmol) and $TlPF_6$ (0.70 g, 2.0 mmol) were heated at reflux in 100 mL 1:1 (V/V) acetonitrile/water under argon in the dark for 24 hours. The solvent was removed by rotary evaporation. The yellow solid was dissolved in minimal acetonitrile (ca. 20 mL) and TlCl was removed by vacuum filtration. Purification was achieved using alumina chromatography with 3:2 toluene/acetonitrile as eluting agent. The product eluted as the second, yellow product band proceeded by a red band. After collecting the yellow band the solvent was removed by rotary evaporation. The yellow product was dissolved in ca. 20 mL acetonitrile and flash precipitated in ca. 200 mL diethyl ether, collected by vacuum filtration and dried under vacuum. Yield: 0.78 g, 0.95 mmol, 95%. ^{1}H NMR: 9.84(dd), 9.38(dd), 8.84(dd), 8.57(d), 8.43(d), 8.34(t), 8.08(dd), 8.04(m), 7.81(d), 7.62(dd), 7.37(m), 7.21(dd), 2.10(s). ^{31}P NMR: -143.38(m). $E_{1/2}$ (V vs. Ag/AgCl): +1.55, -1.06, -1.42. λ_{max}^{abs} = 452 nm. The FAB MS data are summarized in Table 2.2.

Table 2.2 FAB Mass spectral data for $[(tpy)Ru(CH_3CN)(bpm)](PF_6)_2$[a,b]

m/z	rel. abund.	assignment
679	19	$[(tpy)Ru(CH_3CN)(bpm)](PF_6)^+$
533	16	$[(tpy)Ru(CH_3CN)(bpm)]^+$
512	100	$[(tpy)Ru(bpm)F]^+$
492	82	$[(tpy)Ru(bpm)]^+$
334	79	$[Ru(tpy)]^+$

[a] tpy = 2,2':6',6''-terpyridine and bpm = 2,2'-bipyrimidine.

[b] See Appendix 2 (Page 96) for the spectrum.

Synthesis of $[(tpy)Ru(PEt_2Ph)(bpm)](PF_6)_2$

$[Ru(tpy)Cl(bpm)](PF_6)$ (0.67 g, 1.0 mmol) and $TlPF_6$ (0.70 g, 2.0 mmol) were heated at reflux in 30 mL 1:1(V/V) ethanol/water under argon in the dark for 32 hours. After 1 hour, the addition of PEt_2Ph was begun, 180 *u*L (1.0 mmol) of PEt_2Ph was added five times at 6-hour increments while the reaction was heated at reflux under argon. The reaction mixture was added into 15 mL of saturated KPF_6 aqueous solution to induce the precipitation and allowed to sit it in the hood for 2 hours to cool to room temperature. The solvent was removed by rotary evaporation. The yellow solid was then dissolved in minimal acetonitrile (ca. 20 mL) and TlCl precipitate was removed by vacuum filtration. Purification was achieved using alumina chromatography with 3:2 toluene/acetonitrile as eluting solvent. The first band to elute was red and discarded. The second, yellow product band was collected and the solvent was removed by rotary evaporation. The product was dissolved in 20 mL acetonitrile, flash precipitated in 200 mL diethyl ether, collected by vacuum filtration and dried under vacuum. Yield: 0.72 g, 0.75 mmol, 75%. ^1H NMR: 9.75(dd), 9.35(dd), 8.91(t), 8.25(d), 8.19(d), 8.07(dd), 8.03(m), 7.87(d), 7.36(m), 7.27(t),

7.24(dd), 7.03(m), 6.35(m), 1.88(m), 1.75(m), 0.85(p). ^{31}P NMR: -143.26(m), 32.21(s). $E_{1/2}$ (V vs. Ag/AgCl): +1.56, -1.03, -1.38. λ_{max}^{abs} = 450 nm. The FAB MS data are summarized in Table 2.3.

Table 2.3 FAB Mass spectral data for $[(tpy)Ru(PEt_2Ph)(bpm)](PF_6)_2$[a,b]

m/z	rel. abund.	assignment
804	32	$[(tpy)Ru(PEt_2Ph)(bpm)](PF_6)^+$
679	39	$[(tpy)Ru(PEt_2Ph)(bpm)(HF)]^+$
659	14	$[(tpy)Ru(PEt_2Ph)(bpm)]^+$
512	61	$[(tpy)Ru(bpm)F]^+$
492	100	$[(tpy)Ru(bpm)]^+$

[a] tpy = 2,2':6',6''-terpyridine and bpm = 2,2'-bipyrimidine.

[b] See the Appendix 3 (Page 97) for the spectrum.

Synthesis of $[(tpy)Ru(PEt_2Ph)(bpm)PtCl_2](PF_6)_2$

Due to the labile nature of the Pt^{II}-Cl bonds, this product is not stable under typical alumina chromatographic procedures. Thus a synthesis had to be designed to produce a pure product without alumina chromatography. $[(tpy)Ru(PEt_2Ph)(bpm)](PF_6)_2$ (0.19 g, 0.20 mmol) and $Pt(dmso)_2Cl_2$ (0.11 g, 0.25 mmol) were heated at reflux in 140 mL ethanol under argon for 4 hours. The dark product was collected by vacuum filtration and washed with 700 mL hot ethanol followed by 700 mL diethyl ether. The solid was dissolved in minimal acetonitrile (ca. 20 mL) and the unreacted $Pt(dmso)_2Cl_2$ was removed by vacuum filtration. The solvent was removed by rotary evaporation. The dark green product was dissolved in ca.10 mL acetonitrile and flash precipitated in ca. 100 mL diethyl ether. The dark green product was collected by vacuum filtration and dried under vacuum. Yield: 0.15 g , 0.13 mmol, 62%. ^{1}H NMR: 9.92(d), 9.81(d), 9.33(dd), 8.36(t),

8.26(d), 8.19(d), 8.16(d), 8.10(d), 8.06(q), 7.58(m), 7.42(dd), 7.30(t), 7.03(t), 6.35(t), 1.90(m),1.81(m) and 0.90(p). ^{31}P NMR: -143.98(m), 33.30(s). $E_{1/2}$ (V vs. Ag/AgCl): +1.63, +1.82, -0.34, -1.04, -1.45. λ_{max}^{abs} = 416 nm. The FAB MS data are summarized in Table 2.4.

Table 2.4 FAB Mass spectral data for $[(tpy)Ru(PEt_2Ph)(bpm)PtCl_2](PF_6)_2$.[a,b]

m/z	rel. abund.	assignment
1070	41	$[(tpy)Ru(PEt_2Ph)(bpm)PtCl_2](PF_6)^+$
998	18	$[(tpy)Ru(PEt_2Ph)(bpm)Pt](PF_6)^+$
925	100	$[(tpy)Ru(PEt_2Ph)(bpm)PtCl_2]^+$
805	66	$[(tpy)Ru(PEt_2Ph)(bpm)](PF_6)^+$
760	40	$[(tpy)Ru(bpm)PtCl_2]^+$
722	87	$[(tpy)Ru(bpm)PtCl]^+$
685	79	$[(tpy)Ru(bpm)Pt]^+$
658	60	$[(tpy)Ru(PEt_2Ph)(bpm)]^+$

[a] tpy = 2,2':6',6''-terpyridine and bpm = 2,2'-bipyrimidine.

[b] See Appendix 4 (Page 98) for the spectrum

Synthesis of $[(tpy)Ru(CH_3CN)(dpp)](PF_6)_2$

$[Ru(tpy)Cl(dpp)](PF_6)$ (0.75 g, 1.0 mmol) and $TlPF_6$ (0.70 g, 2.0 mmol) were heated at reflux in 100 mL 1:1(V/V) acetonitrile/water under argon in the dark for 24 hours. The solvent was removed by rotary evaporation. The solid was dissolved in a minimal amount of acetonitrile and TlCl was removed by vacuum filtration. Purification was achieved using alumina chromatography with 3:2 toluene/acetonitrile as the eluting solvent. The first band to elute was red and discarded. The second, yellow product band was the

desired product and was collected. The solvent was removed by rotary evaporation. The product was dissolved in ca. 20 mL acetonitrile and flash precipitated in ca. 200 mL diethyl ether, collected by vacuum filtration and dried under vacuum. Yield: 0.86 g, 0.96 mmol, 96%. ^{31}P NMR: -144.003(m). λ_{max}^{abs} = 464 nm.The FAB MS data are summarized in Table 2.5.

Table 2.5 FAB Mass spectral data for $[(tpy)Ru(CH_3CN)(dpp)](PF_6)_2$.[a,b]

m/z	rel. abund.	assignment
753	12	$[(tpy)Ru(CH_3CN)(dpp)](PF_6)^+$
608	13	$[(tpy)Ru(CH_3CN)(dpp)]^+$
588	15	$[(tpy)Ru(dpp)(HF)]^+$
568	29	$[(tpy)Ru(dpp)]^+$
460	100	$[(tpy)Ru(CH_3CN)_3]^+$
334	23	$[Ru(tpy)]^+$

[a] tpy = 2,2':6',6''-terpyridine and dpp = 2,3-bis(2-pyridyl)pyrazine.

[b] See Appendix 5 (Page 99) for the spectrum.

Synthesis of $[(tpy)Ru(PEt_2Ph)(dpp)](PF_6)_2$

$[Ru(tpy)Cl(dpp)](PF_6)$ (0.75 g, 1.0 mmol) and $TlPF_6$ (0.70 g, 2.0 mmol) were heated at reflux in 30 mL 1:1 (V/V) ethanol/water under argon for 32 hours. After 1 hour, the addition of PEt_2Ph was begun, 180 *u*L(1.0 mmol) of PEt_2Ph was added five times at 6-hour increments while the reaction was heated at reflux under argon. The reaction mixture was added into 15 mL of saturated KPF_6 aqueous solution to induce precipitation and allowed to sit in the hood for 2 hours to cool to room temperature. The solvent was

removed by rotary evaporation. The yellow solid was dissolved in ca. 20 mL acetonitrile and TlCl was removed by vacuum filtration. The purification was achieved using alumina chromatography with 3:2 toluene/acetonitrile as eluting solvent. The first band to elute was red and discarded. The second, yellow product band was collected and the solvent was removed by rotary evaporation. The product was dissolved in ca. 20 mL acetonitrile and flash precipitated in ca. 200 mL diethyl ether, collected by vacuum filtration and dried under vacuum. Yield: 0.77 g, 0.75 mmol, 75%. ^{31}P NMR: -143.04(m), 30.62(s), 32.18(s). $E_{1/2}$ (V vs. Ag/AgCl): +1.57, -1.05, -1.42. λ_{max}^{abs} = 460 nm. The FAB MS data are summarized in Table 2.6.

Table 2.6 FAB Mass spectral data for $[(tpy)Ru(PEt_2Ph)(dpp)](PF_6)_2$.[a,b]

m/z	rel. abund.	assignment
880	31	$[(tpy)Ru(PEt_2Ph)(dpp)](PF_6)^+$
734	16	$[(tpy)Ru(PEt_2Ph)(dpp)]^+$
568	94	$[(tpy)Ru(dpp)]^+$
334	100	$[Ru(tpy)]^+$

[a] tpy = 2,2':6',6''-terpyridine and dpp = 2,3-bis(2-pyridyl)pyrazine.

[b] See Appendix 6 (Page 100) for the spectrum

Synthesis of $[(tpy)Ru(PEt_2Ph)(dpp)PtCl_2](PF_6)_2$.

Similar to $[(tpy)Ru(PEt_2Ph)(bpm)PtCl_2](PF_6)_2$, this product is not stable under typical alumina chromatographic procedures due to the labile nature of the Pt^{II}-Cl bonds. Therefore this product was also synthesized using the method that did not involve alumina chromatography. $[(tpy)Ru(PEt_2Ph)(dpp)](PF_6)_2$ (0.21 g, 0.20 mmol) and $Pt(dmso)_2Cl_2$ (0.11 g, 0.25 mmol) were heated at reflux in 140 mL ethanol under argon

for 4 hours. The dark product was collected by vacuum filtration and washed by 700 mL hot ethanol followed by 700 mL diethyl ether. The solid was dissolved in minimal acetonitrile (ca. 20 mL) and the unreacted $Pt(dmso)_2Cl_2$ was removed by vacuum filtration. The solvent was removed by rotary evaporation. The light red product was dissolved in 10 mL acetonitrile and flash-precipitated in 100 mL diethyl ether. The light red product was collected by vacuum filtration and dried under vacuum. Yield: 0.14 g, 0.11 mmol, 55%. ^{31}P NMR: -143.30(m), 29.76(s), 32.12(s). $E_{1/2}$ (V vs. Ag/AgCl): +1.55, +1.70, -0.50, -1.15, -1.40. λ_{max}^{abs} = 506 nm. The FAB MS data are summarized in Table 2.7.

Table 2.7 FAB Mass spectral data for $[(tpy)Ru(PEt_2Ph)(dpp)PtCl_2](PF_6)_2$[a,b]

m/z	rel. abund.	assignment
1146	6	$[(tpy)Ru(PEt_2Ph)(dpp)PtCl_2](PF_6)^+$
1001	21	$[(tpy)Ru(PEt_2Ph)(dpp)PtCl_2]^+$
835	12	$[(tpy)Ru(dpp)PtCl_2]^+$
798	17	$[(tpy)Ru(dpp)PtCl]^+$
763	11	$[(tpy)Ru(dpp)Pt]^+$
603	15	$[(tpy)Ru(dpp)Cl]^+$
568	47	$[(tpy)Ru(dpp)]^+$
500	55	$[(tpy)Ru(PEt_2Ph)]^+$

[a] tpy = 2,2':6',6''-terpyridine and dpp = 2,3-bis(2-pyridyl)pyrazine.

[b] See Appendix 7 (Page 101) for the spectrum.

Method

Preparation and Purification of Plasmid DNA

Plasmid DNA was prepared by Matt Milkevtich.[58] The plasmid, pBluescript, was amplified and purified from *Escherichia coli* strain JM109 according to established protocols[59]. Plasmids were isolated using an alkaline lysis procedure, purified in a cesium chloride gradient, and then extensively dialyzed against TE [10 mM Tris(tris(hydroxymethyl)aminomethane), 1 mM EDTA, pH 7.5]. Following concentration by ethanol precipitation, the DNA was stored in TE at 4 ^{o}C. Plasmid DNA was linearized by overnight incubation at 37 ^{o}C with EcoRI endonuclease. Typically, 200 ug of plasmid DNA was combined with *EcoRI* (3 *u*L, 240 U) and 20 *u*L of 10X buffer in a total volume of 200 *u*L. Protein was removed by extracting with phenol/0.1% hydroxyquinoline (equilibriated with TE pH 8) and 24:1 chloroform /isoamyl alcohol. The DNA was then precipitated with NaCl and ethanol, resuspended in deionized water, and stored at 4 ^{o}C.

Preparation of Molecular Weight Standards

Molecular weight standards for non-denaturing agarose gel electrophoresis were prepared by digestion of bacteriophage lambda DNA with *HindIII* endonuclease. Lambda DNA (50 ug, 100 uL of 500 ug/mL stock solution) was combined with Hind*III* (2 uL, 160 U) in 258 uL of H_2O buffered with 10X buffer (40 uL) and incubated for 12 hours at 37 ^{o}C. Upon completion, 100 uL of 6X type III dye was added and the solution was stored at 4 ^{o}C.

Reactions of Metal Complexes with Plasmid DNA

The concentration of the linearized plasmid DNA solution was determined spectrophotometrically[60]. Concentrations of metal solutions were determined using the known extinction coefficients for $[(tpy)Ru(PEt_2Ph)(bpm)PtCl_2](PF_6)_2$

($\varepsilon = 0.58 \times 10^4\ M^{-1}cm^{-1}$ at 560 nm), [(tpy)Ru(PEt_2Ph)(dpp)$PtCl_2$]$(PF_6)_2$ ($\varepsilon = 1.47 \times 10^4\ M^{-1}cm^{-1}$ at 506 nm), [(tpy)RuCl(dpp)$PtCl_2$](PF_6)[61] ($\varepsilon = 1.33 \times 10^4\ M^{-1}cm^{-1}$ at 548 nm) and [Ru$(bpy)_2$(dpq)$PtCl_2$]$(CF_3SO_3)_2$ ($\varepsilon = 8.10 \times 10^3\ M^{-1}cm^{-1}$ at 582 nm)[58]. All reactions contained 1 ug of linearized plasmid DNA and 10 mM sodium phosphate, pH 7 in a total volume of 100 uL. The samples were analyzed by electrophoresis in 300 mL agarose gels (0.8% agarose, 89 mM Tris, 89 mM boric acid, PH 8) at 104 V for 1.5 hours, with recirculation of the buffer. Gels were then stained in 0.5 ug/mL ethidium bromide for 1 hour and photographed with UV illumination. Polaroid prints were scanned using a MicroTek ScanMaker E_6.

NMR Spectroscopy

^{1}H NMR spectra were obtained on a JOEL 500 MHz instrument while ^{31}P NMR spectra were obtained on a Bruker 360 MHz instrument. All spectra were obtained at room temperature using CD_3CN as the solvent and trimethylsilane as a ^{1}H chemical shift internal standard unless otherwise indicated. The sample was prepared by dissolving 25 mg of the compound into 6 mL dry CD_3CN and the solution was then transferred to the 7-inch NMR tube.

FAB-Mass Spectrometry

FAB Mass spectral analysis was conducted on a Fisons VG Quattro triple-stage quadrupole mass spectrophotometer using m-nitrobenzyl alcohol as the matrix. CH_3CN was added to improve the solubility of the samples.

Electrochemistry

A Bioanalytical Systems, Inc. 100W electrochemical analyzer was used to record the cyclic voltammograms. The supporting electrolyte was 0.1 M Bu_4NPF_6 and the measurements were made in Burdick and Jackson UV-grade acetonitrile. The three-electrode system uses a 1.9 mm diameter platinum disk working electrode, a platinum wire auxiliary electrode, and a Ag/AgCl reference electrode (0.29 V vs. NHE). The Ag/AgCl reference electrode was calibrated against the $FeCp_2/FeCp_2^+$ couple which was assumed to be 0.665 V vs. NHE in 0.1 M Bu_4NPF_6 in acetonitrile[62].

Electronic absorption spectroscopy

Spectra were recorded at room temperature using a Hewlett Packard 8452 diode array spectrophotometer with a 2 nm resolution and a range from 190 to 820 nm, interfaced to an IBM compatible computer. The solvent was Burdick and Jackson UV-grade acetonitrile. The cuvette was a 1 cm pathlength cell with quartz windows. The sample compounds were dissolved into CH_3CN to give a spectrum with absorbance of the largest peak between 0.5 to 1.0.

Chapter 3: Results and Discussion

Ru-Pt bimetallic complex containing A-A type bridging ligand bpm

Synthesis

The Ru-Pt bimetallic complex $[(tpy)Ru(PEt_2Ph)(bpm)PtCl_2](PF_6)_2$ with a bpm bridging ligand and a NMR tag ligand, PEt_2Ph, on the ruthenium metal center is a unique structural type and no previous synthetic method has been reported. Many of the synthetic precursors to the desired Ru-Pt bimetallic complex are also new compounds. Our synthesis follows a building block approach where the complex was assembled step by step by sequentially adding a component building block. The introduction of the phosphorous ligand was achieved by extraction of the chloride ligand with $TlPF_6$ followed by the addition of the phosphorous ligand. The synthetic scheme is shown in Figure 3.1. By taking this step by step approach, the exact nature of each component can be chosen. The use of $TlPF_6$ in the PEt_2Ph introduction step generates a vacancy in the remote metal coordination sphere. The PEt_2Ph ligand is added into the reaction mixture five times to avoid the decomposition of the PEt_2Ph ligand prior to binding. This method greatly improved the reaction yield over a single PEt_2Ph addition.

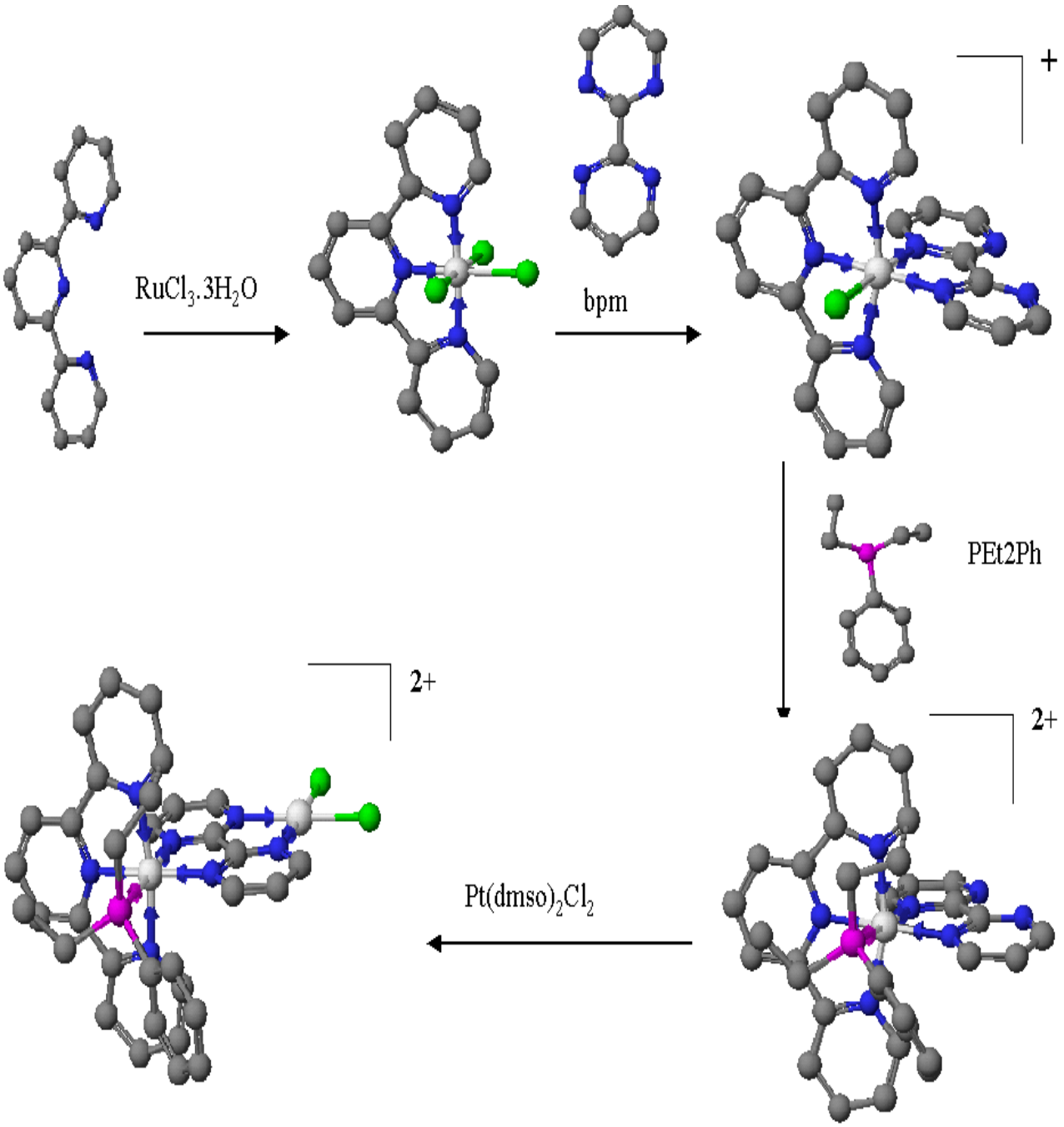

Figure 3.1 Synthetic scheme for the preparation of $[(tpy)Ru(PEt_2Ph)(bpm)PtCl_2](PF_6)_2$.

FAB MS Spectra

The MS spectra for complexes [(tpy)RuCl(bpm)](PF_6), [(tpy)Ru(CH_3CN)(bpm)](PF_6)$_2$, [(tpy)Ru(PEt_2Ph)(bpm)](PF_6)$_2$ and [(tpy)Ru(PEt_2Ph)(bpm)$PtCl_2$](PF_6)$_2$ are included in Appendixces1~4 (Page 95~98). These complexes give quite good FAB MS data with parent ions appearing and fragmentation by ligand and/or metal loss observable. All the spectra show the [M-PF_6]$^+$ peak and the latter three also show the [M-2PF_6]$^+$ peak.

The [(tpy)RuCl(bpm)](PF_6) spectrum shows five major groups of peaks (Table 2.1 at page 17 and Appendix 1 at page 95). The peak at 528(*m/z*) is assigned as the [(tpy)RuCl(bpm)]$^+$. The loss of a chlorine atom from the former yields [(tpy)Ru(bpm)]$^+$ giving rise to the peak at 492(*m/z*). Since the spectrum was obtained with CH_3CN in the matrix, the peak at 460(*m/z*) is assigned as the species [(tpy)Ru(CH_3CN)$_3$]$^+$. The remaining two peaks at 370(*m/z*) and 334(*m/z*) could be easily assigned respectively as the species [(tpy)RuCl]$^+$ and [Ru(tpy)]$^+$.

The [(tpy)Ru(CH_3CN)(bpm)](PF_6)$_2$ spectrum also shows five major groups of peaks (Table 2.2 at 18 and Appendix 2 at page 96). The [M-PF_6]$^+$ peak shows at 679(*m/z*). Because there are two counter ions in this complex, the [M-2PF_6]$^+$ peak is observed at 533(*m/z*). The appearance of these peaks provides a proof of structure. The peak at 512(*m/z*) is assigned as the [(tpy)Ru(bpm)F]$^+$. Also the species [(tpy)Ru(bpm)]$^+$ and [Ru(tpy)]$^+$ are observed at 492(*m/z*) and 334(*m/z*) respectively, consistent with the location of the corresponding peaks in the [(tpy)RuCl(bpm)](PF_6) complex.

The FAB MS spectrum of the complex [(tpy)Ru(PEt_2Ph)(bpm)](PF_6)$_2$ (Table 2.3 at page 19 and Appendix 3 at page 97) shows the expected pattern. The [M-PF_6]$^+$ peak and the [M-2PF_6]$^+$ peak are observed at 804(*m/z*) and 659(*m/z*) respectively. The peak at 679(*m/z*) is for the species [(tpy)Ru(bpm)(HF)]$^+$. It comes from [(tpy)Ru(PEt_2Ph)(bpm)](PF_6)$^+$ with the loss of PF_5. Also the peak at 492(*m/z*) is assigned as the species [(tpy)Ru(bpm)]$^+$ which comes from the [M-2PF_6]$^+$ with the further loss of the phosphine ligand.

The FAB MS spectrum for the Ru-Pt bimetallic complex looks much more complicated than the monometallic complexes (Table 2.4 at page 20 and Appendix 4 at page 98), but the characteristic peaks, ion $[M\text{-}PF_6]^+$ and $[M\text{-}2PF_6]^+$ can be clearly observed at 1070(*m/z*) and 925(*m/z*). With continuous loss of the other components like the chlorine atom, the platinum atom and the phosphine ligand, a series of charged species are observed at 998(*m/z*), 805(*m/z*), 760(*m/z*), 722(*m/z*), 685(*m/z*) and 658(*m/z*). Their assignments are listed in Table 2.4. These high mass/charge ratio peaks along with the characteristic fragmentation by ligand and metal loss is consistent with the proposed structure.

Electrochemistry

The electrochemical data for $[(tpy)RuCl(bpm)](PF_6)$, $[(tpy)Ru(CH_3CN)(bpm)](PF_6)_2$, $[(tpy)Ru(PEt_2Ph)(bpm)](PF_6)_2$ and $[(tpy)Ru(PEt_2Ph)(bpm)PtCl_2](PF_6)_2$ have been studied. The electrochemical behavior of these complexes is characterized by reversible metal based oxidation and ligand based reductions with bpm reduction prior to tpy due to the lower energy π^* on the bpm realtive to tpy. The specific interpretations of the electrochemical data for each complex are described below.

$[(tpy)RuCl(bpm)](PF_6)$

In $[(tpy)RuCl(bpm)]^+$(Figure 3.2), the oxidation occurring at +1.01 V is assigned as the $Ru^{II/III}$ couple, the first reduction at –1.15 V is assigned as the $bpm^{0/-}$ couple, and the second reduction at –1.56 V is assigned as the $tpy^{0/-}$ couple. The $bpm^{0/-}$ couple occurs prior to the $tpy^{0/-}$ due to the lower lying π^* orbital on bpm. The ruthenium based oxidation at + 1.01 V is consistent with the chloride ligitation of this metal center.[24a]

This assignment is also consistent with the assignment made in the previously studied [(tpy)RuCl(dpp)]$(PF_6)_2$ containing the dpp bridging ligand where the reduction at –1.54 V is assigned as the $tpy^{0/-}$ couple and the reduction at –1.21 V is assigned as the $dpp^{0/-}$ couple.[56] The terminal ligand $tpy^{0/-}$ couples in these two analogs occur at very similar potentials.

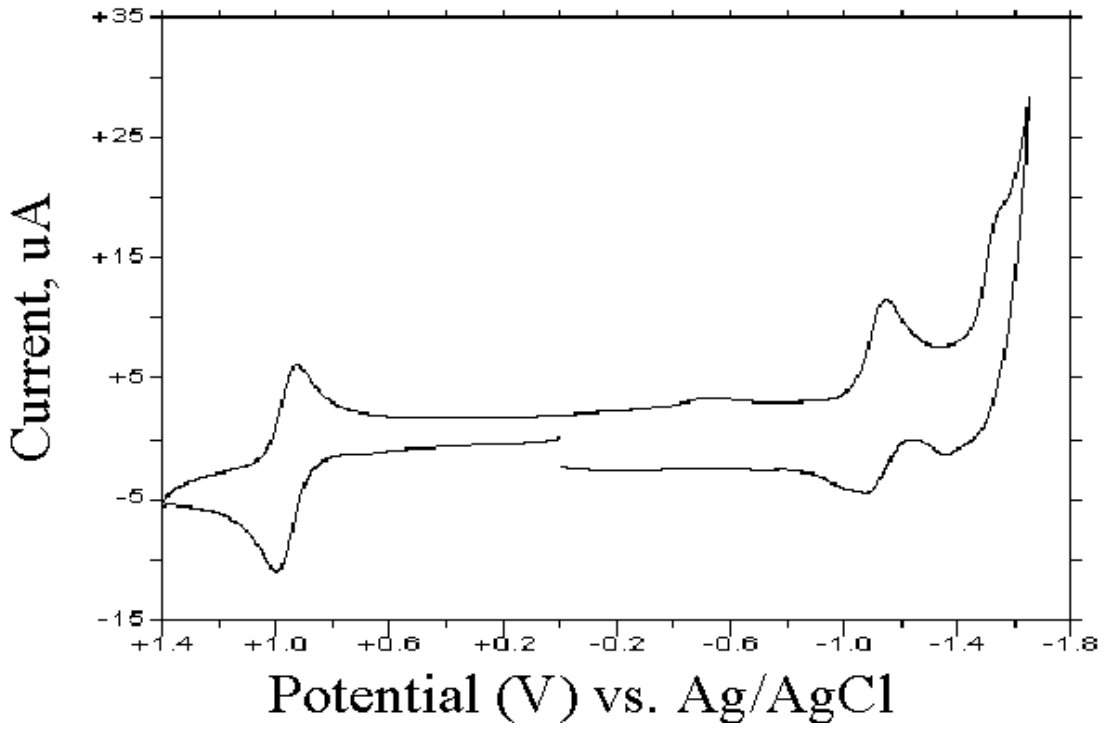

Figure 3.2 Cyclic voltammogram of [(tpy)RuCl(bpm)](PF_6) in 0.1 M Bu_4NPF_6 in CH_3CN (tpy = 2,2':6',6''-terpyridine, bpm = 2,2'-bipyrimidine).

[(tpy)Ru(CH_3CN)(bpm)]$(PF_6)_2$

When the chloride ligand was substituted by CH_3CN to form $[(tpy)Ru(CH_3CN)(bpm)]^{2+}$ (Figure 3.3), both the metal based oxidation and ligand based reductions are shifted to a more positive region with a more substantial shift of the metal based oxidation process.

This is consistent with the chloride substitution. The metal based $Ru^{II/III}$ couple is shifted to +1.55 V from +1.01 V. The bridging ligand reduction $bpm^{0/-}$ couple is shifted much less to –1.06 V from –1.15 V for $[(tpy)Ru(CH_3CN)(bpm)](PF_6)_2$ vs. $[(tpy)RuCl(bpm)](PF_6)_2$. The terminal ligand reduction $tpy^{0/-}$ also experiences a small shift moving to –1.42 V from -1.56 V.

The CH_3CN ligand, compared to chloride ligand, is a poorer σ donor but a much better π acceptor. The coordination of CH_3CN will result in a more electron deficient ruthenium metal center shifting the metal based oxidation to more positive potential. This substitution also shifts slightly the ligand based reductions. This is consistent with the decrease of electron density on the ruthenium metal center accepting more electron density from the other two ligands, bpm and tpy.

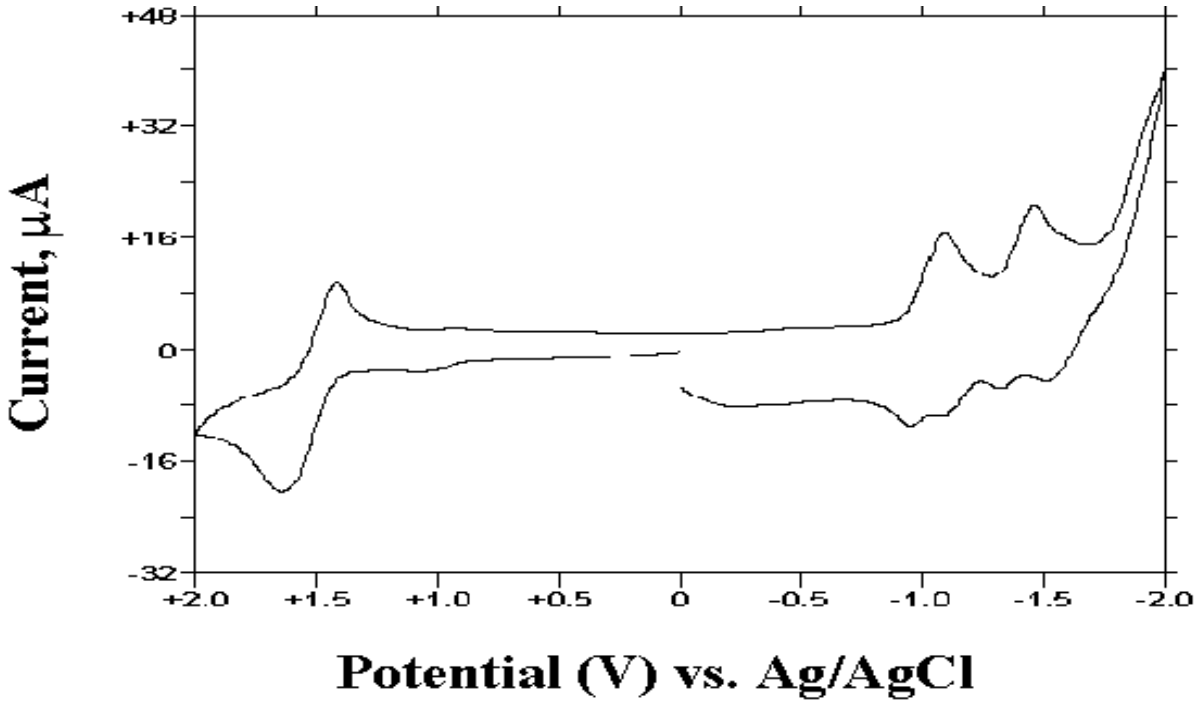

Figure 3.3 Cyclic voltammogram of $[(tpy)Ru(CH_3CN)(bpm)](PF_6)_2$ in 0.1 M

Bu_4NPF_6 in CH_3CN (tpy = 2,2':6',6''-terpyridine, bpm = 2,2'-bipyrimidine)

[(tpy)Ru(PEt_2Ph)(bpm)](PF_6)$_2$

The cyclic voltammogram of the complex [(tpy)Ru(PEt_2Ph)(bpm)](PF_6)$_2$ is shown in Figure 3.4. Upon substitution of the CH_3CN ligand by PEt_2Ph ligand, the metal based oxidation and the ligand based reductions remain almost the same. This is because the CH_3CN ligand and the PEt_2Ph ligand form a very similar coordination bond with the ruthenium metal center. Both ligands are weak σ donors but good π acceptors. There still exists a small difference between these two ligands. The PEt_2Ph ligand coordinates to the ruthenium metal center through the phosphorus atom while the CH_3CN ligand coordinates through the nitrogen atom. The phosphorus is at the third row in the periodical table and its 3d orbital is energetically closer to the ruthenium dπ orbital. This makes the back bonding between the PEt_2Ph ligand and the metal center somewhat stronger, so the ruthenium oxidation shifts slightly to a more positive potential.

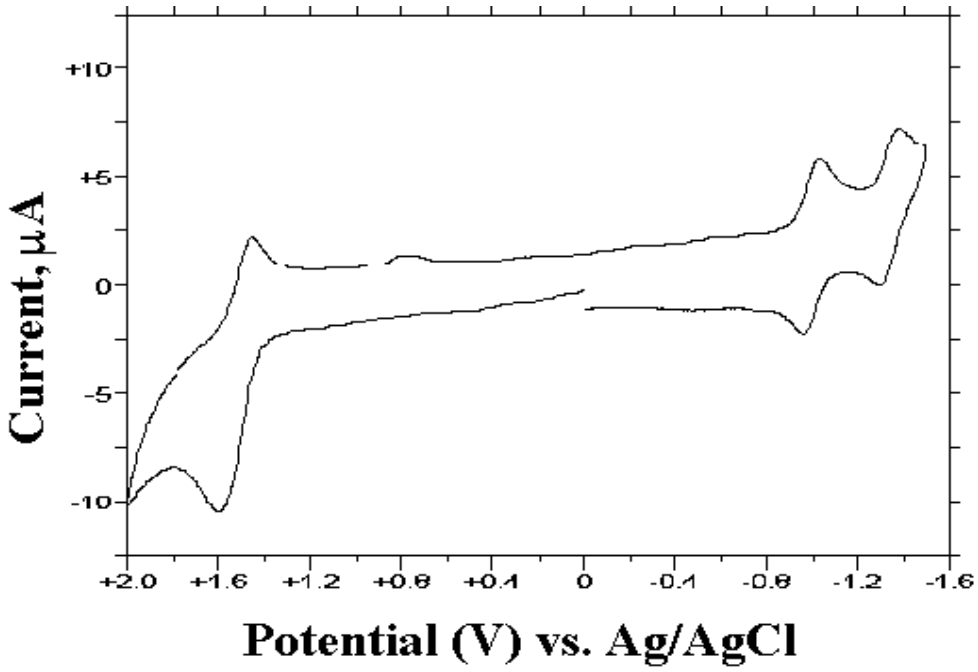

Figure 3.4 Cyclic voltammogram of [(tpy)Ru(PEt_2Ph)(bpm)](PF_6)$_2$ in 0.1 M Bu_4NPF_6 in CH_3CN (tpy = 2,2':6',6''-terpyridine, bpm = 2,2'-bipyrimidine).

$[(tpy)Ru(PEt_2Ph)(bpm)PtCl_2](PF_6)_2$

Upon formation of the bpm-bridged bimetallic complex, the bridging ligand bpm becomes much easier to reduce due to the stabilization of the π^* orbital induced by the coordination of the electron deficient Pt^{II} metal center (Figure 3.5). This is a characteristic of polyazine bridged complexes consistent only with bpm acting in a bridging fashion. In $[(tpy)Ru(PEt_2Ph)(bpm)PtCl_2](PF_6)_2$, the first two reductions are assigned as $bpm^{0/-}$ and $bpm^{-/2-}$ occurring prior to the terminal ligand reduction $tpy^{0/-}$. The first reduction assigned as the $bpm^{0/-}$ is consistent with the assignment made by Rillema et al[19,63] in the bimetallic complex $[(bpy)_2Ru(bpm)Ru(bpy)_2](PF_6)_4$ where peaks at –0.37 V, -1.05 V and –1.50 V were assigned respectively as $bpm^{0/-}$, $bpm^{-/2-}$ and $2bpy^{0/-}$. The presence of the $bpm^{-/2-}$ couple before the reduction of the terminal tpy ligand is indicative of the bimetallic formulation of this complex. Oxidatively, one sees a quasi-reversible oxidation of the ruthenium and an irreversible oxidation of platinum. Compared to the monometallic complex, the $Ru^{II/III}$ couple is shifted from 1.56 V to 1.63 V.

In the complexes $[(bpy)_2Ru(BL)PtCl_2]^{2+}$ where BL = dpq or dpb, similar irreversible platinum oxidations just prior to 1.72 V and 1.61 V were observed.[24a] The irreversible platinum oxidation in our complex appears to occur after the reversible ruthenium oxidation while the two oxidations occurred in reverse order in the $[(bpy)_2Ru(BL)PtCl_2]^{2+}$ complexes. This might result from the change of the bridging ligands that could impact the platinum oxidation potential.

A summary of the electrochemical behavior of these bpm complexes is provided in Table 3.1.

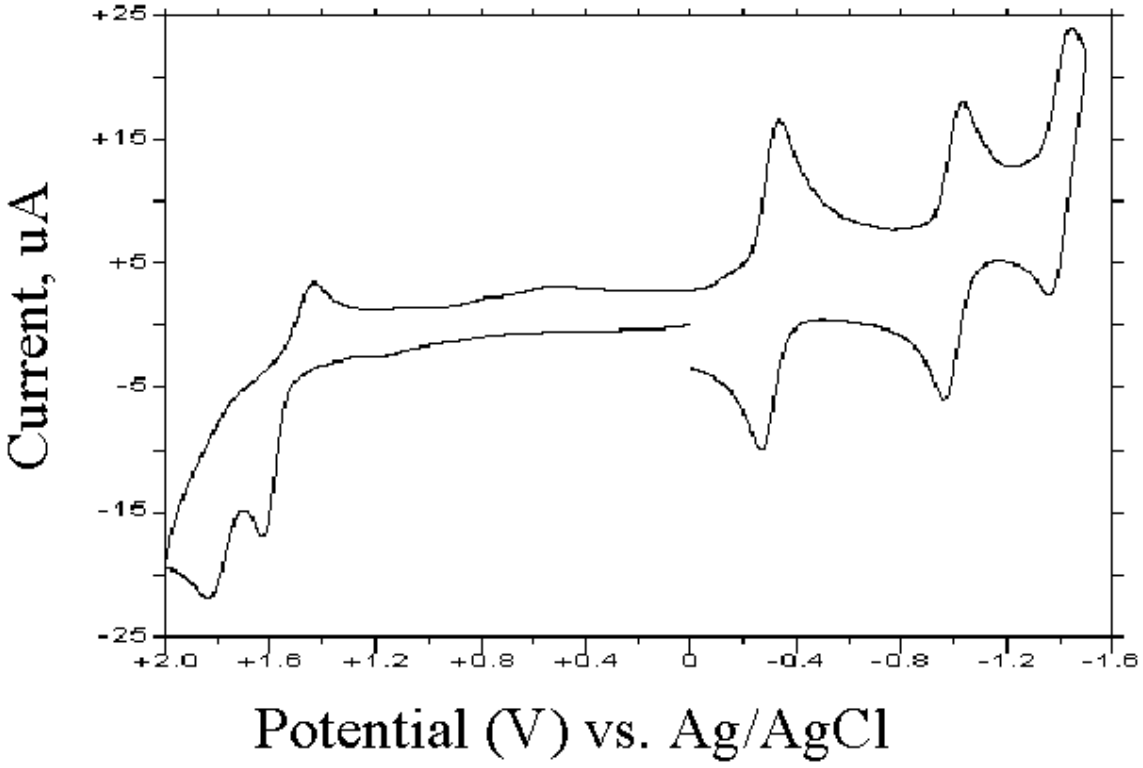

Figure 3.5 Cyclic voltammogram of $[(tpy)Ru(PEt_2Ph)(bpm)PtCl_2](PF_6)_2$ in 0.1 M Bu_4NPF_6 in CH_3CN (tpy = 2,2':6',6''-terpyridine, bpm = 2,2'-bipyrimidine).

Table 3.1 Electrochemical data for a series of ruthenium complexes incorporating bridging ligand bpm[a,b].

Complex	$E_{1/2}$ oxidation (V)	$E_{1/2}$ reduction (V)
$[(tpy)RuCl(bpm)](PF_6)$	+1.01 $Ru^{II/III}$	-1.15 $bpm^{0/-}$
		-1.56 $tpy^{0/-}$
$[(tpy)Ru(CH_3CN)(bpm)](PF_6)_2$	+1.55 $Ru^{II/III}$	-1.06 $bpm^{0/-}$
		-1.42 $tpy^{0/-}$
$[(tpy)Ru(PEt_2Ph)(bpm)](PF_6)_2$	+1.56 $Ru^{II/III}$	-1.03 $bpm^{0/-}$
		-1.38 $tpy^{0/-}$
$[(tpy)Ru(PEt_2Ph)(bpm)PtCl_2](PF_6)_2$	+1.63 $Ru^{II/III}$	-0.34 $bpm^{0/-}$
	+1.82 $Pt^{II/IV}$ [c]	-1.04 $bpm^{-/2-}$
		-1.45 $tpy^{0/-}$

[a] bpm = 2,2'-bipyrimidine, tpy = 2,2':6',6''-terpyridine, and PEt_2Ph = diethylphenylphosphine.

[b] Potentials reported in CH_3CN solution with 0.1 M Bu_4NPF_6 and reported versus Ag/AgCl (0.29 V vs. NHE).

[c] All irreversible processes reported as E_p^c.

Electronic Absorption Spectroscopy

The spectroscopy of mixed-ligand ruthenium based complexes containing the bpm bridging ligand is characterized by intense ligand $\pi \rightarrow \pi^*$ and $n \rightarrow \pi^*$ transitions in the ultraviolet region and metal ($d\pi$) $\rightarrow$ ligand (π^*) charge transfer transitions in the visible region based on each acceptor ligand. The electronic absorption data were summarized at Table 3.2.

The electronic absorption spectrum of $[(tpy)RuCl(bpm)](PF_6)$ is shown in Figure 3.6. The lowest energy transition at 516 nm is a $Ru(d\pi) \rightarrow bpm(\pi^*)$ CT transition and the shoulder at 490 nm is expected to be a $Ru(d\pi) \rightarrow tpy(\pi^*)$ CT transition. This assignment is consistent with those assignments made by D.P. Rillema[19] in the complex $[Ru(bpy)_2(bpm)](ClO_4)_2$, where the two lowest transitions at 478 nm and 422 nm are assigned as the $Ru(d\pi) \rightarrow bpm(\pi^*)$ CT transition and $Ru(d\pi) \rightarrow bpy(\pi^*)$ CT transition respectively. From comparison with other polypyridyl complexes, the intense transitions in the UV region are assigned as bpm and tpy $\pi \rightarrow \pi^*$ transitions.

The electronic absorption spectrum for $[(tpy)Ru(CH_3CN)(bpm)](PF_6)_2$ is also shown in Figure 3.6. The lowest transitions at 452 nm and the shoulder 412 nm are assigned to the $Ru(d\pi) \rightarrow bpm(\pi^*)$ CT transition and $Ru(d\pi) \rightarrow tpy(\pi^*)$ CT transition respectively. The intense transitions in the UV region of the spectrum are assigned as bpm and tpy $\pi \rightarrow \pi^*$ transitions. Compared to the complex with the chloride ligand, $[(tpy)RuCl(bpm)](PF_6)$, the lowest lying MLCT transition is significantly blue-shifted for the CH_3CN complex. This is because the CH_3CN ligand, compared to chloride ligand, is a poorer σ donor but better π acceptor. Thus its coordination with the ruthenium metal center would substantially stabilize the ruthenium $d\pi$ orbital. Since the bpm π^* orbital and the tpy π^* orbital remain almost the same, the energy gaps for those two MLCT transitions are greatly increased and the blue shift for these MLCT transitions results.

Table 3.2 Electronic absorption spectroscopy of the ruthenium and platinum complexes containing bpm ligand[a,b].

Complex	λ_{max}(nm)	$\varepsilon(M^{-1}cm^{1})/10^{4}$	assignment
[(tpy)RuCl(bpm)] (PF_6)	516	0.99	Ru(dπ)→bpm(π*) CT
	490	0.86	Ru(dπ)→tpy(π*) CT
	370	0.96	Ru(dπ)→tpy(π*) CT
	316	3.78	π→π*
	268	2.86	π→π*
	240	4.37	π→π*
[(tpy)Ru(CH_3CN)(bpm)](PF_6)$_2$	452	0.85	Ru(dπ)→bpm(π*) CT
	412	0.65	Ru(dπ)→tpy(π*) CT
	332	2.34	
	304	3.33	π→π*
	268	3.08	π→π*
	240	3.50	π→π*
[(tpy)Ru(PEt_2Ph)(bpm)](PF_6)$_2$	450	0.91	Ru(dπ)→bpm(π*) CT
	404	0.69	Ru(dπ)→tpy(π*) CT
	334	2.16	
	308	3.75	π→π*
	268	3.34	π→π*
	234	4.99	π→π*
[(tpy)Ru(PEt_2Ph)(bpm)$PtCl_2$] (PF_6)$_2$	554	0.53	Ru(dπ)→bpm(π*) CT
	416	1.34	Ru(dπ)→tpy(π*) CT
	336	2.61	
	304	3.48	π→π*
	274	3.98	π→π*
	232	5.11	π→π*

[a] Spectra recorded in CH_3CN at room temperature.

[b] tpy = 2,2':6',6''-terpyridine, bpm = 2,2'-bipyrimidine.

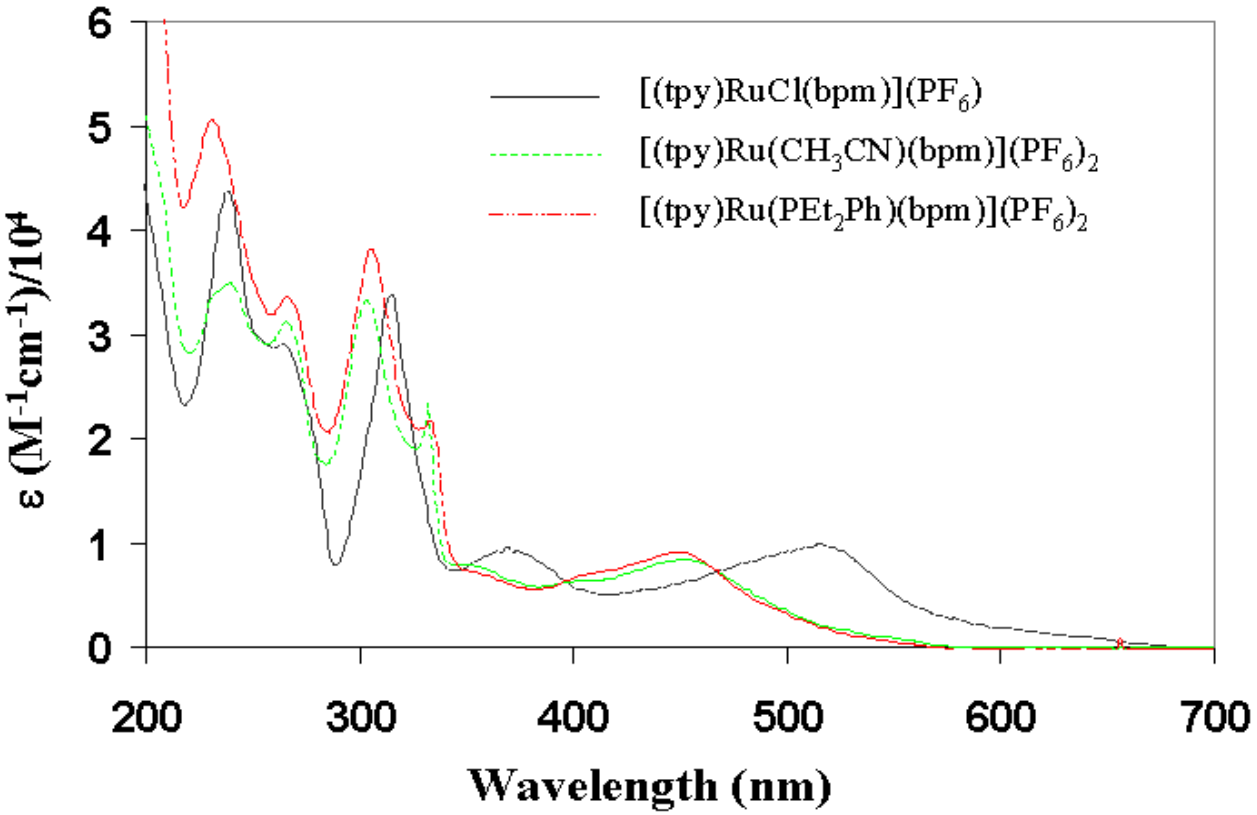

Figure 3.6 Electronic absorption spectrum of [(tpy)RuCl(bpm)](PF_6), [(tpy)Ru(CH_3CN)(bpm)](PF_6)$_2$ and [(tpy)Ru(PEt_2Ph)(bpm)](PF_6)$_2$ in CH_3CN at RT.

The electronic absorption spectrum for [(tpy)Ru(PEt_2Ph)(bpm)](PF_6)$_2$, is shown in Figure 3.6. It is very close to that of the CH_3CN complex. As before, the two lowest transitions, at 450 nm and the shoulder at 404 nm, are assigned as Ru(dπ)→bpm(π*) CT transition and Ru(dπ)→tpy(π*) CT transition respectively. The similar spectra for the two complexes are consistent with the electrochemical data. This indicates a very similar nature of the coordination bonds between the ruthenium metal and these two ligand sets.

The electronic absorption spectrum for the bimetallic complex is shown in Figure 3.7. The transition at 554 nm is assigned to the Ru(dπ)→bpm(π*) CT transition and the peak at 416 nm is assigned as overlapping Ru(dπ)→bpm(π*) and Ru(dπ)→tpy(π*) CT transitions. The other intense transitions at the UV region are then assigned as the bpm π→π* and tpy π→π* transitions. The Ru(dπ)→bpm(π*) CT transition is red shifted to

554 nm in this bimetallic from 450 nm in the monometallic complex. This is consistent with bridging ligand coordinating to the electron-deficient platinum metal center and reflective of the electrochemical data.

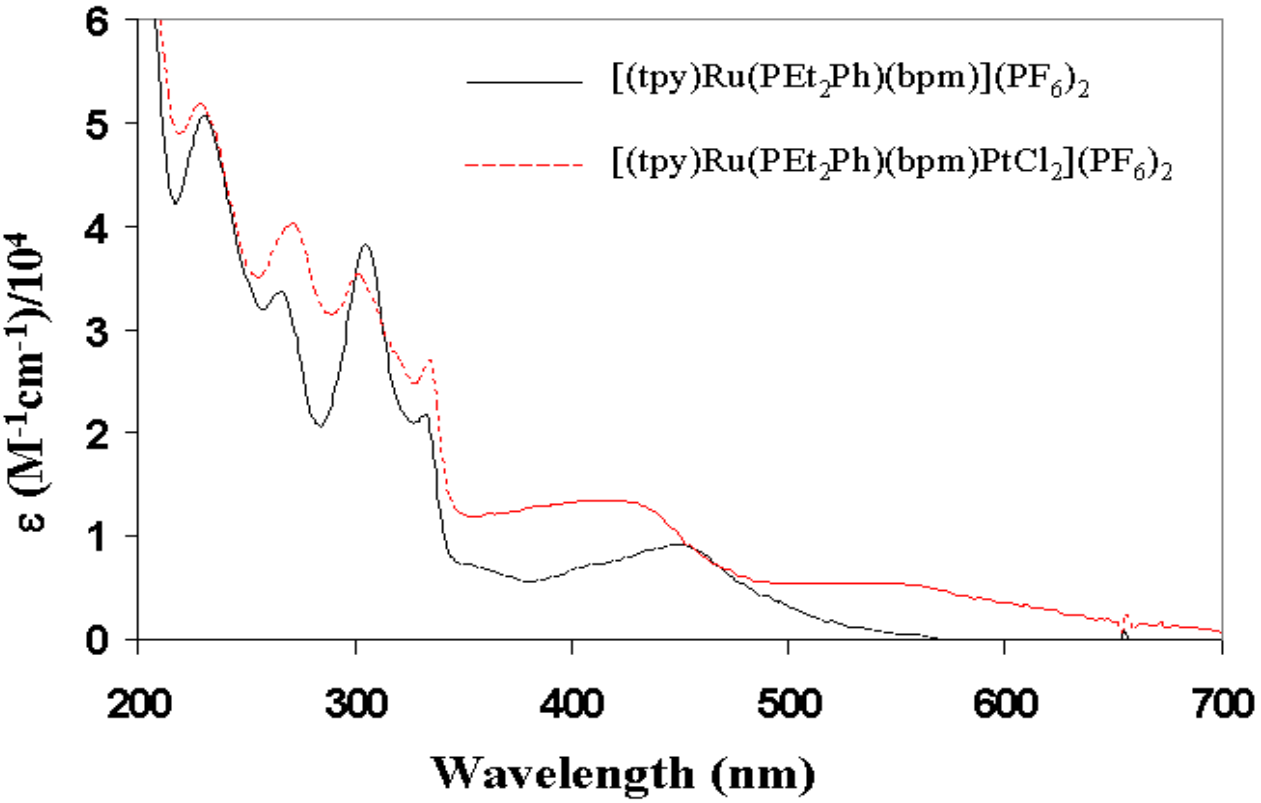

Figure 3.7 Electronic absorption spectrum of $[(tpy)Ru(PEt_2Ph)(bpm)](PF_6)_2$ and $[(tpy)Ru(PEt_2Ph)(dpp)PtCl_2](PF_6)_2$ in CH_3CN at RT.

^{1}H and ^{31}P NMR Spectra

^{1}H and ^{31}P NMR data for these complexes provide further proof of the structures of these metal complexes as well as showing the utility of the phosphine as a ^{31}P NMR tag for the structures of the polymetallic complexes. The ^{1}H NMR of these types of complexes is typically ill-defined. Our use of a phosphine ligand has made NMR a valuable technique of analysis. The spectral assignments of the ^{31}P and ^{1}H NMR spectra for free ligand PEt_2Ph are provided.

The ^{31}P NMR spectrum of PEt_2Ph (Figure 3.8) is relatively straightforward: one strong peak at -10.28 ppm and a minor peak at 46.96 ppm. The peak at –10.28 ppm is assigned as the phosphorus peak from the free ligand PEt_2Ph and the peak at 46.96 ppm is assigned as the phosphorus peak from the phosphorous oxide. The peak for the phosphorous oxide appears downfield because it is deshielded by coordination to the oxygen atom.

The ^{1}H spectrum of free ligand PEt_2Ph (Figure 3.9) shows 5 peaks, as expected, two aliphatic and 3 aromatic. The peak at 7.51 is assigned to the proton at position 1 because these two protons are immediately adjacent to the electron withdrawing phosphorus atom. The peaks at 7.39 ppm and 7.36 ppm are assigned to protons 2 and 3 respectively. In the aliphatic region of the spectrum, two groups of peaks are assigned to the $-CH_2-$ and $-CH_3$ protons respectively. The methyl proton peak split into 5 lines with intensity ratio of 1:2:2:2:1. This could be seen as the combination of the two first order 1:2:1 split from H-H and H-P coupling where the last line in one group of peak lines overlaps with the first line in the other group of lines. The $–CH_2-$ proton peak is split into 4 lines as a normal quartet. So there is no coupling between the $–CH_2-$ protons and the phosphorus atom. This is because the phosphorus sometimes only couples to the protons on the even-numbered carbons but not to those protons on the odd-numbered carbons.[64]

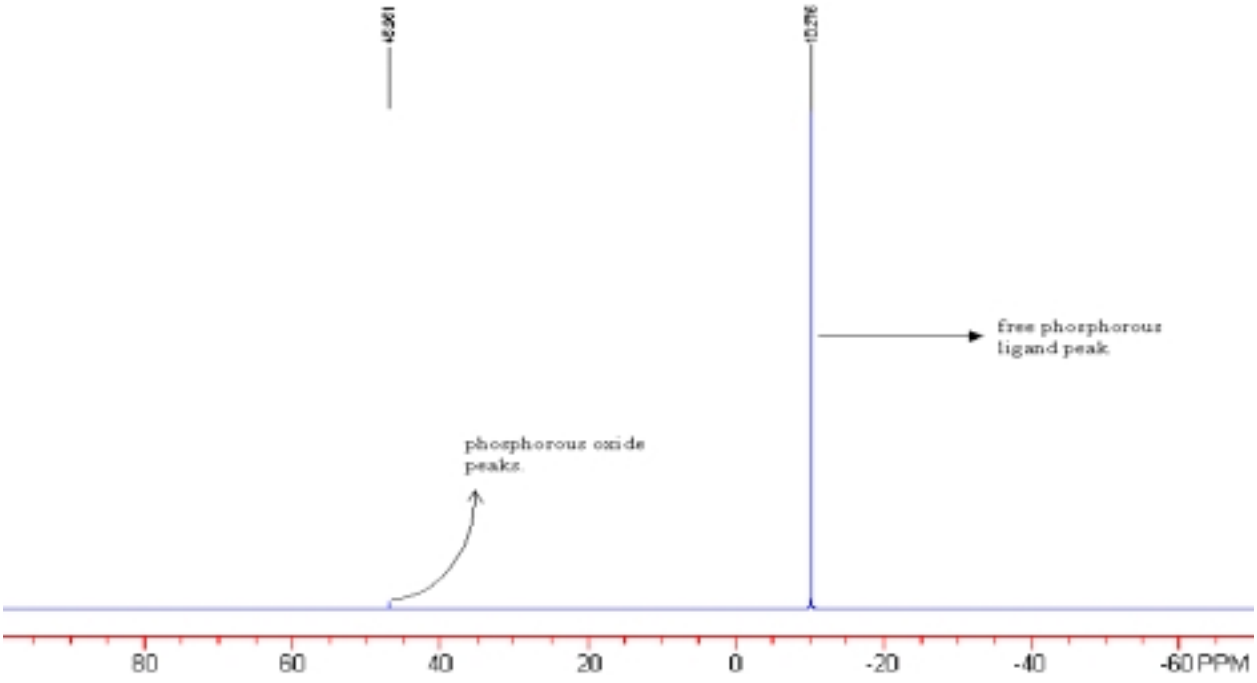

Figure 3.8 ^{31}P NMR spectrum of free ligand PEt_2Ph in CD_3CN at RT

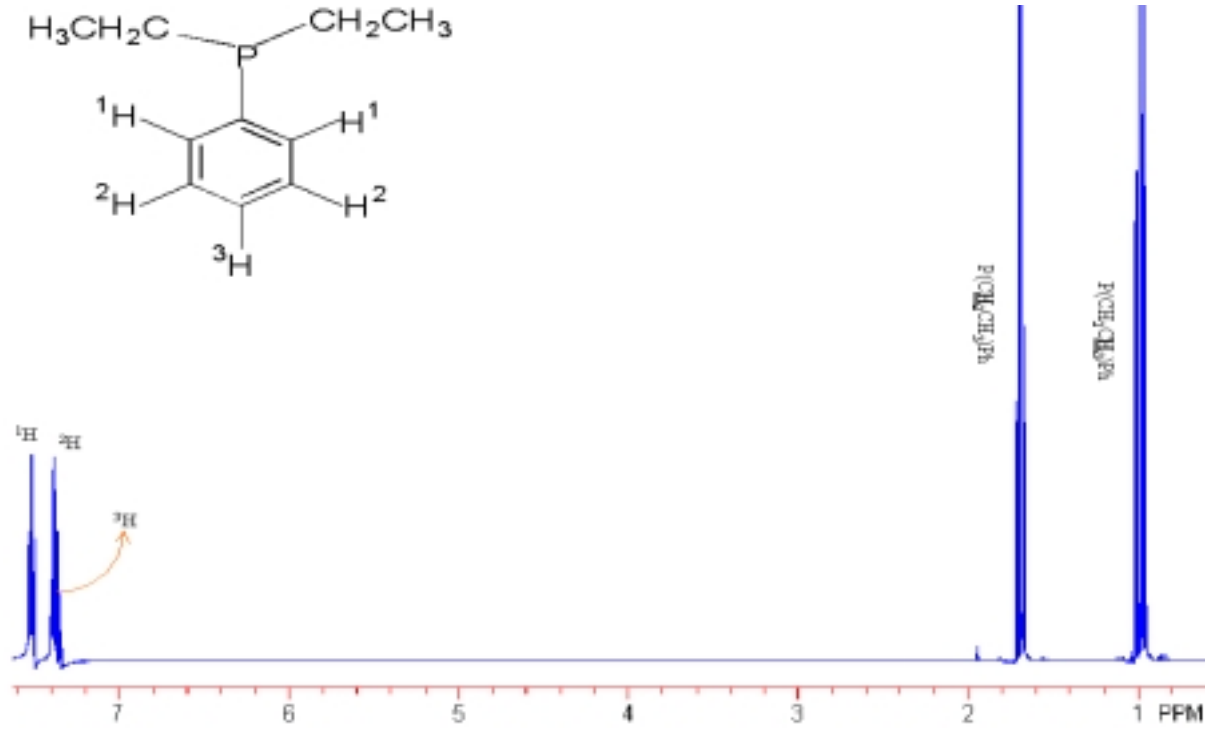

Figure 3.9 ^{1}H NMR spectrum of free ligand PEt_2Ph in CD_3CN at RT

The interpretations of for ^{1}H NMR spectrum for PEt_2Ph are summarized below in Table 3.3.

Table 3.3 ^{1}H NMR data for free ligand PEt_2Ph[a,b].

Postion	Chemical shift	Integration	Multiplicity
1	7.51	2	multiplet
2	7.39	2	multiplet
3	7.36	1	multiplet
$P(C\underline{\mathbf{H}}_2CH_3)Ph$	1.69	4	quartet
$P(CH_2C\underline{\mathbf{H}}_3)Ph$	0.98	6	pentet

[a] Data were recorded in CD_3CN at 500MHz.

[b] The chemical shift are measured in ppm.

The ^{1}H NMR of the polypyridyl ligand tpy and the bridging ligands bpm and dpp are well studied and the ^{1}H spectra are summarized below (see Figure 3.10 for the numbering of the protons from these three ligands).

The ^{1}H NMR spectrum of free tpy ligand shows six groups of peaks[65]: δ(ppm) 8.62 (H^3 and $H^{5''}$), 7.86(H^4 and $H^{4''}$) 7.33(H^5 and $H^{3''}$), 8.70(H^6 and $H^{2''}$), 8.46($H^{3'}$ and $H^{5'}$) and 7.96($H^{4'}$).

The ^{1}H NMR spectrum of free bpm ligand shows two groups of peaks[66]: δ(ppm) 8.99(H^4, H^6, $H^{4'}$ and $H^{6'}$) and 7.64(H^5 and $H^{5'}$).

The ^{1}H NMR spectrum of free dpp ligand shows five groups of peaks[67]: δ(ppm) 8.68(H^{4} and H^{5}), 8.24($H^{3'}$ and $H^{3''}$), 7.84($H^{4'}$ and $H^{4''}$), 7.84($H^{5'}$ and $H^{5''}$) and 7.25($H^{6'}$ and $H^{6''}$).

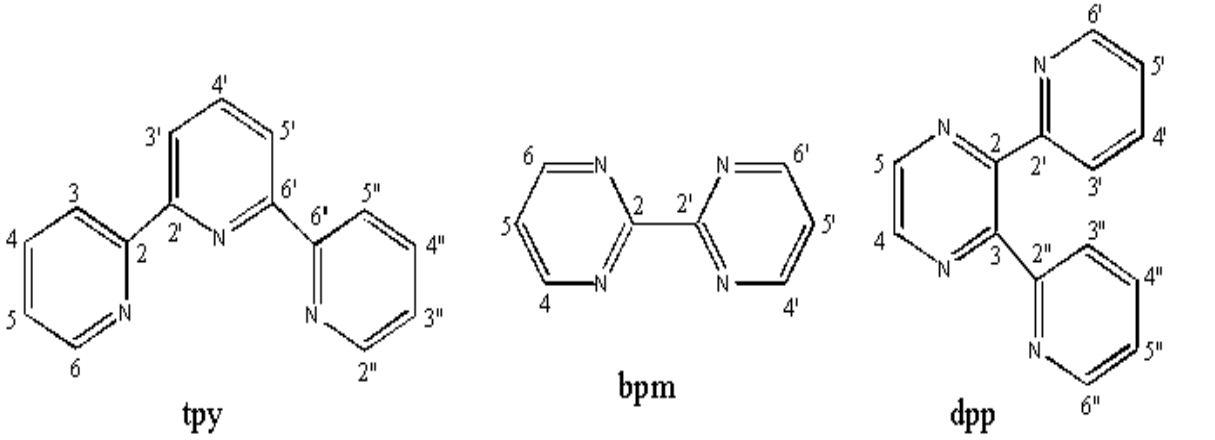

Figure 3.10 The numbering of protons for ligands tpy, bpm and dpp

[(tpy)RuCl(bpm)](PF$_6$)

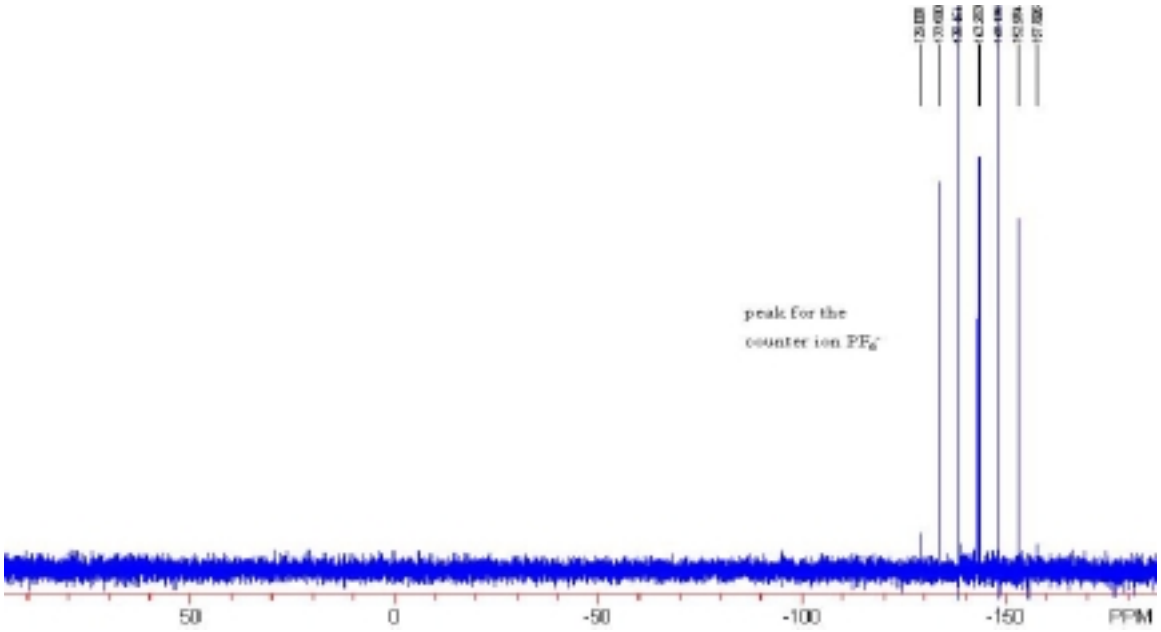

Figure 3.11 The ^{31}P NMR spectrum for [(tpy)RuCl(bpm)](PF$_6$) in CD_3CN at RT.

The ^{31}P and ^{1}H NMR spectra for [(tpy)RuCl(bpm)](PF_6) are shown in Figures 3.11 and 3.12. The tentative proton peaks assignments are summarized in Table 3.4.

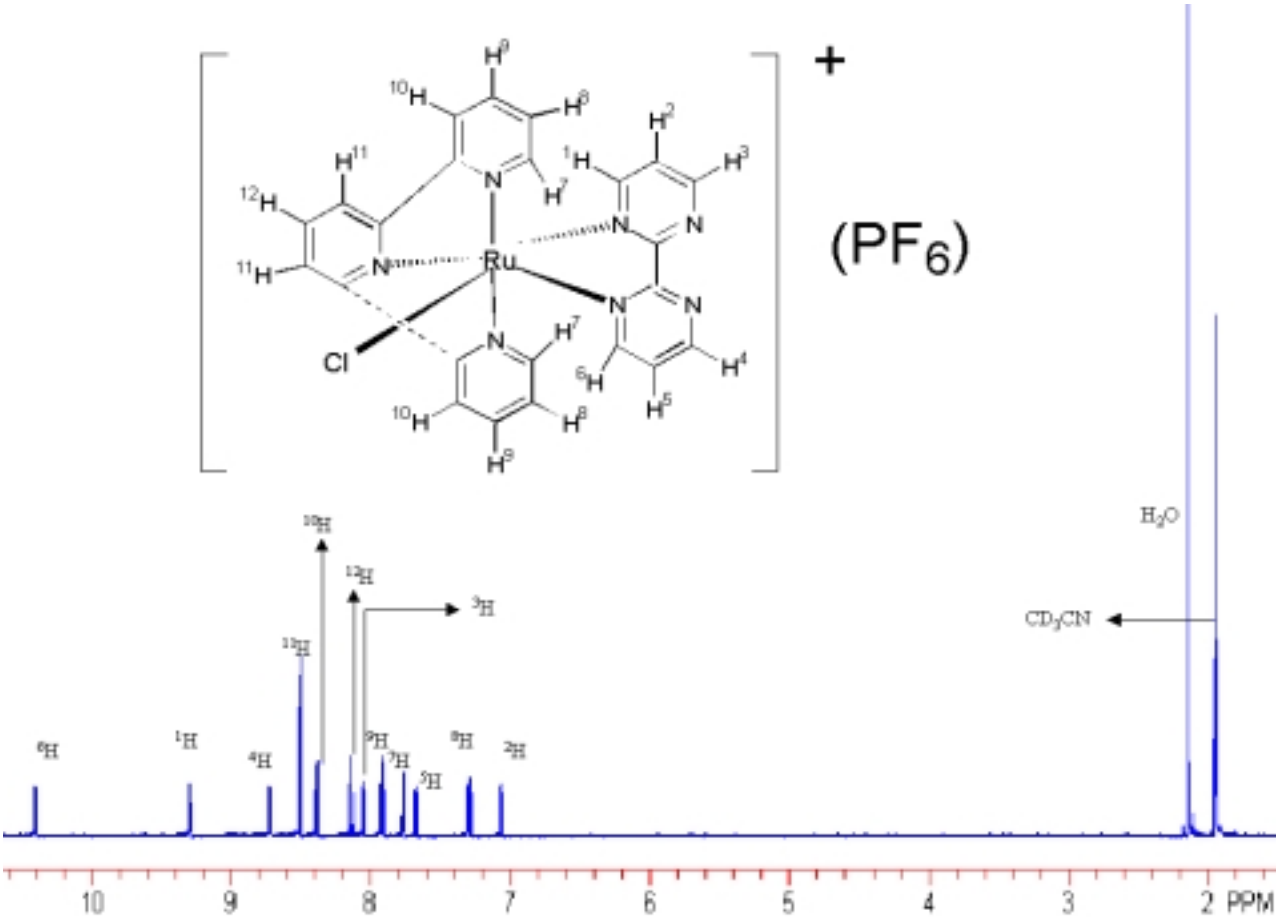

Figure 3.12 The ^{1}H NMR spectrum for [(tpy)RuCl(bpm)](PF_6) in CD_3CN at RT.

The ^{31}P NMR spectrum is very simple, with only one group of peaks at –143.3 ppm. The peak is assigned as the phosphorus from the counter ion PF_6^-. It is split into seven lines due to the coupling of the phosphorus atom to the six adjacent fluorine atoms.

Table 3.4 ^{1}H NMR for $[(tpy)RuCl(bpm)](PF_6)$[a,b].

Position	Chemical Shift	Integration	Multiplicity
1	9.29	1	doublet doublet
2	7.06	1	doublet doublet
3	8.05	1	doublet doublet
4	8.72	1	doublet doublet
5	7.68	1	doublet doublet
6	10.04	1	doublet doublet
7	7.75	2	doublet
8	7.29	2	multiplet
9	7.92	2	multiplet
10	8.38	2	doublet
11	8.50	2	doublet
12	8.14	1	triplet

[a] The data were recorded in CD_3CN in 500 MHz.

[b] The chemical shifts were measured in ppm.

The ^{1}H NMR spectrum is relatively complicated and therefore the following peak assignments are tentative. There are no aliphatic protons in this complex and no peak is expected to appear in this region. From the ^{1}H spectrum, there still exist two groups of protons respectively at 1.94 ppm and 2.14 ppm. According to H.E. Gottlieb[68], the peak at 1.94 ppm is assigned as the NMR solvent CD_3CN peak and the peak at 2.14 ppm is assigned as the water (either H_2O or HOD) peak.

The aromatic region of the spectrum shows twelve peaks as expected. The tridentate ligand tpy binds to metal in mer fashion in the octahedral complex. Thus the complex, [(tpy)Ru(Cl)(bpm)](PF_6), has an inherent reflection plane defined by the ruthenium-chloride bond and the two coordination bonds between ruthenium and the two nitrogen donors in the bpm ligand. So there should be twelve types of protons (as shown in the chemical structure in Figure 3.12) in this complex. In the aromatic region of the spectrum, seven groups of peaks at 10.04, 9.29, 8.72, 8.14, 8.05, 7.68 and 7.06 ppm have the integration of one hydrogen and the other five groups of peaks at 8.50, 8.38, 7.92, 7.75 and 7.06 ppm have the integration of two hydrogens. So these seven groups of peaks are assigned as protons 1 to 6 from bpm ligand and proton 12 from tpy ligand. The other five groups of peaks are then assigned as protons 7 to 11 from the tpy ligand.

First consider the seven peaks with the integration of one hydrogen. The peak at 8.14 ppm is a triplet while the other six groups of peaks are a doublet of doublets. This difference makes the peak at 8.14 ppm assigned as proton 12 and the other six groups of peaks assigned to protons 1 to 6 from the bridging ligand bpm.

Among these six groups of peaks, the peak at 10.04 ppm is assigned to proton 6 and the peak at 9.29 ppm is assigned to proton 1 because they are close to the two electron withdrawing nitrogen atoms. These two protons have chemical shifts of 8.98 ppm in the free ligand and move to a more positive region in the bound ligand. The difference between proton 1 and 6 is that they are trans to different ligands in the complex. It is believed that chloride ligand is a better σ donor and cannot π accept like the tpy ligand. This makes the aromatic ring with proton 1 more electron-rich than the other in the bpm ligand. Therefore the peak at 9.29 ppm is assigned to proton 1 and the peak at 10.04 ppm is assigned to proton 6. Both peaks are a doublet of doublets. This is due to their coupling to the other two protons in each ring.

In the remaining four peaks at 8.72, 8.05, 7.68 and 7.06 ppm, peaks at 8.72 and 8.05 ppm should be assigned to protons 3 and 4 because these two protons are adjacent to the two

electron withdrawing nitrogen atoms. The difference between protons 3 and 4 is that they are in different rings with different electron densities as discussed above. Thus the peak at 8.72 ppm is assigned to proton 4 and peak at 8.05 ppm is assigned to proton 3. The last two peaks at 7.68 and 7.06 ppm are then assigned to protons 5 and 2, respectively, for the same reason.

Now consider the five groups of peaks with the integration of two hydrogens. The peak at 7.92 and 7.29 ppm are split to multiple lines while the three other group of peaks at 8.50, 8.38 and 7.73 ppm are nicely split doublets. Thus the peaks at 7.92 and 7.29 ppm are assigned to protons 8 and 9. In the free tpy ligand proton 8 shows at 7.33 ppm and proton 9 shows at 7.86 ppm. It is expected that proton 9 still has a larger chemical shift than proton 8 in the bound tpy. Therefore the peak at 7.92 ppm is assigned to proton 9 and the peak at 7.29 ppm is assigned to proton 8. This is also consistent with those assignments made by R.P. Thummel[65] in the complex, $[Ru(tpy)_2](PF_6)_2$.

The remaining three groups of peaks at 8.50, 8.38 and 7.73 ppm are less easily assigned. In free tpy ligand, protons 7, 10 and 11 appear at 8.70, 8.62 and 8.46 ppm respectively. According to R.P. Thummel's assignment of ^{1}H NMR peaks for the complex, $[Ru(tpy)_2](PF_6)_2$, the chemical shift of proton 7 changed to 7.34 ppm from 8.70 ppm, the chemical shift of proton 10 changed to 8.50 ppm from 8.62 ppm and the chemical shift of proton 11 changed to 8.76 ppm from 8.46 ppm. The chemical shifts for protons 7 and 10 from the two side rings of the tpy ligand become smaller in the complex while the chemical shift for proton 11 from the middle ring of the tpy ligand becomes larger. Also proton 7 has a smaller chemical shift than proton 10 in the complex. So in our complex the peak at 8.50 ppm is assigned to proton 11 and the peaks at 8.38 and 7.75 ppm are assigned to protons 10 and 7 respectively.

Now consider these assignments of peaks from the perspective of the three aromatic rings of the tpy ligand. Protons 11 and 12 in the middle ring move to more positive regions by 0.04 and 0.18 ppm respectively. Protons 7, 8 and 10 in the two side rings move to more

negative regions by –0.97, -0.04 and –0.24 ppm respectively. Proton 9 in the two side rings move to a somewhat more positive region by 0.06 ppm. All these changes of chemical shifts between the corresponding protons in free tpy ligand and bound tpy ligand in the metal complex, summarized in Table 3.5, are consistent with R.P. Thummel's results for $[Ru(tpy)_2](PF_6)_2$.

Table 3.5 Chemical shift change of the protons in the tpy ligand between the free ligand, $[Ru(tpy)_2](PF_6)_2$ and $[(tpy)RuCl(bpm)](PF_6)$[a].

Complex							
tpy [65]	δ (ppm)	H^3, $H^{5''}$ 8.62	H^4, $H^{4''}$ 7.86	H^5, $H^{3''}$ 7.33	H^6, $H^{2''}$ 8.70	$H^{3'}$, $H^{5'}$ 8.46	$H_{4'}$ 7.96
$[Ru(tpy)_2](PF_6)_2$ [65]	δ (ppm)	H^3, $H^{5''}$ 8.50	H^4, $H^{4''}$ 7.92	H^5, $H^{3''}$ 7.17	H^6, $H^{2''}$ 7.34	$H^{3'}$, $H^{5'}$ 8.76	$H_{4'}$ 8.42
	Δ (ppm)	-0.12	+0.06	-0.16	-1.36	+0.30	+0.46
$[(tpy)RuCl(bpm)](PF_6)$	δ (ppm)	H_{10} 8.38	H_9 7.92	H_8 7.29	H_7 7.75	H_{11} 8.50	H_{12} 8.14
	Δ (ppm)	-0.24	+0.06	-0.04	-0.95	+0.04	+0.18

[a] The Δ (chemical shift change) is calculated against the corresponding proton chemical shift in the free tpy ligand.

[(tpy)Ru(CH_3CN)(bpm)](PF_6)$_2$

The ^{31}P NMR spectrum for [(tpy)Ru(CH_3CN)(bpm)](PF_6)$_2$ (Figure 3.13) is also very simple, with only one group of peaks at –143.3 ppm. The peak is assigned as the phosphine peak from the counter ion, PF_6^-.

The ^{1}H NMR spectrum for [(tpy)Ru(CH_3CN)(bpm)](PF_6)$_2$ (Figure 3.14) is similar to that for [(tpy)RuCl(bpm)](PF_6)$_2$ except that it has a single peak for bound CH_3CN showing at 2.10 ppm. In the aliphatic region there also exist two more peaks at 2.14 and 1.94 ppm respectively. The peak at 1.94 ppm is assigned to NMR solvent CD_3CN and the peak at 2.14 ppm is assigned to H_2O or HOD.[68]

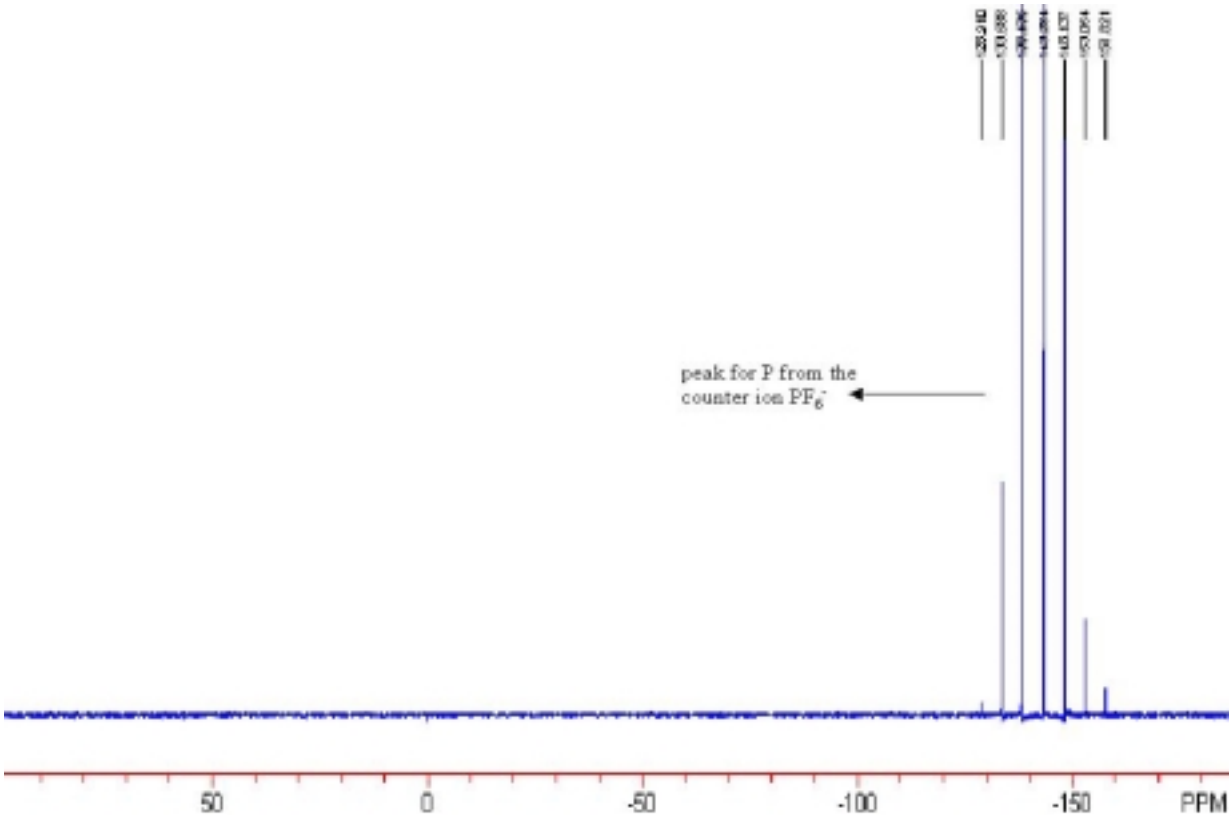

Figure 3.13 ^{31}P NMR spectrum for [(tpy)Ru(CH_3CN)(bpm)](PF_6)$_2$ in CD_3CN at RT .

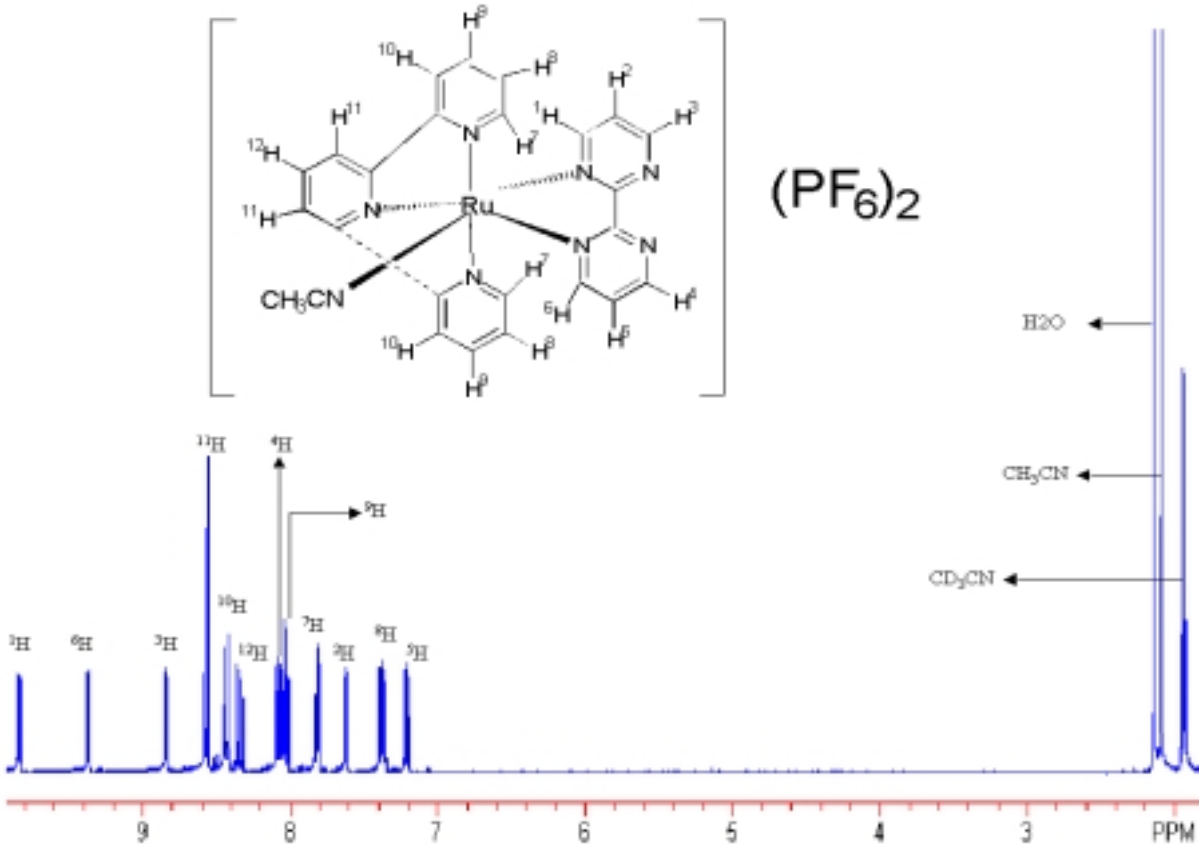

Figure 3.14 ^{1}H NMR for [(tpy)Ru(CH_3CN)(bpm)]$(PF_6)_2$ in CD_3CN at RT .

[(tpy)Ru(CH_3CN)(bpm)]$(PF_6)_2$ also has a reflection plane and thus its ^{1}H NMR spectrum in the aromatic region is almost identical to that of [(tpy)Ru(Cl)(bpm)]$(PF_6)_2$. Due to the difference in the nature of the ruthenium-chloride bond and ruthenium-CH_3CN bond, the assignments of some peaks differ.

First consider those seven groups of peaks with the integration of one hydrogen. They appear at 9.84, 9.38, 8.84, 8.34, 8.03, 7.62 and 7.21 ppm respectively. The peak at 8.34 is assigned to proton 12 since it is a triplet. Among the remaining six groups of peaks, the peak at 9.84 ppm is assigned to proton 1 and the peak at 9.38 ppm is assigned to proton 6. This is different from the corresponding assignments in [(tpy)Ru(Cl)(bpm)]$(PF_6)_2$ because the change of the ligand from chloride to CH_3CN reverses the order of electron density for the two aromatic rings in the bpm ligand. In [(tpy)Ru(CH_3CN)(bpm)]$(PF_6)_2$ the aromatic ring trans to CH_3CN becomes more electron deficient compared to the other

ring because CH_3CN is a π acceptor and a poorer σ donor than chloride. For the same reason, the peak at 8.84 ppm is assigned to proton 3 and the peak at 8.08 ppm is assigned to proton 4, the peak at 7.62 ppm is assigned to proton 2 and the peak at 7.21 ppm is assigned to proton 5.

The remaining five groups of two hydrogen peaks are assigned to protons in the same order as they are in the complex $[(tpy)Ru(Cl)(bpm)](PF_6)_2$ because it is believed that the change of the chloride ligand to CH_3CN ligand would not change the order of electron density of the three aromatic rings in the tpy ligand. Also the multiplicities of these peaks are consistent with these assignments.

The tentative assignments of ^1H NMR peaks for $[(tpy)Ru(CH_3CN)(bpm)](PF_6)_2$ are summarized in Table 3.6.

Table 3.6 ^{1}H NMR for $[(tpy)Ru(CH_3CN)(bpm)](PF_6)_2$ [a,b].

Position	Chemical Shift	Integration	Multiplicity
1	9.84	1	doublet doublet
2	7.62	1	doublet doublet
3	8.84	1	doublet doublet
4	8.08	1	doublet doublet
5	7.21	1	doublet doublet
6	9.38	1	doublet doublet
7	7.81	2	doublet
8	7.37	2	multiplet
9	8.04	2	multiplet
10	8.43	2	doublet
11	8.57	2	doublet
12	8.34	1	triplet
$C\underline{H}_3CN$	2.10	3	singlet

a The data were recorded in CD_3CN on 500 MHz JOEL.

b The chemical shifts were measured in ppm.

[(tpy)Ru(PEt$_2$Ph)(bpm)](PF$_6$)$_2$

The ^{31}P NMR spectrum for [(tpy)Ru(PEt$_2$Ph)(bpm)](PF$_6$)$_2$ (Figure 3.15) shows two groups of peaks. There exists a single peak at 32.2 ppm that is assigned to phosphine peak from the bound PEt$_2$Ph ligand. The phosphine chemical shift in the bound ligand, 32.2 ppm, falls between the phosphine peaks for the free PEt$_2$Ph ligand (at -10.3 ppm) and the phosphine oxide (at 47.0 ppm). This is consistent with binding of the PEt$_2$Ph to the electron deficient metal center. At –143.3 ppm there appears a 7-line peak, which is assigned to the phosphine peak from the counter ion PF_6^-. The phosphine peak for the PF_6^- and the bound PEt$_2$Ph integrate to 2.01/1, which is very close to the expected 2/1 ratio.

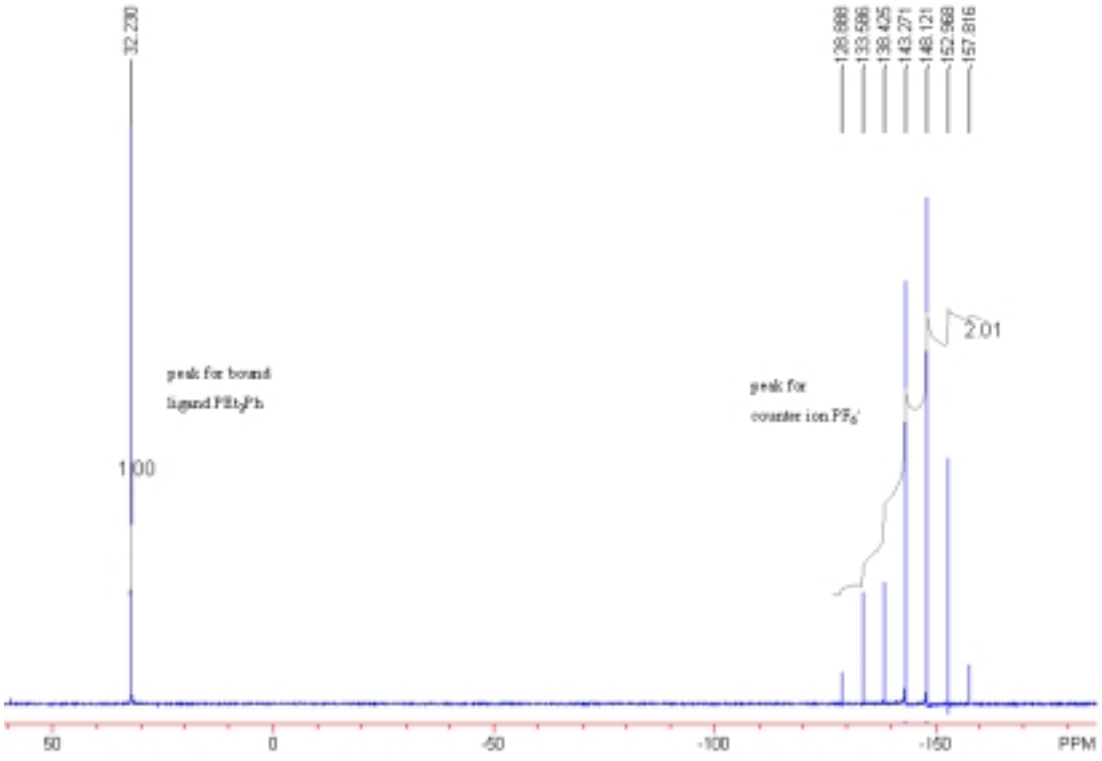

Figure 3.15 ^{31}P NMR spectrum for [(tpy)Ru(PEt$_2$Ph)(bpm)](PF$_6$)$_2$ in CD$_3$CN at RT.

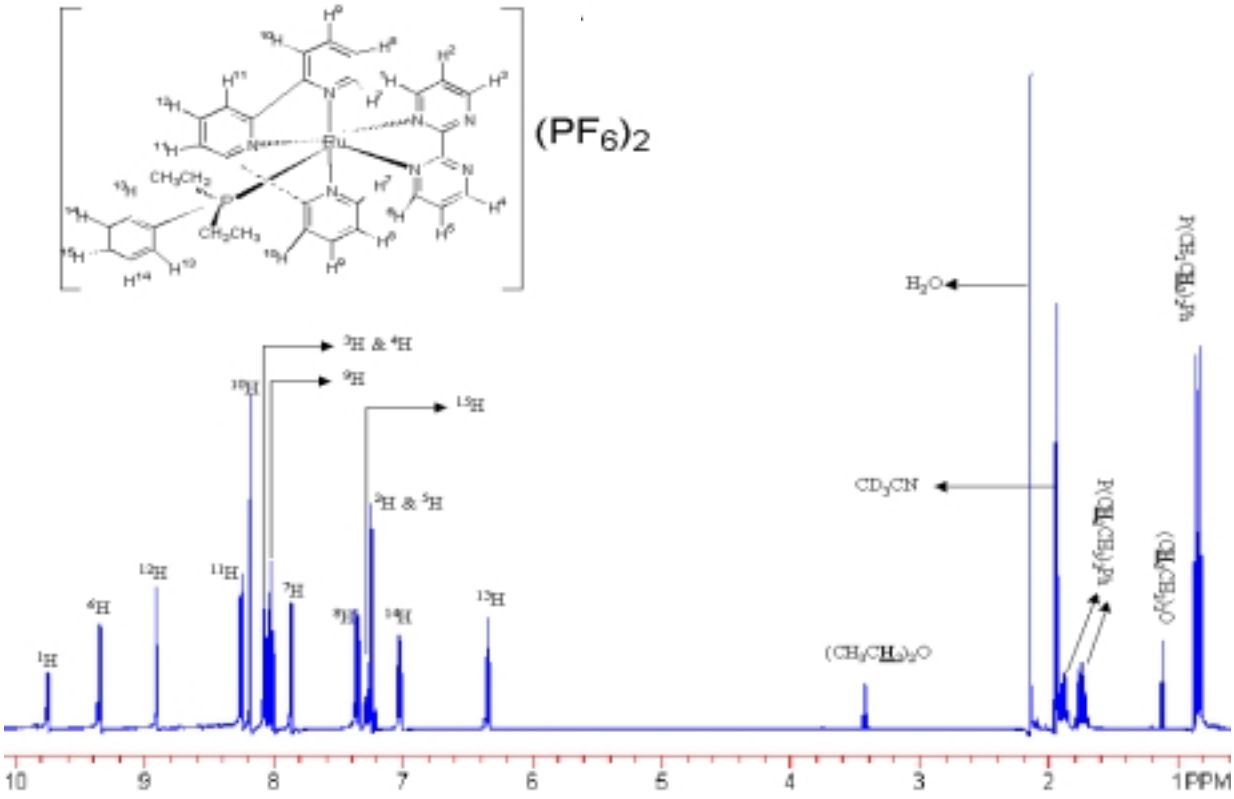

Figure 3.16 ^{1}H NMR spectrum for [(tpy)Ru(PEt_2Ph)(bpm)]$(PF_6)_2$ in CD_3CN at RT.

The ^{1}H NMR spectrum of [(tpy)Ru(PEt_2Ph)(bpm)]$(PF_6)_2$ (Figure 3.16) becomes much more complicated due to the introduction of five more aromatic protons from the PEt_2Ph ligand. In the aliphatic region of the spectrum, there are peaks at 0.85, 1.12, 1.75, 1.88, 1.94, 2.14 and 3.42 ppm. The peaks at 1.12 ppm and 3.42 ppm are assigned to the -CH_3 and –CH_2- protons in diethyl ether. As above, the peak at 2.14 ppm is the water peak and the peak at 1.94 ppm is from proton-containing impurities in the CD_3CN NMR solvent.[68] The peak at 0.85 ppm split into a pentet with a ratio of 1:2:2:2:1, matching the pattern of the –CH_3 proton peaks in the free PEt_2Ph ligand. This represents the methyl protons in the bound PEt_2Ph ligand. The remaining two groups of peaks at 1.75 ppm and 1.88 ppm in the aliphatic region are assigned to two –CH_2- protons. These two peaks integrate as 2:2:6 relative to the –CH_3 protons at 0.85 ppm. Theoretically the protons in the two -CH_2-

groups are homotopic and should have the same chemical shifts. A possible reason for the different chemical shifts might be the bulky phenyl group in this ligand. The bulky phenyl ring could restrict the free rotation of the ruthenium-phosphorus coordination bond because it is unfavorable for this ring to point toward the tpy or the bpm ligand. Thus the protons in the two $–CH_2$- groups are then exposed to different chemical environments and have slightly different chemical shifts.

Comparing the aromatic regions of the spectra of $[(tpy)Ru(PEt_2Ph)(bpm)](PF_6)_2$ and $[(tpy)Ru(CH_3CN)(bpm)](PF_6)_2$, it is quite easy to assign peaks at 7.03 and 6.35 ppm to protons 13 and 14 from the aromatic ring in the phosphine ligand. This time the peak of high chemical shift at 7.03 ppm is assigned as proton 14 instead of proton 13. This is because this phenyl ring is in partial overlap with one of the tpy side rings and proton 13 is protruding much closer to the inside of one tpy side ring (see calculated 3D structure in Figure 3.17). Therefore proton 13 is in the shielding cone of the tpy side ring and chemical shift becomes much smaller than proton 14 and 15. Thus the peak at 6.35 ppm is assigned to proton 13.

The remaining eleven groups of peaks in the aromatic region are attentatively assigned in the following way. There are four groups of peaks at 9.75, 9.35, 8.91 and 7.27 ppm having the integration of one hydrogen. This makes the assignment of the peaks somewhat difficult. The peaks at 9.75 and 9.35 ppm are a doublet of doublets and assigned to protons 1 and 6 from the bpm bridging ligand. More specifically, the peak at 9.75 ppm is assigned to proton 1 and the peak at 9.35 ppm is assigned to proton 6. This is similar to the assignments made in the solvato complex. The peak at 8.91 ppm is a triplet and assigned to proton 12 from the middle ring of the tpy ligand. The peak at 7.27 ppm is split into multiple lines and is assigned to proton 15 from the phosphine ligand. This assignment of proton 15 is consistent with the previous assignment of the peaks at 7.03 and 6.35 ppm because all the protons in the PEt_2Ph ligand have lower chemical shifts in the complex than in the free ligand.

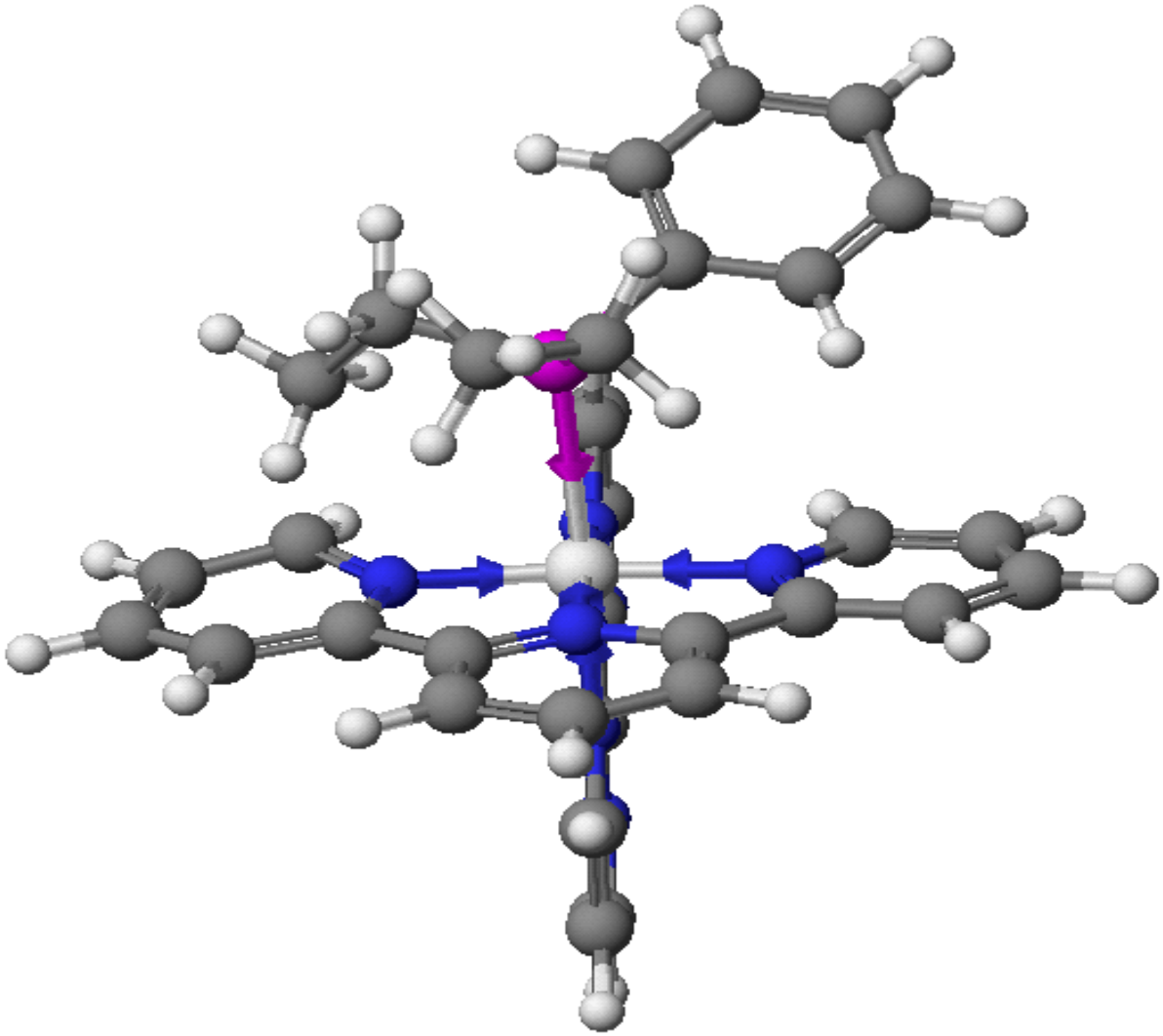

Figure 3.17 Calculated structure of [(tpy)Ru(PEt_2Ph)(bpm)](PF_6)$_2$ using CAChe ZINDO method of computing molecular geometries

In the remaining 7 groups of peaks with integration of two hydrogens, the peaks at 8.07 and 7.24 ppm are doublet doublets, which are assigned to the remaining four protons from the bpm bridging ligand. The peak at 8.07 is assigned to proton 3 and proton 4 and the peak at 7.24 ppm is assigned to proton 2 and 5. This is because proton 3 and 4 are

closer to the electron withdrawing nitrogen atoms. The last 5 groups of peaks belong to protons 7 to 11 from the tpy ligand. In these groups, the peaks at 8.03 and 7.36 ppm are split to multiple lines and should be assigned to protons 8 and 9. As with the assignments made in the solvato complex, the peak with higher chemical shift at 8.03 ppm is assigned to proton 9 and the peak at 7.36 ppm is then assigned to proton 8. The last three groups of peaks at 7.87, 8.19 and 8.25 ppm are assigned to proton 7, 10 and 11 respectively.

The attentative assignments of ^{1}H NMR peaks for $[(tpy)Ru(PEt_2Ph)(bpm)](PF_6)_2$ are shown in the Table 3.7.

Table 3.7 ^{1}H NMR for [(tpy)Ru(PEt$_2$Ph)(bpm)](PF$_6$)$_2$[a,b].

Position	Chemical Shift[b]	Integration	Multiplicity
1	9.75	1	doublet doublet
2	7.24	1	doublet doublet
3	8.07	1	doublet doublet
4	8.07	1	doublet doublet
5	7.24	1	doublet doublet
6	9.35	1	doublet doublet
7	7.87	2	doublet
8	7.36	2	multiplet
9	8.03	2	multiplet
10	8.19	2	doublet
11	8.25	2	doublet
12	8.91	1	triplet
13	6.35	2	multiplet
14	7.03	2	multiplet
15	7.27	1	triplet
P(C**H**$_2$CH$_3$)$_2$Ph	1.88	2	multiplet
	1.75	2	multiplet
P(CH$_2$C**H**$_3$)$_2$Ph	0.85	6	pentet

[a] The data were recorded at 500 MHz in CD$_3$CN at RT.

[b] The chemical shift were measured in ppm.

[(tpy)Ru(PEt$_2$Ph)(bpm)PtCl$_2$](PF$_6$)$_2$

The ^{31}P NMR spectrum (Figure 3.18) is quite similar to that of the monometallic complex with the PF6$^-$ peak appearing at –144.0 ppm and the bound PEt$_2$Ph peak at 33.3 ppm. The two peaks integrate as 1.84:1, close to the expected 2:1 ratio.

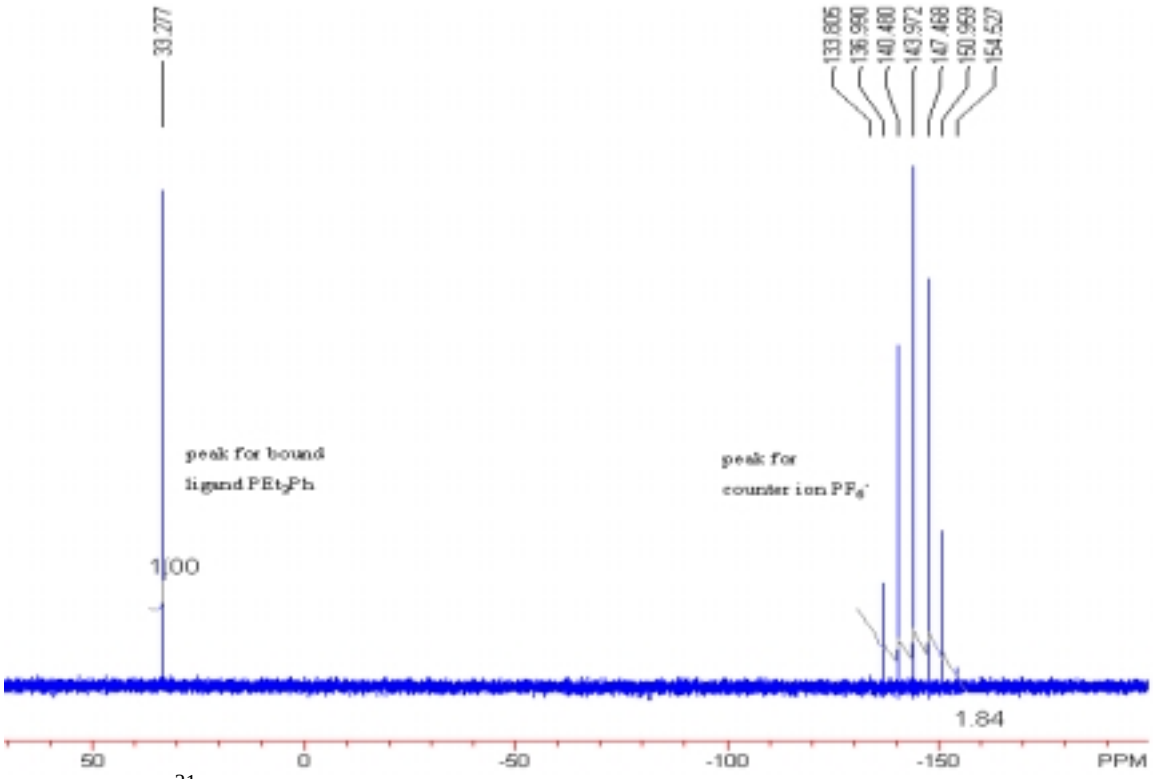

Figure 3.18 ^{31}P NMR spectrum for [(tpy)Ru(PEt$_2$Ph)(bpm)PtCl$_2$](PF$_6$)$_2$ in CD$_3$CN at RT

The ^{1}H NMR spectrum of [(tpy)Ru(PEt$_2$Ph)(bpm)PtCl$_2$](PF$_6$)$_2$ is very close to that of monometallic, as shown in Figure 3.19. The peaks are assigned with reference to the order of the chemical shifts of the corresponding peaks in the monometallic complex. As in the monometallic complex, the protons from the two –CH$_2$- group in the PEt$_2$Ph ligand give two different peaks respectively at 1.81 ppm and 1.90 ppm. They integrate as 2:2:6 relative to the -CH$_3$ protons in same ligand.

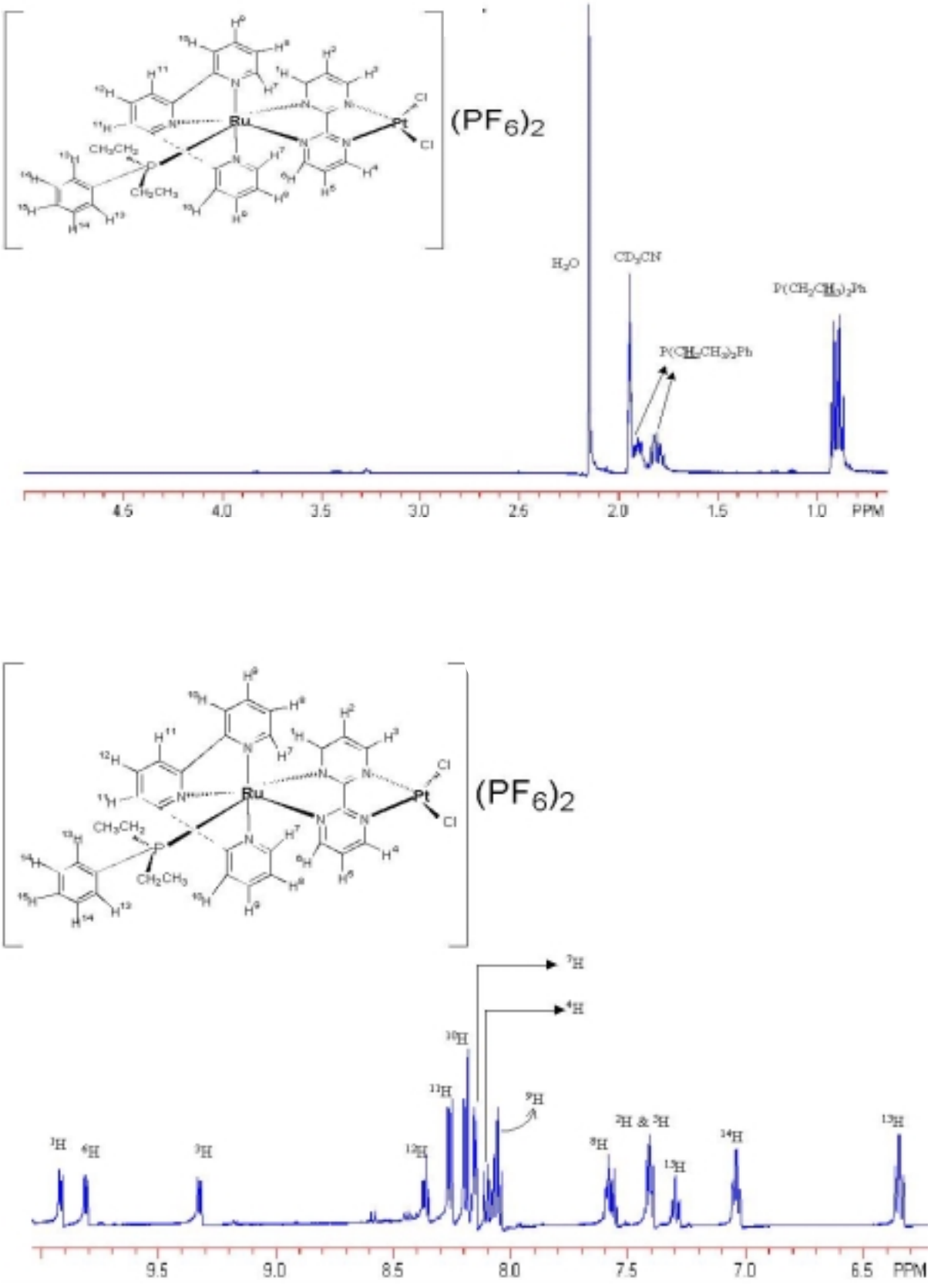

Figure 3.19 ^{1}H NMR spectrum for $[(tpy)Ru(PEt_2Ph)(bpm)PtCl_2](PF_6)_2$ in CD_3CN at RT.

The change of the chemical shifts between the corresponding protons in the monometallic and the bimetallic complexes is also consistent with the coordination of the second electron deficient metal center. The most obvious example is the change in the chemical shifts for proton 3 and 4. The chemical shifts for proton 3 and 4 changed from 8.07 in the monometallic complex to 9.33 and 8.10 ppm, respectively, in the bimetallic complex.

The attentative assignments of ^{1}H NMR peaks are summarized in Table 3.8.

Table 3.8 ^{1}H NMR for $[(tpy)Ru(PEt_2Ph)(bpm)PtCl_2](PF_6)_2$[a].

Position	Chemical Shift[b]	Integration	Multiplicity
1	9.92	1	doublet
2	7.42	1	doublet doublet
3	9.33	1	doublet doublet
4	8.10	1	doublet
5	7.42	1	doublet doublet
6	9.81	1	doublet
7	8.16	2	doublet
8	7.58	2	multiplet
9	8.06	2	quartet
10	8.19	2	doublet
11	8.26	2	doublet
12	8.36	1	triplet
13	6.35	2	triplet
14	7.03	2	triplet
15	7.30	1	triplet
$P(C\underline{\mathbf{H}}_2CH_3)_2Ph$	1.90	2	multiplet
	1.81	2	multiplet
$P(CH_2C\underline{\mathbf{H}}_3)_2Ph$	0.90	6	pentet

[a] The data were recorded in CD_3CN at 500 MHz at RT.

[b] The chemical shift were measured in ppm.

Ru and Pt complexes containing asymmetrical bridging ligand dpp

Synthesis.

The ruthenium-platinum bimetallic complex bridged by a dpp ligand was synthesized using a building block approach analogous to the bpm-bridged analog. This step by step scheme, shown in Figure 3.20, allows for the choice of the exact nature of each component. Due to the asymmetric nature of the dpp bridging ligand bearing an AB chelate, all the complexes described herein with this ligand have two stereoisomers. In this project, all the complexes were characterized as mixtures of the two geometric isomers without any further separations. This practice is common to polyazine bridged ruthenium chemistry. As discussed later, our complexes are unique in that the phosphine probe unit allows us to see the existence of the two stereoisomers.

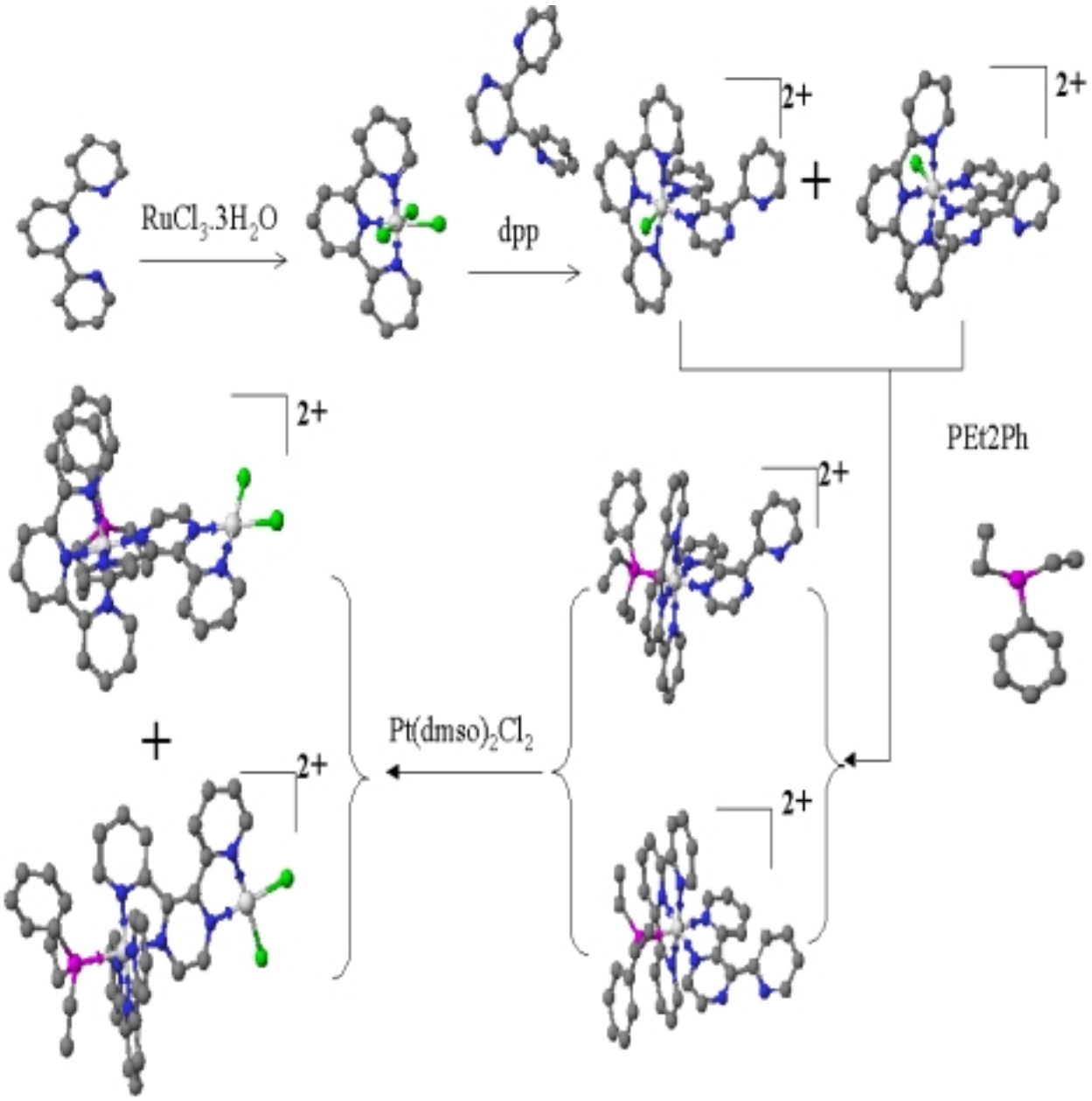

Figure 3.20 Synthetic scheme for the preparation of $[(tpy)Ru(PEt_2Ph)(dpp)PtCl_2](PF_6)_2$.

FAB MS Spectrum.

The MS spectra for monometallic complex $[(tpy)Ru(PEt_2Ph)(dpp)](PF_6)_2$ and bimetallic complex $[(tpy)Ru(PEt_2Ph)(dpp)PtCl_2](PF_6)_2$ are included in Appendices 6 and 7 (Page 100 and 101). The two complexes also give quite good FAB MS data with parent ions appearing and fragmentation by ligand and/or metal loss observable. Both spectra show the $[M\text{-}PF_6]^+$ peak and the $[M\text{-}2PF_6]^+$ peak.

The FAB MS spectrum of the complex, $[(tpy)Ru(PEt_2Ph)(dpp)](PF_6)_2$, shows four major groups of peaks (Table 2.6 at page 22 and Appendix 6 at page 100). The peaks at 880(*m/z*) and 734(*m/z*) are assigned as the species $[(tpy)Ru(PEt_2Ph)(dpp)](PF_6)^+$ and $[(tpy)Ru(PEt_2Ph)(dpp)]^+$ respectively. The loss of the phosphine ligand, PEt_2Ph, from $[(tpy)Ru(PEt_2Ph)(dpp)]^+$ gives rise to the $[(tpy)Ru(dpp)]^+$ peak at 568(*m/z*). The peak at 334(m/z) is assigned as the $[Ru(tpy)]^+$ species.

The FAB MS spectrum for the Ru-Pt bimetallic complex has a much more complicated fragmentation than the monometallic complex (Table 2.7 at page 23 and Appendix 7 at page 101). However the characteristic peaks for $[M\text{-}PF_6]^+$ and $[M\text{-}2PF_6]^+$ can be clearly observed at 1146(*m/z*) and 1001(*m/z*). With continuous loss of the other components like the phosphine ligand, the chlorine atom and the platinum atom, a series of species are observed at 835(*m/z*), 798(*m/z*), 763(*m/z*), 603(*m/z*) and 568(*m/z*). Their assignments are listed in Table 2.7 (page 23). These high mass/charge ratio peaks along with the characteristic fragmentation by ligand and metal loss are consistent with the proposed structure.

Electrochemistry

The electrochemistry of [(tpy)RuCl(dpp)](PF_6), [(tpy)Ru(PEt_2Ph)(dpp)]($(PF_6)_2$ and [(tpy)Ru(PEt_2Ph)(dpp)$PtCl_2$]($(PF_6)_2$ have been studied.

[(tpy)RuCl(dpp)](PF_6)

The electrochemical behavior of these complexes is characterized by metal based oxidation(s) and ligand based reductions. [(tpy)RuCl(dpp)](PF_6) has been previously studied[1] by the Brewer group but the properties reported herein are for my sample studied under my conditions to make comparison more valid. In [(tpy)RuCl(dpp)](PF_6), the oxidation is assigned as $Ru^{II/III}$, the first reduction is assigned as $dpp^{0/-}$, and the second reduction is assigned as $tpy^{0/-}$. The $dpp^{0/-}$ couple occurs prior to the $tpy^{0/-}$ due to the lower lying π^* orbitals.[10, 69-73]

[(tpy)Ru(PEt_2Ph)(dpp)]($(PF_6)_2$

When the chloride ligand in [(tpy)RuCl(dpp)](PF_6) is substituted by PEt_2Ph to form the new complex [(tpy)Ru(PEt_2Ph)(dpp)]($(PF_6)_2$, the metal based oxidation shifts to a more positive potential to 1.57 V from 1.00 V (see Figure 3.21). This is due to the decrease in electron density on the metal center upon PEt_2Ph substitution. As PEt_2Ph is substituted for chloride to form [(tpy)Ru(PEt_2Ph)(dpp)]($(PF_6)_2$ the dpp and tpy ligands become slightly more electron-deficient and thus much easier to reduce. The dpp reduction is shifted from –1.21 V to –1.05 V and the tpy reduction is shifted from -1.54 V to –1.42 V in [(tpy)Ru(PEt_2Ph)(dpp)]($(PF_6)_2$ relative to the [(tpy)RuCl(dpp)]($(PF_6)_2$ synthon.

The assignments in [(tpy)Ru(PEt_2Ph)(dpp)]($(PF_6)_2$ are consistent with those made in the analog complex [(tpy)Ru(PEt_2Ph)(bpm)]($(PF_6)_2$. Comparing the corresponding ligand based reductions and metal based oxidations, one can see that the tpy terminal ligand reductions occur at very close potentials, at -1.38 V in the bpm analog and –1.42 V in the

dpp analog. The ruthenium based oxidation occurs at 1.56 V in the bpm analog and at 1.57 V in the dpp analog. It is very interesting to notice that the two bridging ligand reductions in the two analog complexes also occur at very close potential, -1.03 V for the bpm analog and –1.05 V for the dpp analog consistent with the similar π^* orbital energy in these two systems.

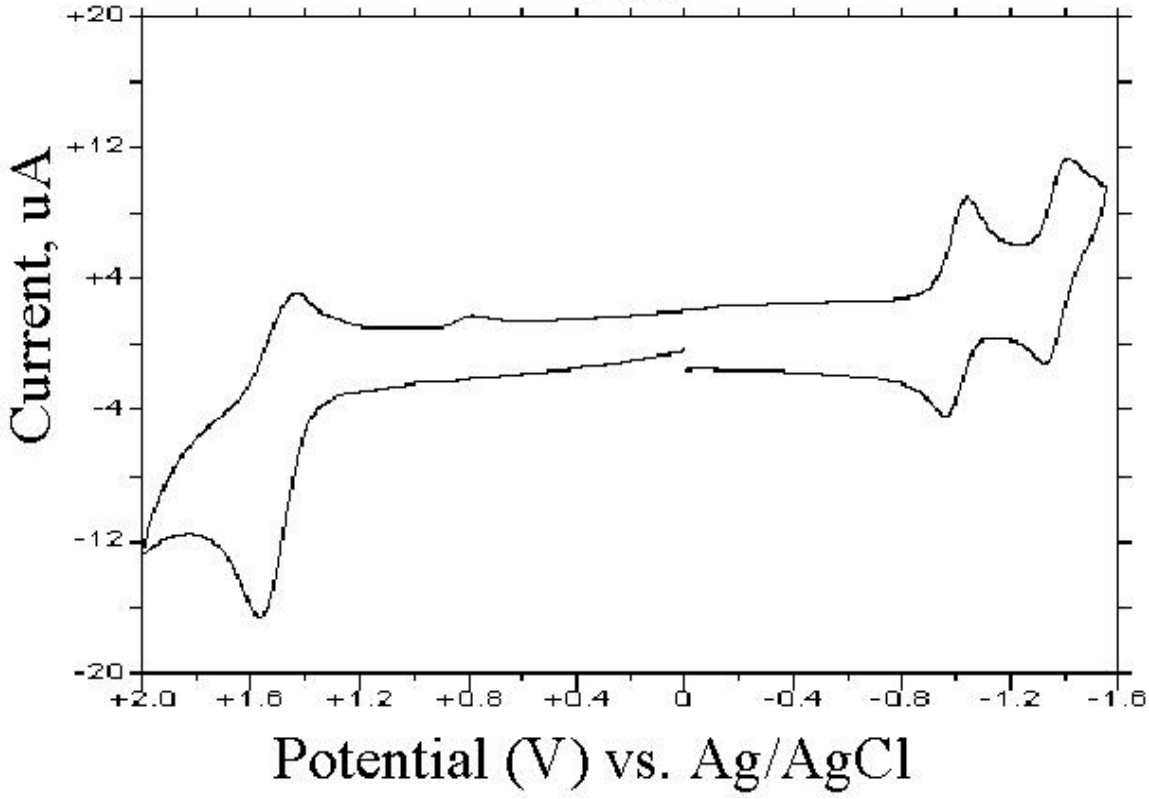

Figure 3.21 Cyclic voltammogram of $[(tpy)Ru(PEt_2Ph)(dpp)](PF_6)_2$ in 0.1 M Bu_4NPF_6 in CH_3CN (tpy = 2,2':6',6''-terpyridine, dpp = 2,3-bis(2-pyridyl)pyrazine.

$[(tpy)Ru(PEt_2Ph)(dpp)PtCl_2](PF_6)_2$

When the electron-deficient metal center platinum is bound to the monometallic compound, $[(tpy)Ru(PEt_2Ph)(dpp)](PF_6)_2$, the bridging dpp ligand becomes much easier

to reduce. The first reduction $dpp^{0/-}$ couple is shifted from –1.05 V to –0.50 V. This is due to the stabilization of the π^* orbital induced by the coordination of the platinum metal center (Figure 3.22). In $[(tpy)Ru(PEt_2Ph)(dpp)PtCl_2](PF_6)_2$, the first two reductions are assigned as $dpp^{0/-}$ and $dpp^{-/2-}$, occuring prior to the terminal ligand reduction $tpy^{0/-}$. The assignment of the third reduction peak at –1.40 V to the $tpy^{0/-}$ is consistent with similar assignment in the bpm analog where the third reduction at –1.45 V is assigned as the $tpy^{0/-}$. The presence of the $dpp^{-/2-}$ couple before the reduction of the tpy ligand indicates the formation of the bimetallic complex bridged by this dpp ligand.[24a] In the oxidative region, there exist two peaks. The first one is assigned to the $Ru^{II/III}$. Compared to the ruthenium oxidation in the monometallic complex, no significant shift of the oxidation potential occurs upon bimetallic formation. The second oxidation occurring at 1.70 V is assigned as the irreversible oxidation of the Pt^{II} metal center.

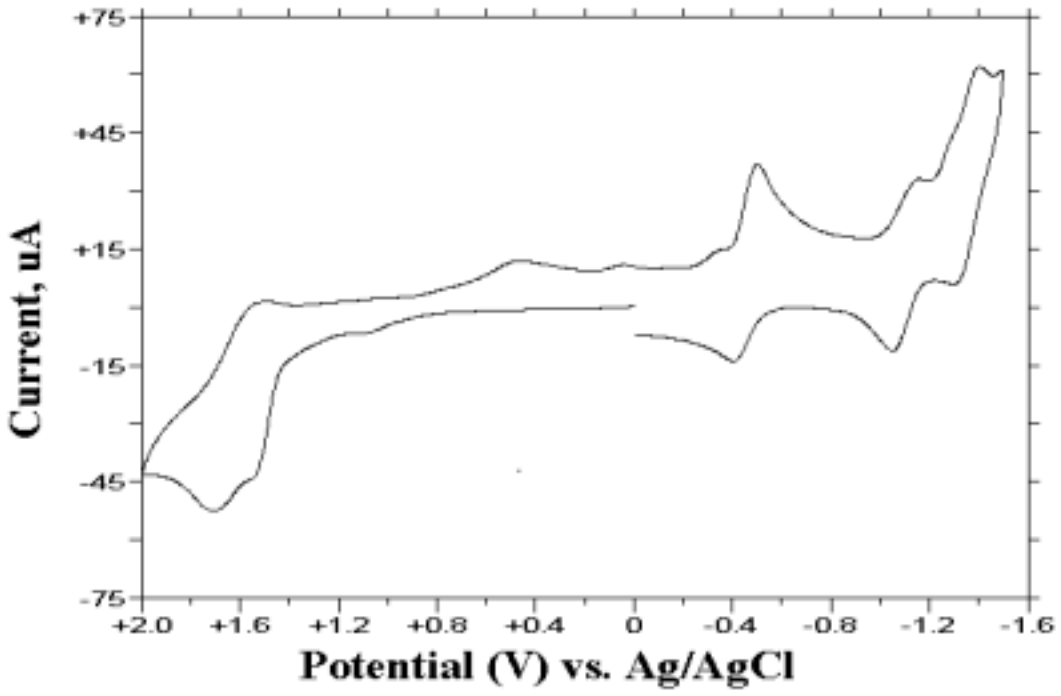

Figure 3.22 Cyclic voltammogram of $[(tpy)Ru(PEt_2Ph)(dpp)PtCl_2](PF_6)_2$ in 0.1 M Bu_4NPF_6 in CH_3CN (tpy = 2,2':6',6''-terpyridine, dpp = 2,3-bis(2-pyridyl)pyrazine).

Compared to the Ru-Pt bimetallic analog with the bpm bridging ligand, the two metal based oxidations in this dpp complex occur at closer potential. In the bpm analog, both metal based oxidations occur at a correspondingly more positive region than in the dpp analog. However in the bpm analog, the irreversible platinum oxidation occurs in a much more positive region. Thus the two oxidation peaks look well separated in that complex. This may be due to the difference in the matching of the platinum dπ orbital and the different bridging ligands based π orbitals.

The electrochemistry of the complexes containing dpp bridging ligand is summarized in Table 3.9.

Table 3.9 Electrochemical data for a series of ruthenium complexes incorporating the dpp bridging ligand [a,b].

Complex	$E_{1/2}$ oxidation (V)	$E_{1/2}$ reduction (V)
$[(tpy)RuCl(dpp)](PF_6)$	+1.00 $Ru^{II/III}$	-1.21 $dpp^{0/-}$
		-1.54 $tpy^{0/-}$
$[(tpy)Ru(PEt_2Ph)(dpp)](PF_6)_2$	+1.57 $Ru^{II/III}$	-1.05 $dpp^{0/-}$
		-1.42 $tpy^{0/-}$
$[(tpy)Ru(PEt_2Ph)(dpp)PtCl_2](PF_6)_2$	+1.55 $Ru^{II/III}$	-0.50 $dpp^{0/-}$
	+1.70 $Pt^{II/IV}$ [c]	-1.15 $dpp^{-/2-}$
		-1.40 $tpy^{0/-}$

[a] dpp = 2,3-bis(2-pyridyl)pyrazine, tpy = 2,2':6',6''-terpyridine, and PEt_2Ph = diethylphenylphosphine.

[b] Potentials reported in CH_3CN solution with 0.1 M TBAH and reported versus Ag/AgCl (0.29V vs. NHE).

[c] All irreversible process reported as E_p^c.

Electronic absorption spectroscopy

The spectroscopy of the complexes containing the dpp bridging ligand is characterized by intense ligand π→ π* transitions in the ultraviolet region and metal (dπ) → ligand (π*) charge transfer transitions in the visible region. The spectral data of the dpp complexes prepared in this project are summarized at Table 3.10.

The electronic absorption spectrum of $[(tpy)Ru(PEt_2Ph)(dpp)](PF_6)_2$ is shown in Figure 3.23. The lowest energy transition at 460 nm is a Ru(dπ)→dpp(π*) CT transition and the transition at 416 nm is a Ru(dπ)→tpy(π*) CT transition. The intense transitions in the UV region are assigned as dpp π→π* and tpy π→π* transitions.

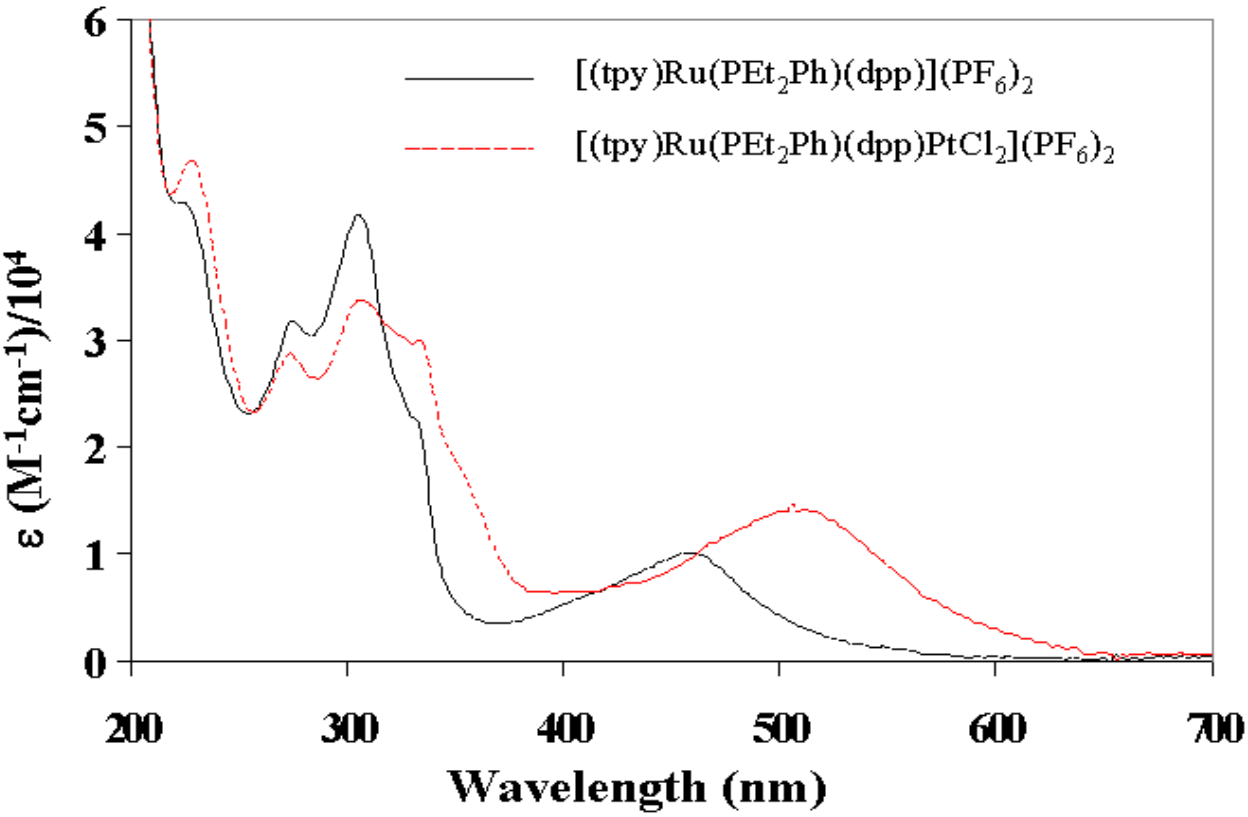

Figure 3.23 Electronic absorption spectrum for $[(tpy)Ru(PEt_2Ph)(dpp)](PF_6)_2$ and $[(tpy)Ru(PEt_2Ph)(dpp)PtCl_2](PF_6)_2$ in CH_3CN at RT.

Compared to the complex, [(tpy)RuCl(dpp)](PF_6), with chloride ligand, the MLCT transition is significantly blue-shifted for the complex, [(tpy)Ru(PEt_2Ph)(dpp)](PF_6)$_2$. This is consistent with the replacement of the chloride by the PEt_2Ph ligand. The coordination of the PEt_2Ph ligand would stabilize the Ru dπ orbital and thus widen the energy gap between the ruthenium based dπ HOMO and the dpp based π* LUMO, blue shifting the MLCT transition.

The electronic absorption spectrum of [(tpy)Ru(PEt_2Ph)(dpp)$PtCl_2$](PF_6)$_2$ is shown in Figure 3.23. The lowest energy transition at 506 nm is a Ru(dπ)→dpp(π*) CT transition and the shoulder at 424 nm is a Ru(dπ)→tpy(π*) CT transition. The intense transitions in the UV region are assigned as dpp π→π* and tpy π→ π* transition with a shoulder appearing in the [(tpy)Ru(PEt_2Ph)(dpp)$PtCl_2$](PF_6)$_2$ at ~370 nm likely representing the red-shifted dpp π→ π* upon coordination of the Pt^{II} center. Compared to the monometallic complex, the lowest energy Ru(dπ)→dpp(π*) CT transition is significantly red shifted. This is because the coordination of the electron deficient Pt metal pulls more electron density from the bridging dpp ligand and substantially stabilizes dpp π* acceptor orbital. This decrease in the energy gap between the Ru(dπ) based HOMO and the dpp(π*) based LUMO red shifts this MLCT transition.

Table 3.10 Electronic absorption spectroscopy of the ruthenium and platinum complexes containing dpp ligand[a,b].

Complex	λ_{max}(nm)	$\varepsilon(M^{-1}cm^{1})/10^{4}$	Assignment
$[(tpy)RuCl(dpp)](PF_6)$ [c]	512		Ru(dπ)→ dpp(π*) CT
	480		Ru(dπ)→ tpy(π*) CT
	370		tpy π→ π*
	314		π→ π*
	276		π→ π*
$[(tpy)Ru(PEt_2Ph)(dpp)](PF_6)_2$	460	1.00	Ru(dπ)→ dpp(π*) CT
	416	0.64	Ru(dπ)→ tpy(π*) CT
	334	2.20	tpy π→ π*
	308	4.14	π→ π*
	278	3.14	π→ π*
	226	4.27	π→ π*
$[(tpy)Ru(PEt_2Ph)(dpp)PtCl_2](PF_6)_2$	506	1.47	Ru(dπ)→ dpp(π*) CT
	424	0.70	Ru(dπ)→ tpy(π*) CT
	336	2.94	tpy π→ π*
	308	3.37	π→ π*
	276	2.85	π→ π*
	230	4.67	π→ π*

[a] Spectra recorded in CH_3CN at room temperature.

[b] tpy = 2,2':6',6''-terpyridine, dpp = 2,3-bis(2-pyridyl)pyrazine.

[c] Reference 24a.

^{31}P NMR Spectra

The ^{1}H NMR spectra for the complexes containing the asymmetric bridging ligand, dpp, are very complicated and not interpretable due to the two stereoisomers. Only the ^{31}P NMR spectra are included here as one purpose of the incorporation of the phosphine ligand was to provide an NMR handle to this type of complexes typically not amenable to NMR characterization.

[(tpy)Ru(PEt$_2$Ph)(dpp)](PF$_6$)$_2$

The ^{31}P NMR for [(tpy)Ru(PEt$_2$Ph)(dpp)](PF$_6$)$_2$ is shown in Figure 3.24. It is very simple. The peak for the phosphorus from the PF_6^- counter ion appears at –143.0 ppm. There are two single peaks at 30.5 ppm and 32.2 ppm. The two peaks are assigned to phosphorus from the bound PEt$_2$Ph ligand. There are two single peaks because there are two stereoisomers for the complex [(tpy)Ru(PEt$_2$Ph)(dpp)](PF$_6$)$_2$.

The sum of the integration of two single peaks has a fixed ratio of about 1:2 relative to the integration of the PF_6^- peak, although the ratio of the two single peaks changes for different submitted samples. A series of ratios from about 1:1 to more than 10:1 for the two single peaks have been observed. One possibility is that sometimes when the alumina chromatography was performed, only part of the second yellow product band following the band for starting material was collected, so one can see the changed ratio of the two isomers.

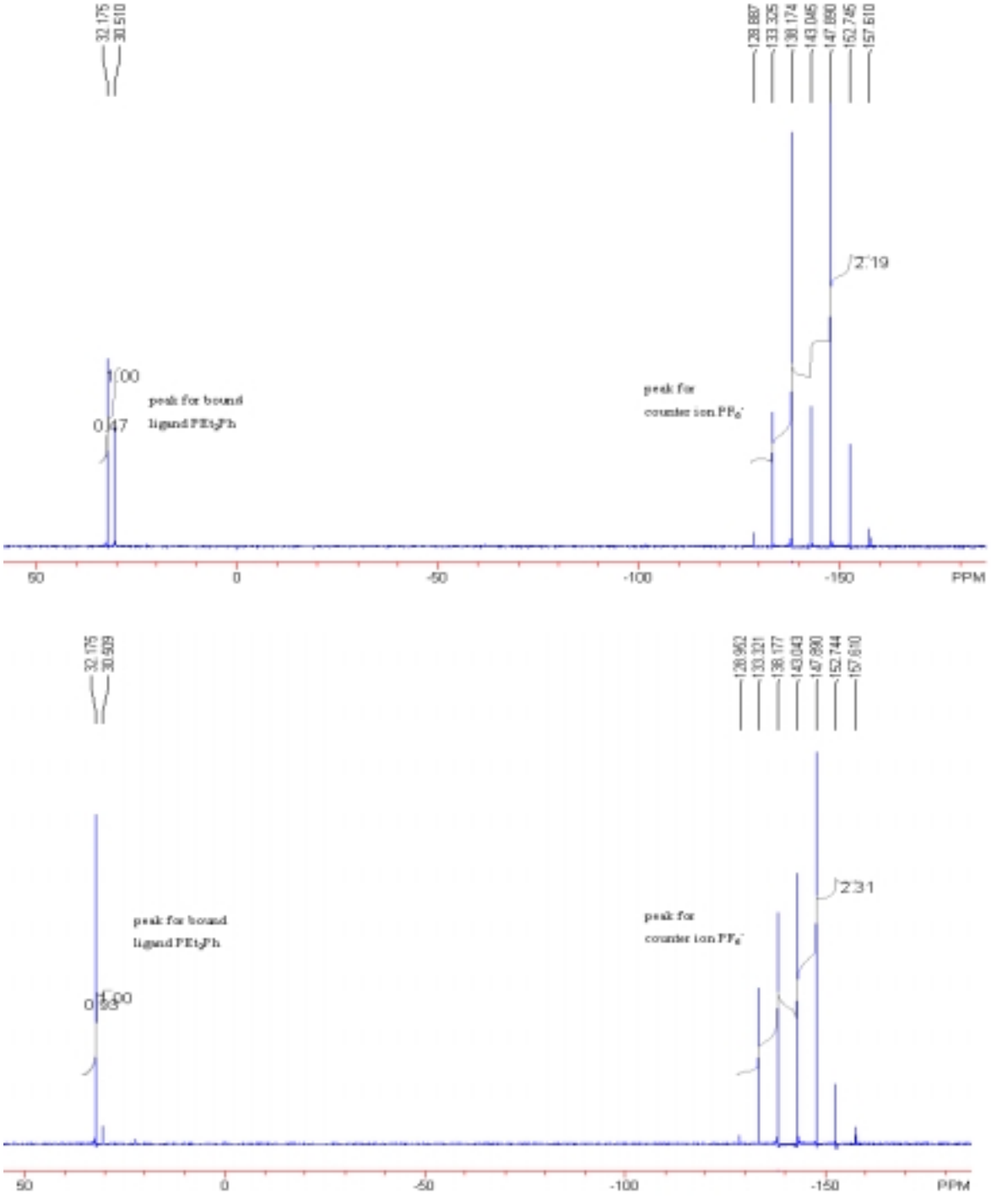

Figure 3.24 ^{31}P NMR spectra for two different samples of $[(tpy)Ru(PEt_2Ph)(dpp)](PF_6)_2$ in CD_3CN at RT.

[(tpy)Ru(PEt$_2$Ph)(dpp)PtCl$_2$](PF$_6$)$_2$

The ^{31}P NMR spectrum for the bimetallic complex, [(tpy)Ru(PEt$_2$Ph)(dpp)PtCl$_2$](PF$_6$)$_2$, is shown in Figure 3.25. This bimetallic is made from the monometallic whose spectrum is the top spectrum in Figure 3.24. Its spectrum is similar to that for the monometallic complex.

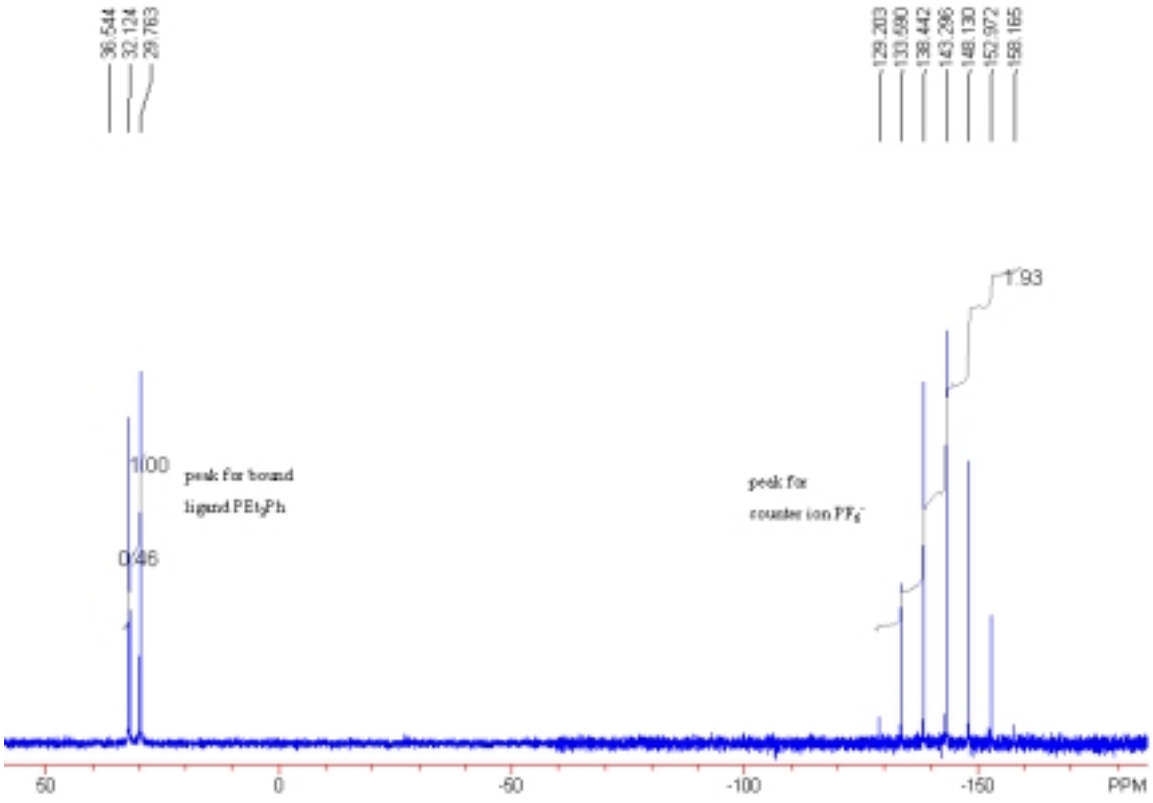

Figure 3.25 ^{31}P NMR for the complex [(tpy)Ru(PEt$_2$Ph)(dpp)PtCl$_2$](PF$_6$)$_2$ in CD$_3$CN at RT.

As above, the peak at –143.3 ppm is assigned as the phosphorus from the PF_6^- counter ion and the other two single peaks at 29.8 ppm and 32.1 ppm are assigned as the phosphorus peak from the bound PEt$_2$Ph ligand. Again the two peaks for PEt$_2$Ph ligand are due to the presence of the two stereoisomers. As in the monometallic complex, the sum of the integration of two singlet peaks keeps a fixed ratio of 1:2 relative to the integration of the

peak for the PF_6^- counter ion while the ratio of the two singlet peaks sometimes changes for different samples.

DNA binding study by non-denaturing agarose gel electrophoresis

Ru-Pt bimetallic complex containing bpm bridging ligand

The DNA interactions of the monometallic and bimetallic complexes containing a bpm bridging ligand were studied using agarose gel electrophoresis. The results are shown in Figure 3.26. The results for two known platinum-based DNA binding agents, cisplatin and the bimetallic complex $[Ru(bpy)_2(dpq)PtCl_2](CF_3SO_3)_2$ [24c], are included for comparison. In Figure 3.26, lanes 1 and 10 contain a molecular weight standard; lanes 2 and 9 contain the linearized plasmid DNA control that was incubated in the absence of the any metal complex; lanes 3 to 8 show the plasmid DNA incubated with varying ratio of the corresponding metal complex, given the bp:mc (bp = DNA base pair, mc = metal complex) ratio of 5:1, 10:1, 20:1, 100:1, 200:1 and 300:1. The highest bp:mc ratio means the lowest relative amount of metal complex. It is clear that for all compounds at high bp:mc ratio, from 100:1 to 300:1, the DNA migrated through the gel at approximately the same rate as the DNA control that was treated with no metal complex. At low bp:mc ratio, from 5:1 to 20:1, the DNA migrated at different rates for the three Pt-containing complexes. The monometallic complex $[(tpy)Ru(PEt_2Ph)(bpm)](PF_6)_2$ did not retard DNA migration even at very low bp:mc ratios. For the DNA binding study standard, cisplatin, the DNA migration through the gel was retarded but to a significantly lower extent than the other two bimetallic complexes. The bimetallic complex $[(tpy)Ru(PEt_2Ph)(bpm)PtCl_2](PF_6)_2$ shows a more pronounced retardation effect on DNA migration at low bp:mc ratios than the cisplatin standard but a less pronounced effect than the $[Ru(bpy)_2(dpq)PtCl_2](CF_3SO_3)_2$ complex. For the two platinum-containing bimetallic complexes, with the decrease of the bp:mc ratio, the intensity of the stained DNA band's emission also decreased. This is attributed to the quenching of the emissions of the fluorescent stain ethidium bromide.[58] The absolute and relative distances traveled by the DNA-metal complexes were measured in mm and are summarized in Table 3.11. The

standard shown in lanes 1 and 10 contains six DNA bands. The lowest molecular weight or most rapidly migrating band was used to normalize migration of the sample bands.

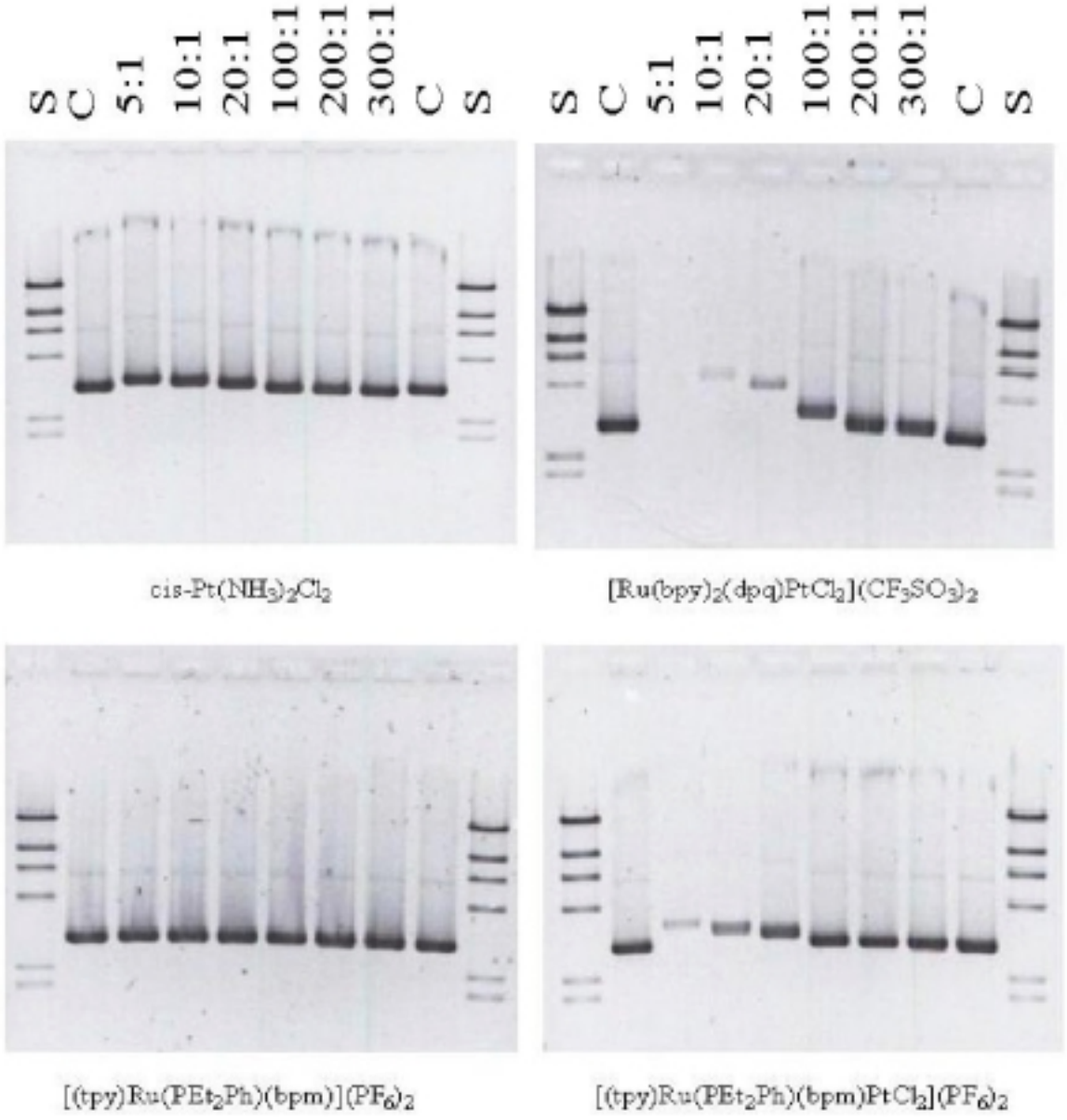

Figure 3.26 Gel electrophoresis results for the complexes containing the bpm ligand.

Table 3.11 Absolute and relative migration distance of the DNA-metal complex containing bpm ligand in the non-denaturing agarose gel electrophoresis study [a,b].

Complex Lanes	cis-$Pt(NH_3)_2Cl_2$	$[Ru(bpy)_2(dpq)PtCl_2](CF_3SO_3)_2$	$[(tpy)Ru(PEt_2Ph)(bpm)](PF_6)_2$	$[(tpy)Ru(PEt_2Ph)(bpm)PtCl_2](PF_6)_2$
Standard[c]	30.0/1.15	25.0/1.15	29.0/1.15	27.6/1.15
Control[c]	26.1/1.00	21.8/1.00	25.2/1.00	24.0/1.00
BP:Metal 5:1	24.8/0.95	15.4/0.706	24.8/0.984	21.5/0.896
BP:Metal 10:1	25.0/0.958	17.0/0.780	24.8/0.984	22.0/0.917
BP:Metal 20:1	25.2/0.966	17.6/0.807	24.8/0.984	22.3/0.929
BP:Metal 100:1	25.5/0.977	20.0/0.917	24.8/0.984	23.0/0.958
BP:Metal 200:1	25.7/0.985	21.0/0.963	24.8/0.984	23.4/0.975
BP:Metal 300:1	25.9/0.992	21.2/0.968	24.8/0.984	23.7/0.988

[a] The absolute migration distances (in mm) and relative distances are separated by a slash.

[b] The relative migration distances are calculated against the average of absolute migration distances for two controls in each gel.

[c] The absolute migration distances for the molecular weight standard and the control are the average of two distances values (the distance between the well and the first band in these lanes) collected from two lanes in each gel.

McMillin and coworkers have shown that $[Pt(tpy)X]^+$ (X=Cl, OH, CH_3CN) is a bifunctional DNA-binding agent that competitively binds to DNA covalently through the platinum(II) metal site and intercalatively through the terminal ligand tpy.[28] This

suggested that the new bimetallic complex, $[(tpy)Ru(PEt_2Ph)(bpm)PtCl_2](PF_6)_2$, also has two possible modes of binding to DNA, even though no report about tpy intercalation to DNA from octahedral complexes. Previous studies in our group have shown that covalent binding appears to be necessary to alter DNA migration through the gel.[24] Our monometallic complex $[(tpy)Ru(PEt_2Ph)(bpm)](PF_6)_2$ does not have the cis-$Pt^{II}Cl_2$ moiety and could not bind to DNA in a covalent manner. Comparison of the gel electrophoresis results for the monometallic and bimetallic complexes at low bp:mc ratios strongly suggest that covalent binding to DNA through the Pt^{II} metal center is responsible for retardation of DNA migration in the agarose gel.

In the agarose gel electrophoresis experiments, covalent binding to DNA through the platinum(II) metal site alters DNA migration through the gel by changing molecular weight, molecular shape and molecular charge of the DNA fragment.[24c] Although the voltage applied in the electrophoresis experiment has a large impact on DNA migration rate, it does not account for the differences observed for the various DNA-binding agents as all of the electrophoresis experiments were performed at the same voltage of 105 V.

Based on molecular weight considerations, one would expect binding of cisplatin and the other two bimetallic complexes to impact DNA migration differently. The complexes $[Ru(bpy)_2(dpq)PtCl_2](CF_3SO_3)_2$ (increasing DNA molecular weight by 894 g/mole) and $[(tpy)Ru(PEt_2Ph)(bpm)PtCl_2](PF_6)_2$ (increasing DNA molecular weight by 854 g/mol) have much greater molecular weights than the cisplatin (increasing DNA molecular weight by 229 g/mol) standard and therefore these two complexes are expected to have more pronounced molecular weight-based retardation effects on DNA migration than cisplatin. This is consistent with the observed results. However, the significantly different retardation effects between these two bimetallic complexes on DNA migration could not be satisfactorily explained by molecular weight difference alone, as the two complexes are very similar in molecular weight.

The change in DNA charge from metal binding will also impact DNA migration in gel electrophoresis. The DNA strand has an overall negative charge due to the sugar phosphate backbone. When the metal complexes bind to DNA a decrease in the overall negative charge results due to the cationic metal center. The two bimetallic complexes, $[Ru(bpy)_2(dpq)PtCl_2](CF_3SO_3)_2$ and $[(tpy)Ru(PEt_2Ph)(bpm)PtCl_2](PF_6)_2$, become 4^+ cations upon substitution of the two chloride ligands on platinum(II) metal by water before binding to the DNA strand. Cisplatin becomes the generally-accepted active species[35, 37a, 38b] $[Pt(NH_3)_2(H_2O)_2]^{2+}$, which is a 2^+ cation prior to the binding to DNA strand. So it will decrease the DNA overall negative charge by 4 per complex binding for the bimetallic complexes relative to 2 per complex binding for cisplatin. Therefore DNA bound to cisplatin has a larger negative charge than DNA bound with equivalent amount of either the two bimetallic complexes and is expected to migrate faster in the gel electrophoresis experiments. This factor may contribute to the different migration rates of DNA bound with the bimetallic complexes versus that bound with cisplatin. However, speculated above, if the two bimetallic complexes, $[Ru(bpy)_2(dpq)PtCl_2](CF_3SO_3)_2$ and $[(tpy)Ru(PEt_2Ph)(bpm)PtCl_2](PF_6)_2$, bind to DNA with the same efficiency, the migration rate difference of the DNA bound with either complex could also not be explained by difference in charge.

The molecular shape of DNA is a third factor that can have a dramatic effect on DNA migration in gel electrophoresis.[24c] There is an obvious difference between the cisplatin standard and the two bimetallic complexes in the experiments shown in Figure 3.26. The DNA bound to cisplatin standard forms a much tighter band in terms of molecular size than the two ruthenium-platinum bimetallic complexes. Cisplatin is generally accepted to form a variety of adducts with DNA[38c,74,75], primarily (>90%) by 1,2 intrastrand crosslinks at adjacent purine bases.The bimetallic complex $[Ru(bpy)_2(dpq)PtCl_2](CF_3SO_3)_2$ exhibits DNA binding that is primarily intrastrand crosslink in nature but has more interstrand crosslinks with DNA than does cisplatin.[24b,c] Since in our native gel electrophoresis experiments the DNA is in a double-stranded

form, both interstrand and intrastrand crosslinks can produce differences in the shape of the linearized plasmid DNA. According to the work of Marzilli, platinum-based anticancer agents sometimes induce an unusual hairpinlike structure in DNA.[76] However, how one complex impacts DNA shape relative to the other, especially in our case, is still unclear. The dramatic difference in migration of DNA bound with the bimetallic complexes, $[(tpy)Ru(PEt_2Ph)(bpm)PtCl_2](PF_6)_2$ or $[Ru(bpy)_2(dpq)PtCl_2](CF_3SO_3)_2$, relative to cisplatin points to a more pronounced impact of metal binding on DNA shape.

The difference in the retardation effects of $[(tpy)Ru(PEt_2Ph)(bpm)PtCl_2](PF_6)_2$ and $[Ru(bpy)_2(dpq)PtCl_2](CF_3SO_3)_2$ on DNA migration is still unclear and requires further study. There are three striking structural differences between these two complexes: a tridentate terminal ligand tpy in the new complex versus two bidentate terminal ligands bpy in $[Ru(bpy)_2(dpq)PtCl_2](CF_3SO_3)_2$, the small bpm bridging ligand in the new complex versus quite bulky dpq bridging ligand in $[Ru(bpy)_2(dpq)PtCl_2](CF_3SO_3)_2$, and the unique phosphine ligand PEt_2Ph only in the new complex. The incorporation of the PEt_2Ph ligand will influence sterically or electronically the nature of the ruthenium(II) center and indirectly the nature of the platinum(II) metal center. All these structural differences might contribute to the observed migration rate difference of the bound DNA either by affecting the binding mode and/or binding efficiency. It is important to realize that the exact nature of the DNA-metal complex interaction in these experiments is not known. Studies are in progress to probe the DNA binding to these complexes in more detail.[77]

Ru-Pt bimetallic complex containing dpp bridging ligand

DNA binding of the monometallic and bimetallic complexes containing a dpp bridging ligand was also studied using agarose gel electrophoresis. The results are shown in Figure 3.27. The absolute and relative distances traveled by DNA-metal complex were measured in the same manner as for the analogs containing bpm and are summarized in Table 3.12. The gels for cis-$Pt(NH_3)_2Cl_2$ and $[Ru(bpy)_2(dpq)PtCl_2](CF_3SO_3)_2$ are the exact same gels as in Figure 3.26. The results are very similar to what was observed for the bpm analogs containing bpm as the bridging ligand. This provides good evidence that this class of compounds, with a tridentate tpy terminal ligand and a PEt_2Ph ligand on the remote metal center, form a new type of DNA binding agent and produce different

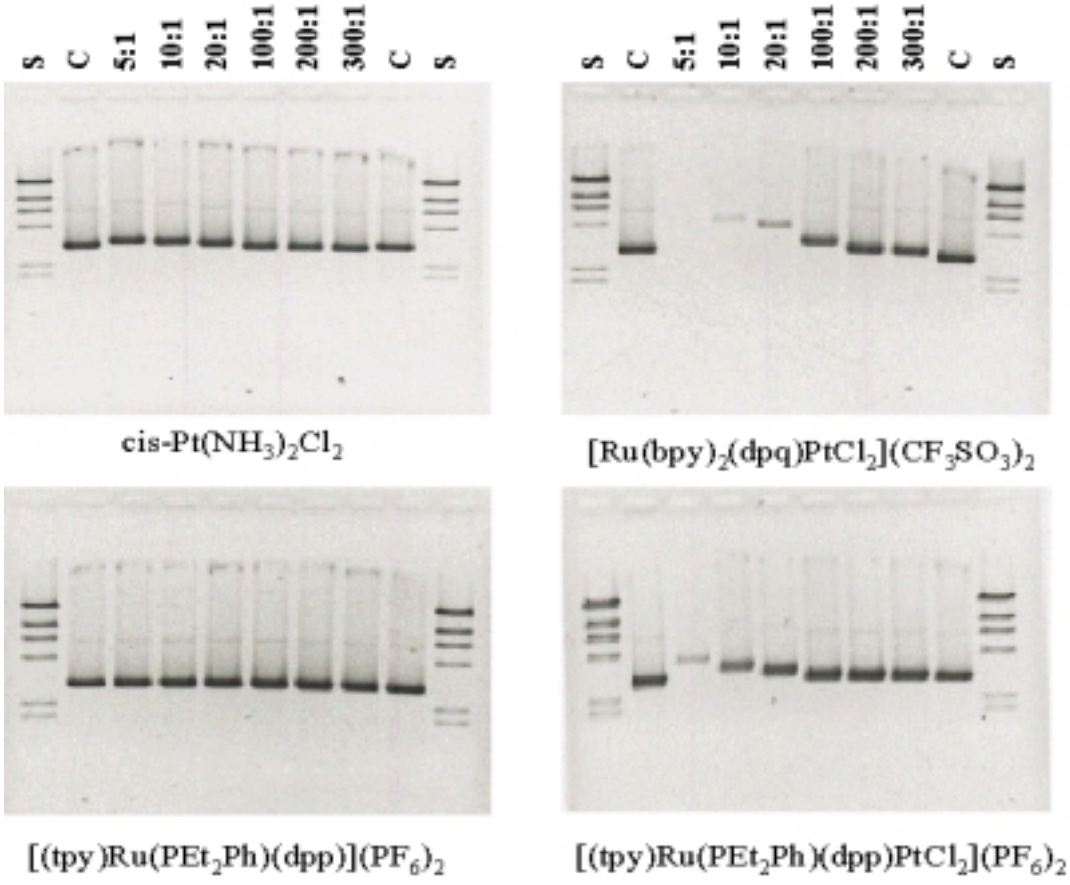

Figure 3.27 Gel electrophoresis results for the complexes containing the dpp ligand.

retardation effects on DNA migration through the agarose gel from complexes such as $[Ru(bpy)_2(dpq)PtCl_2](CF_3SO_3)_2$. The dpp bimetallic complex retards DNA migration more than the bpm analog at low bp:mc (5:1) ratio. This might be because the larger size of the dpp bridging ligand makes the bound DNA fragment more bulky. At high bp:mc ratios, the bpm and dpp analogs retard DNA migration almost to the same extent.

Table 3.12 Absolute and relative migration distance of the DNA-Metal Complex containing dpp ligand in the non-denaturing agarose gel electrophoresis study [a,b].

Complex Lanes	cis-$Pt(NH_3)_2Cl_2$	$[Ru(bpy)_2(dpq)PtCl_2](CF_3SO_3)_2$	$[(tpy)Ru(PEt_2Ph)(dpp)](PF_6)_2$	$[(tpy)Ru(PEt_2Ph)(dpp)PtCl_2](PF_6)_2$
Standard [c]	30.0/1.15	25.0/1.15	29.0/1.14	27.6/1.15
Control [c]	26.1/1.00	21.8/1.00	25.4/1.00	24.0/1.00
BP:Metal 5:1	24.8/0.95	15.4/0.706	25.1/0.988	20.8/0.867
BP:Metal 10:1	25.0/0.958	17.0/0.780	25.1/0.988	21.8/0.908
BP:Metal 20:1	25.2/0.966	17.6/0.807	25.1/0.988	22.2/0.925
BP:Metal 100:1	25.5/0.977	20.0/0.917	25.1/0.988	23.0/0.958
BP:Metal 200:1	25.7/0.985	21.0/0.963	25.1/0.988	23.3/0.971
BP:Metal 300:1	25.9/0.992	21.2/0.968	25.1/0.988	23.7/0.988

a The absolute migration distances (in mm) and relative distances are separated by a slash.

b The relative migration distance is calculated against the average of absolute migration distances for two controls in each gel.

c The absolute migration distances for the molecular weight standard and the control are the average of the two distances (the distance between the well and the first band in these lanes) collected from two lane in each gel.

Chapter 4: Conclusions and Future Work

Conclusion

The Ru-Pt bimetallic complexes containing the bridging ligands, bpm or dpp, and precursors were designed, successfully synthesized and characterized. The synthesis followed a building block approach, allowing variation of each part of the supramolecular system. The final bimetallic complexes were made without need for alumina chromatography purification, which is very important to labile cis-$Pt^{II}Cl_2$ site.

The bimetallic complexes and all of their monometallic precursors were fully characterized by FAB MS, electrochemistry, electronic absorption spectroscopy and ^{31}P and ^{1}H NMR. The FAB MS spectra of the complexes is characterized by the appearance of the parent ion peaks $[M\text{-}PF_6]^+$. The fragments observed are characteristic of the loss of counter ions, intact ligands and/or metals. The cyclic voltammogram of all complexes show observable metal based oxidation(s) and ligand based reductions. The change of the redox potential is consistent with the variation of the ligand set and the coordination of the additional metal centers. Substitution of the chloride with phosphine ligand, PEt_2Ph, in the monometallic complexes $[(tpy)RuCl(BL)](PF_6)$ (BL = bpm or dpp) shift the ruthenium(II) based oxidations to significantly more positive potentials. Coordination of the platinum(II) metal center to the monometallic complexes $[(tpy)Ru(PEt_2Ph)(BL)](PF_6)_2$ (BL = bpm or dpp) significantly shift the bridging ligands based first reductions to less negative potentials. The electronic absorption spectra of the complexes are characteristic of the lowest lying MLCT transitions and the higher energy bridging and terminal ligands $\pi \rightarrow \pi^*$ transitions. Substitution of the chloride with PEt_2Ph blue shifts the lowest lying MLCT transitions while coordination of the platinum(II) metal center red shifts the MLCT transitions. The electronic absorption data are

consistent with the electrochemical data. The ^{31}P NMR technique provides a very efficient and easy characterization method for the complexes.

The DNA binding activity of the bimetallic complex was studied by non-denaturing agarose gel electrophoresis, which showed that these bimetallic complexes can bind to DNA through the cis-$Pt^{II}Cl_2$ moiety and this binding has a more pronounced retardation effect on DNA migration than cis-$[Pt(NH_3)_2Cl_2]$ (cisplatin), but less than $[Ru(bpy)_2(dpq)PtCl_2](CF_3SO_3)_2$. The DNA binding study established these tagged bimetallic complexes as a new kind of DNA binding agent.

Future work

The Ru-Pt bimetallic complexes synthesized in this project have PF_6^- as the counter ion and do not have good solubility in water. This imposes a limit on the DNA-metal complex interaction study via ^{31}P NMR, for DNA studies need to be carried out in aqueous solutions. Future work could therefore include the synthesis of analogs with better water solubility. This might be achieved by changing the counter ion from PF_6^- to $CF_3SO_3^-$.[24a] There are two possible ways to change the counter ions: (1) change the counter ions during the synthetic pathway or (2) change the counter ions using ion-exchange chromatography. The study of DNA-metal complex interaction could then be carried out using ^{31}P NMR method with the analogs of improved water solubility.

The other possible future work could include making Ru-Pt bimetallic complexes with varied terminal ligands as well bridging ligands. The change of the ligand sets in the remote metal center would have steric and electronic impact on the whole supramolecular systems and therefore allow further exploration of structure-activity relationships. Tuning of the ligand sets could also possibly make these complexes much better DNA binding

agents that could be photoactivated upon exposure to photons of a specific wavelength in the near IR region.

The third possibility for future work would include searching the alternatives of the tag ligand PEt_2Ph that could provide characterization using simpler methods than NMR. One possibility is the use of CO for IR probing.

Finally, it is vey desirable as well as necessary to know the modes and efficiency of binding to DNA by the new bimetallic complexes. The denaturing gel electrophoresis experiment is a good tool for the binding modes study. For the binding efficiency study, it is possible to take advantage of the fact the DNA binding studies was carried out in aqueous solutions. We can add some solvents that are insoluble to water but can dissolve our metal complexes into the DNA-metal complex reaction mixture. This would allow the separation of the unreacted metal complexes and therefore indirect detection of DNA binding efficiency.

References

1 (a) Sabbatini, N.; Balzani, V., *J. Am. Chem. Soc*., **1972**, *94*, 7587; (b) Balzani, V.; Moggi, L.; Manfin, M.F.; Bolletta, F.; Laurence, G.A., *Coord. Chem. Rev*., **1975**, *15*, 321.

2 (a)Gafney, H.D.; Adamson, A.W., *J. Am. Chem. Soc*., **1979**, *94*, 8238; (b) Demas, J.N.; Adamson, A.W., *J. Am. Chem. Soc*., **1972**, *93*, 1800.

3 (a) Bock, C.R.; Meyer, T.J.; Whitten, D.G., *J. Am. Chem. Soc*., **1974**, *96*, 4710; (b) Bock, C.R.; Connor, J.A.; Gutierrez, A.R.; Meyer, T.J.; Whitten, D.G.; Sullivan, B.P.; Nagle, J.K., *J. Am. Chem. Soc*., **1979**, *101*, 4815; (c) Meyer, T.J., *Acc. Chem. Res*., **1978**, *11*, 94.

4 Bard, A.J.; Faulkner, L.R., *Electrochemical Methods, Fundamentals and Applications* **1980**, John Wiley and Sons, New York, 213.

5 Kalyanasundaram, K., *Coord. Chem. Rev*. **1982**, *46*, 159.

6 Juris, A.; Balzani, V.; Barigelletti, F.; Campagna, S.; Belser, P.; Von Zelewsky, A., *Coord Chem. Rev*. **1988**, *84*, 85.

7 Krausz, E.; Ferguson, J., *Prog. Inorg. Chem*. **1989**, *37*, 293.

8 Balzani, V.; Scando, F., *Supramolecular Photochemistry*, Horwood: Chichester, England, **1990**.

9 Ramamurthy,V.; Schanze, K.S., *Multimetallic and Macromolecular Inorganic Photochemistry*, Marcel Dekker, Inc, **1999**, p 151-183.

10 Winkler, J.R.; Netzel, T.L.; Creutz, C.; Sutin, N., *J. Amer. Chem. Soc*. **1987**, *109*, 2381.

11 Van Houten, J.; Watts, R.J., *J. Amer. Chem. Soc*. **1975**, *97*, 3843.

12 (a) Kirchhoff, J.R.; McMillin, D.R.; Marnot, P.A.; Sauvage, J.-P, *J. Amer. Chem. Soc*. **1985**, *107*, 1138. (b) Calvert, J.M.; Caspar,, J.V.; Binstead, R.A.; Westmoreland, T.D.; Meyer, T.J., *J. Amer. Chem. Soc*. **1982**, *104*, 6620.

13 (a) Hecker, C.R.; Fanwick, P.E.; McMillin, D.R., *Inorg. Chem*. **1991,** *30*, 659. (b) Leisning, R.A.; Kubow, S.A.; Churchill, M.R.; Buttery, L.A.; Ziller, J.W.; Takeuchi,

K.J., *Inorg. Chem*. **1990**, *29*, 1306. (c) Constable, E.C.; Cargill Thompson, A.M.W.; Tocher, D.A.; Daniels, M.A.M.N., *J. Chem*. **1992**, *16*, 855.

14 Balzani, V.; Juris, A.; Venturi, M.; Campagna, S.; Seroni, S., *Coord Chem. Rev*. **1996**, *96*, 759.

15 (a) Molnar, S.M; Nallas, G.; Bridgewater, J.S; Brewer, K.J., *J. Am. Chem. Soc*. **1994**, *116*, 5206 (b) Molnar, S.M.; Jensen, G.E.; Volger, L.M.; Jones, S.W.; Laverman, L.; Bridgewater, J.S.; Richter, M.M.; Brewer, K.J., *J. Photochem. Photobiol. A: Chem.* **1994**, *80*, 315 (c) Bridgewater, J.S.; Volger, L.M.; Molnar, S.M.; Brewer, K.J., *Inorg. Chim. Acta* **1993**, *208*, 179 (d) Rasmussen, S.C.; Richter, M.M.; Yi, E.; Place, H.; Brewer, K.J., *Inorg. Chem*. **1990**, *29*, 3926

16 Petersen, J.D.; Murphy, Jr., W.R.; Sahai, R.; Brewer, K.J.; Ruminski, R.R., *Coord Chem. Rev*. **1985**, *64*, 261.

17 Braustein, C.H.; Baker, A.D.; Streakas, T.C; Gafney, H.D. *Inorg. Chem*. **1984**, *23*, 857.

18 Hunziker, M.; Ludi, A., *J. Am. Chem. Soc*. **1977**, *99*, 7370.

19 (a) Rillema, D.P.; Mack, K.B.; *Inorg. Chem*. **1982**, *21*, 3849 (b) Rillema, D.P; Allen, G.; Meyer, T.J.; Conrad, D., *Inorg. Chem*. **1983**, *22*, 1617 (c) Sahai, R.; Morgan, L.; Rillema, D.P., *Inorg. Chem*, **1988**, *27*, 3495.

20 Krejcik, M.; Vlcek, A.A., ***Inorg. Chem***. **1992**, *31*, 2390.

21 Pavinato, R.A.; Walk, J.A.; McGuire, M.E., *Inorg. Chem*. **1993**, *32*, 4982

22 (a) Sahai, R.; Rillema, D.P., *J. Chem. Soc., Chem Commun.*,**1986**, 1133;
(b) Sahai, R.; Baucom, D.A.; Rillema, D.P., *Inorg. Chem*., **1986**, *25*, 3843.

23 (a) Yam, V.; Lee, V.; Cheung, K., *J. Chem. Soc., Chem Commun*., **1994**, 2075; (b) Yam, V.; Tam, K.K.; Lai, T.F., *J. Chem. Soc., Dalton Trans*., **1993**, 651; (c) Yam, V.; Choi, S.W.K.; Lai, T.F.; Lee, W.K., *J. Chem. Soc., Dalton Trans*, **1993**, 1001;

24 (a) Milkevitch, M.; Brauns, E.; Brewer, K.J., *Inorg. Chem*. **1996**, *35*, 1737
(b) Milkevitch, M.; Shirley, B.W.; Brewer, K.J., Inorg. Chim. Acta **1997**, *264*, 249
(c) Milkevitch, M.; Storrie, H.; Brauns, E.; Brewer, K.J.; Shirley, B.W., *Inorg. Chem*. **1997**, *36*, 4535.

25 Rosenberg, B.; Van Camp, L.; Krigas, T., *Nature* **1965**, *205*, 698.

26 Sherman, S.E.; Lippard, S.J., *Chem. Rev*. **1987**, *87*, 1153.

27 (a) Aldridge, T.K.; Stacy, E.M.; McMillin, D.R., *Inorg. Chem*. **1994**, *33*, 722 (b) McMillin, D.R.; Liu, F.; Meadows, K.A.; Aldridge, T.K.; Hudson, B.P., *Coord. Chem. Rev*. **1994**, *132*, 105.

28 (a) Peyratout, C.S.; Aldridge, T.K.; Crites, D.K.; McMillin, D.R., *Inorg. Chem*. **1995**, *34*, 4484; (b) Buchner, R.; Field, J.S.; Haines, R.J.; McMillin, D.R., *Inorg. Chem*., **1997**, *36*, 3952; (c) Crites, D.K.; Cunningham, C.T.; McMillin, D.R., *Inorg. Chim. Acta.*, **1998**, *273*, 346.

29 Rosenberg, B.; Van Camp, L.; Trosko, J.E.; Mansour, V.H., *Nature* **1969**, *222*, 385.

30 Rugge, J. et al, *Origins of Human Cancer*; Coldspring Harbor Laboratory Press; **1991**, p147-148.

31 Franks, L.M.; Teich, N.M., *Introduction to the Cellular and Molecular Biology of Cancer*, Oxford University Press, **1986**, p 1-3, 27-34, 363-367.

32 (a) Chaloner, P.A.; *Coord. Chem. Rev.* **1986**, *71*, p 64, 68-72. (b) Takahara, P.M.; Frederik, C.A.; Lippard, S.J., *J. Amer Chem. Soc.* **1996**, *118*, 12309. (c) Hartley, F.R., *Coord. Chem. Rev.* **1985**, *67*, 35. (d) Chaloner, P.A., *Coordination Chemistry Reviews* **1986**, *72*, 281.

33 (a) Huang, H.; Woo, J.; Ally, S.C.; Hopkins, P.B., *Bioorganic & Medical Chemistry* **1995**, *3*, 659.

34 Kobayashi, S.; Furukawa, M.; Hamajima, H.; Arai, T.; Ihsii,Y.; Tobinaga, S.; Tanaka, A., *Nucleic Acids Symposium* **1993**, *29*, 137.

35 Bloemink, M.J; Reedijk, J., *Metal Ions in Biological Systems* **1996**, *32*, 641.

36 Clarke, M.J.; Stubbs, M., *Metal Ions in Biological Systems* **1996**, *32*, 727.

37 (a) Zable, D.B.; Lippard, S.J., *Trends Biochem. Sci.* **1995**, *20*, 435. (b) Whitehead, J.P; Lippard, S.J., *Met. Ions. Biol. Syst*., **1996**, *32*, 687.

38 (a) Bruhm, S.J.; Toney, J.H.; Lippard, S.J., *Coord. Chem. Rev*. **1990**, *100*, 293. (b) Sherman, S.E.; Lippard, S.J., *Chem. Rev.* **1987**, *87*, 1153. (c) Takahara, P.M.; Rosenzweis, A.C.; Frederick, P.M.; Lippard, S.J., *Nature* **1995**, *377*, 649. (d) Brown,

S.J.; Kellett, P.J.; Lippard, S.J., *Science* **1993**, *261*, 603; (e) Ziegler, C.J.; Silverman, A.P.; Lippard, S.J., *J Biol Inorg Chem* **2000**, *5*, 774; (f) Sandman, K.E.; Lippard, S.J., *Cisplatin*; Verlag Helvetica Chimica Acta, Zurich, Switzland; **1999**, p 523-536.

39 Pendyla, L. Kidoni, Y.; Perz, R.; Wilkes, J.; Bernacki, R.J.; Creaven, P.J., *Cancer Lett.* **1995**, *97*, 117.

40 Yoshido, M.; Khokhar, A.R.; Siddik, Z.H., *Anticancer Drug Des*. **1994**, *9*, 425.

41 Blommaert, F. A., van dijk-Kinjnenburg, H.C.M.; Dijt, F.J.; den Engelse, L.; Baan, R.A.; Berends, F.; Fichtinger-Scheptman, A.M.J., *Biochemistry* **1995**, *34*, 8474.

42 Amato, R.J.; Ellerhorst, J.; Banks, M.; Logothetis, C.J., *Eur. J. Cancer* **1995**, *31A*, 2223.

43 Weiss, R.B.; Christian, M.C., *Drugs* **1993**, *46*, 360.

44 (a) Barton, J.K.; Danishefsky, A.T.; Goldberg, J.M., *J. Amer. Chem. Soc*. **1984**, *106*, 2172. (b) Barton, J.K., *Science* **1986**, *233*, 727. (c) Barton, J.K.; Goldberg, J.M.; Kumar, C.V.; Turro, N.J., *J. Amer. Chem. Soc*. **1986**, *108*, 2081. (d) David, S.S.; Barton, J.K., *J. Amer. Chem. Soc.* **1993**, *113*, 2984. (e) Turro, C.; Bossmann, S.H.; Jenkins, Y.; Barton, J.K.; Turro, N.J., *J. Amer. Chem. Soc*. **1995**, *117*, 9026. (f) Holmlin, R.E.; Barton, J.K., *Inorg. Chem*. **1995**, *34*, 7.

45 (a) Morgan, R.J.; Chartterjee, S.; Baker, A.D.; Strekas, T.C., *Inorg Chem*. **1991**, *30*, 2687. (b) Tysoe, S.A.; Morgan, R.J.; Baker, A.D.; Strekas, T.C., *J. Phys. Chem*. **1993**, *97*, 1707.

46 Sigman, D.S.; Mazumder, A.; Perrin, D.M., *Chem Rev*. **1993**, *93*, 2295.

47 Satyanarayana, S.; Dabrowiak, J.C.; Chaires, J.B, *Biochemistry* **1993**, *32*, 2573.

48 Lecomte, J-P.; DeMesmaeker, A.K.; Orellana, G., *J. Phys. Chem*. **1994**, *98*, 5382.

49 Naing, K.; Takahashi, M.; Taniguchi, M.; Yamagishi, A., *Inorg. Chem*. **1995**, *34*, 350.

50 Atounaguiri, S.; Maiya, B.G., *Inorg. Chem*. **1996**, *35*, 4267.

51 Carlson, D.L.; Huchital, D.H.; Mantilla, E.J.; Sheardy, R.D.; Murphy, W.R., *J. Am. Chem. Soc*. **1993**, *115*, 6424.

52 (a) Mital, R.; Ray, K.S.; Srivastava, T.S.; Bhattacharya, R.K., *J. Inorg. Biochem*. **1986**, *27*, 133. (c) Mital, S.;Srivastava, T.S.; Parekh, H.K.; Chitnis, M.P., *J. Inorg. Biochem*. **1991**, *41*, 93.

53 Rickwood, D.; Hames, B.D., *Gel electrophoresis of nucleic acids*, Oxford University Press, **1990**, 2nd edition, p 51-59.

54 Fangman, W.L., *Nucleic Acid Res* **1978**, *5*, 653.

55 Sullivan, B. P.; Calvert, J. M.; Meyer, T. J., *Inorg. Chem.* **1980**, *19*, 1404.

56 Vogler, L. M.; Franco, C.; Jones, S. W.; Brewer, K. J., *Inorg. Chim. Acta* **1994**, *221*, 55.

57 Sahai, R.; Rillema, D. P., *Inorg. Chim. Acta* **1986**, *118*, L35.

58 Milkevitch, M., *PhD dissertation*, Virginia Polytechnic Institute and State University, **2000**.

59 Ish-Horowitz, D.; Burke, J. F., *Nucl. Acids Res.* **1981**, *9*, 2989.

60 Ausubel, F.; Brent, R.; Kingston, R. E.; Moore, D. D.; Seidman, J. G.; Smith, J. A.; Struhl, R., *Short Protocols in Molecular Biology, 3rd ed*.; Wiley: New York, **1995**.

61 Williams, L; Brewer, K.J., Work in progress.

62 Bard, A.J.; Faulkner, L.R., *Electrochemical Methods, Fundamentals and Applications* **1980**, John Wiley and Sons, New York, 701.

63 Jones, S. W., PhD dissertation, Virginia Polytechnic Institute and State University, 1998.

64 (a) Muller, N.; Lauterbur, P. C.; Goldensun, J., *J. Amer. Chem. Soc.* **1956**, *78*, 3357. (b) Albrand, J. P.; Cogne, A.; Robert, J.-B., *Chem. Phys. Lett*, **1977**, *48*, 524.

65 Thummel, R. P.; Chirayil, S., *Inorg. Chim. Acta* **1988**, *154*, 77.

66 Klein, A.; Kaim, W.; Horung, F. M.; Fileder, J.; Zalis, S., *Inorg. Chim. Acta* **1997**, *264*, 269.

67 Prederi, G.; Vignali, C.; Denti, G.; Ferroni, S., *Inorg. Chim. Acta* **1993**, *205*, 145.

68 Gottlieb, H. E.; Kotlyar, V.; Nudelman, A., *J. org. Chem.* **1997**, *62*, 7512.

69 Goodwin, H.A.; Lions, F., *J. Amer. Chem. Soc.* **1959**, *81*, 6415.

70 Escuer, A.; Comas, T.; Ribas, J., Vicente, R.; Solans, X.; Zanchini, C. and Gatteshi, D., *Inorg. Chim. Acta* **1989**, *162*, 97.

71 Buu-Hoi, N.P.; Saint-Ruf, G., *J. Chem. Soc*., **1961**, 2259.

72 Trusell, F.C.; McKenzie, W.F., *Anal. Chim. Acta*, **1968**, *40*, 350.

73 Stephen, W.I.; Uden, P.C., *Anal. Chim. Acta*, **1967**, *39*, 357.

74 Huang, H.; Zhu, L.; Reid, B.R.; Drobny, G.P., and Hopkins, P.B., *Science* **1995**, *270*, 1842.

75 Fichtinger-Schepman A.M.; van der Veer, J.L.; den Hartog, J.H.; Lohma, P.H.; and Reedijk, J., *Biochemistry* **1985**, *24*, 707.

76 Yohannes, P.G.; Zon, G.; Doetsch, P.W.; Marzilli, L.G., *J. Amer. Chem. Soc*. **1993**, *115*, 5105. (b) Iwamoto, M.; Mukandan, S., Jr.; Marzilli, L.G., *J. Amer. Chem. Soc*. **1994**, *116*, 6238.

77 Fang, Z.; Swavey, S.; Winkel, B.S.; Brewer, K.J., work in progress.

Appendix 1

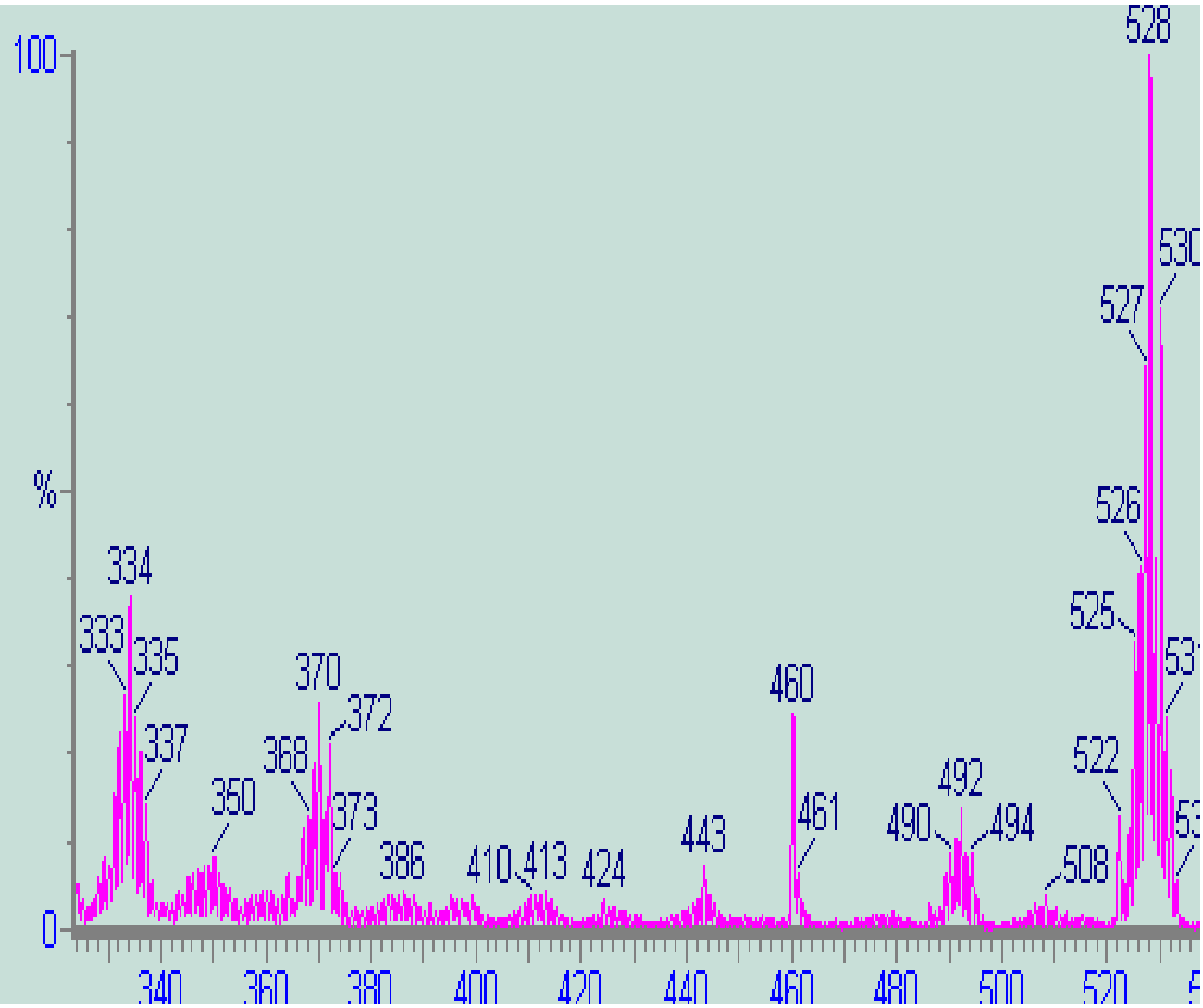

FAB MS spectrum for [(tpy)RuCl(bpm)](PF_6)

Appendix 2

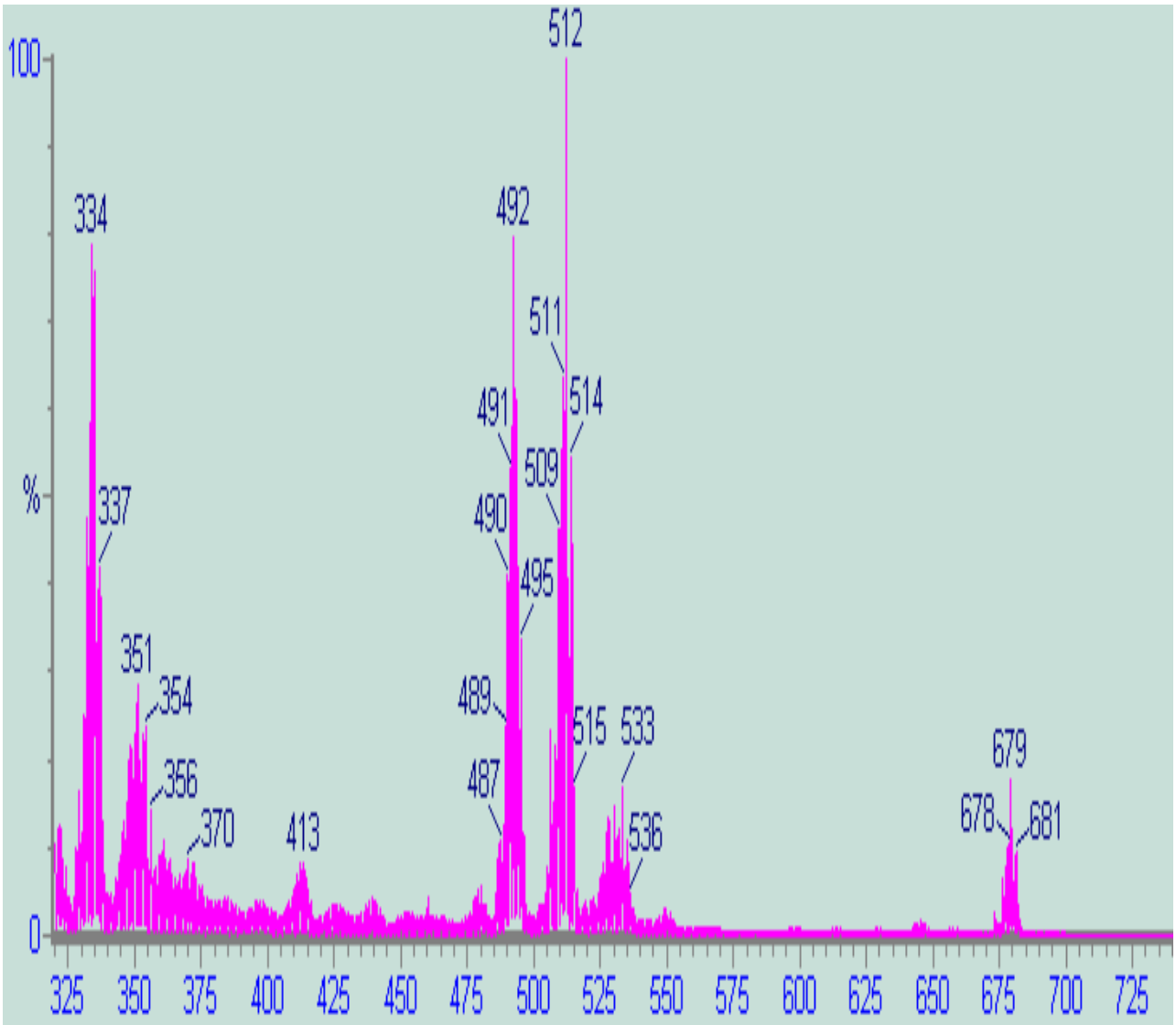

FAB MS spectrum for $[(tpy)Ru(CH_3CN)(bpm)](PF_6)_2$

Appendix 3

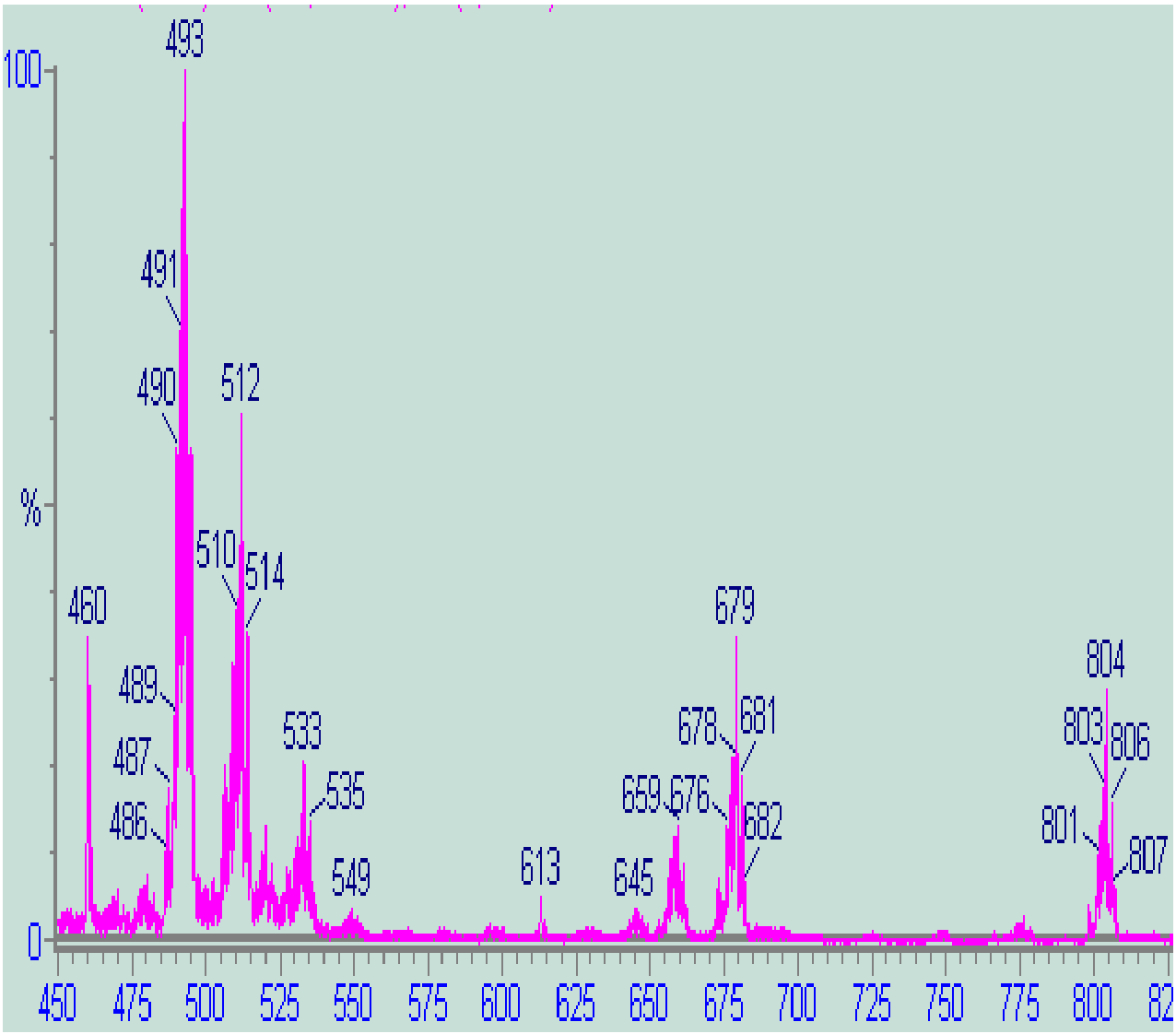

FAB MS spectrum for [(tpy)Ru(PEt_2Ph)(bpm)](PF_6)$_2$

Appendix 4

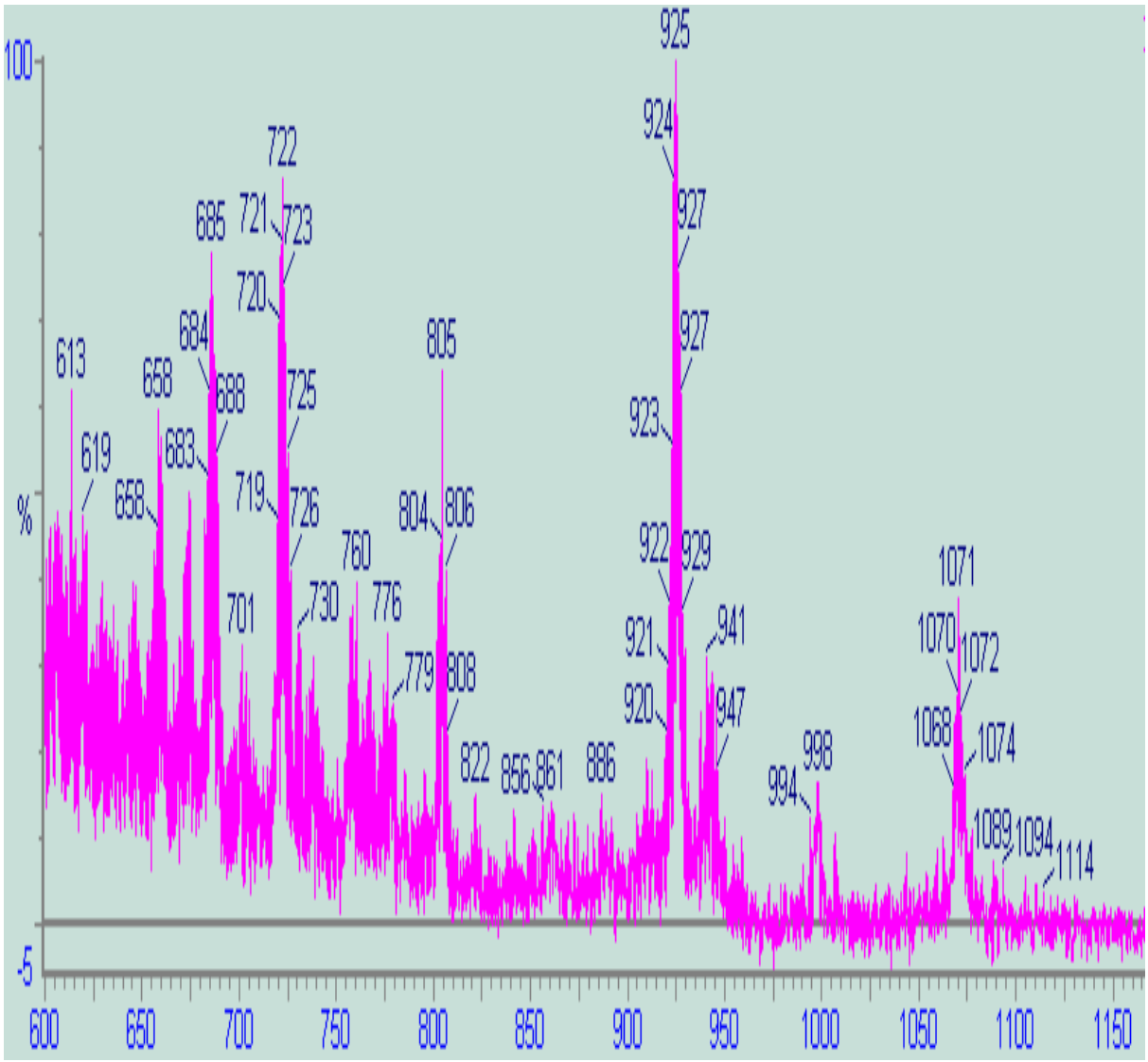

FAB MS spectrum for $[(tpy)Ru(PEt_2Ph)(bpm)PtCl_2](PF_6)_2$

Appendix 5

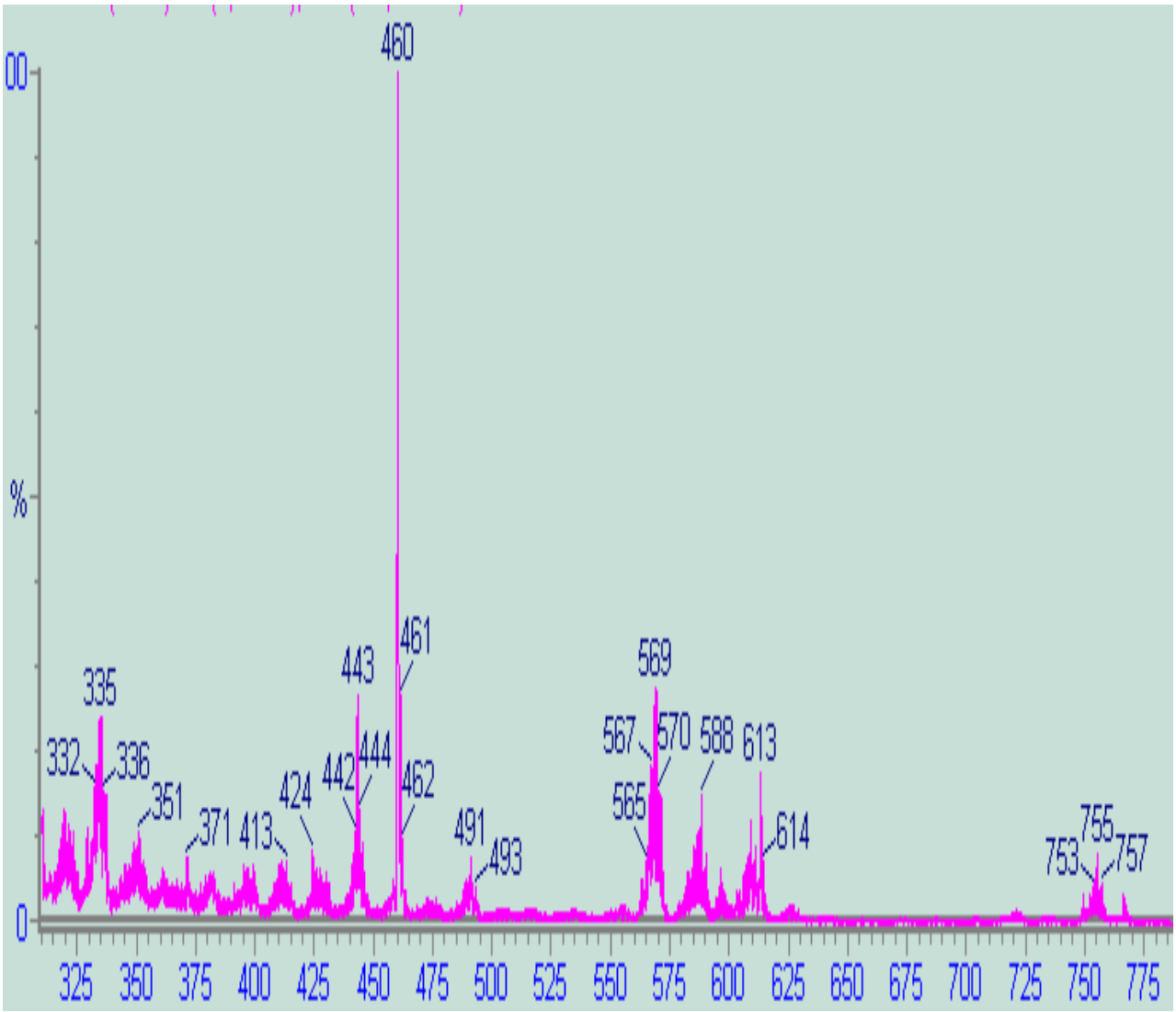

FAB MS spectrum for $[(tpy)Ru(CH_3CN)(dpp)](PF_6)_2$

Appendix 6

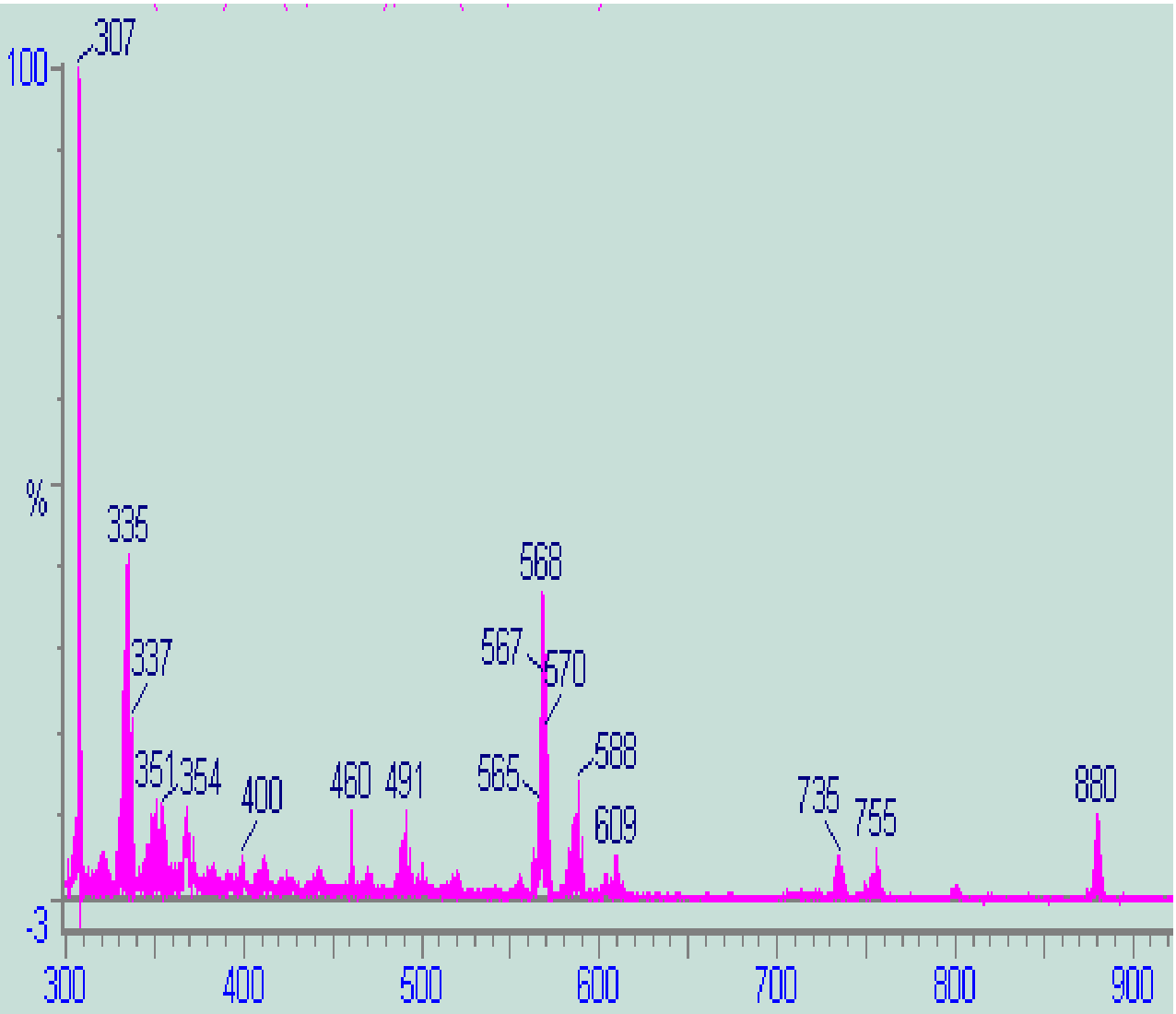

FAB MS spectrum for $[(tpy)Ru(PEt_2Ph)(dpp)](PF_6)_2$

Appendix 7

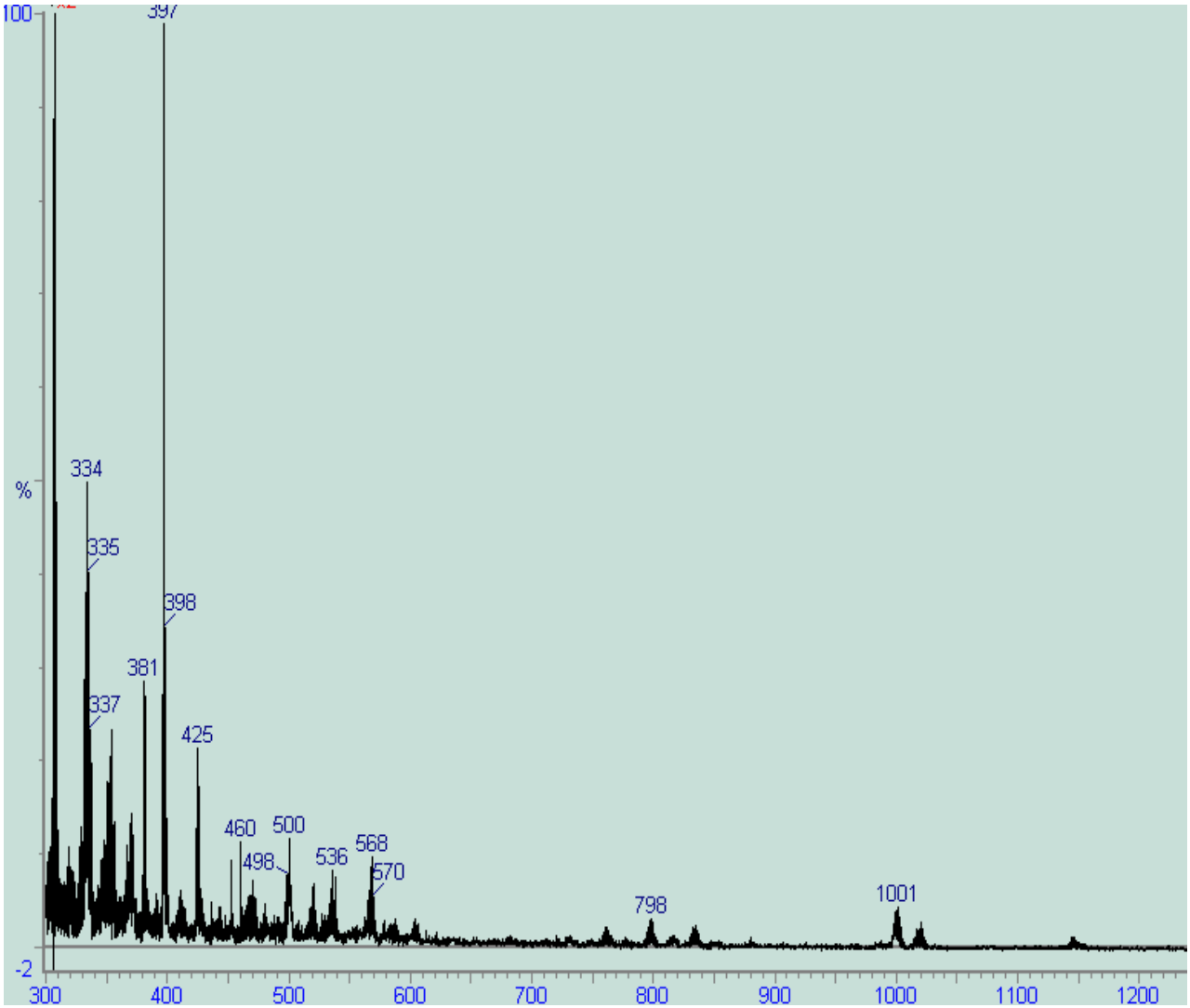

FAB MS spectrum for $[(tpy)Ru(PEt_2Ph)(dpp)PtCl_2](PF_6)_2$

Vitae

Zhenglai Fang was born in May 5, 1971 in a remote village in Anhui province, east China. In 1989 he joined Nanjing University majoring in chemistry. He graduated with BS in July 1993 and joined Research Institute of Petroleum Processing (RIPP) in Beijing, where he maintained until he joined Virginia Tech in August, 1998.

After two years in Blacksburg, Zhenglai moved to Columbia University in the New York city. Right now he is a graduate student in the chemistry department.